Evaluation of Flood Mitigation Strategies for the Santa Catarina Watershed using a Multi-model Approach

by

Jorge E. Cázares Rodríguez

A Thesis Presented in Partial Fulfillment
of the Requirements for the Degree
Master of Science

Approved November 2015 by the
Graduate Supervisory Committee:

Enrique R. Vivoni, Chair
Zhihua Wang
Larry W. Mays

ARIZONA STATE UNIVERSITY

May 2016

ABSTRACT

The increasingly recurrent extraordinary flood events in the metropolitan area of Monterrey, Mexico have led to significant stakeholder interest in understanding the hydrologic response of the upstream Santa Catarina watershed to these high intensity events. This study analyzes a flood mitigation strategy proposed by stakeholders through a participatory engagement process and are assessed using two hydrological models: The Hydrological Modeling System (HEC-HMS) and the Triangulated Irregular Network (TIN)-based Real-time Integrated Basin Simulator (tRIBS).

The stakeholder-derived flood mitigation strategy consists of placing new hydraulic infrastructure in addition to the current flood controls in the basin. This is done by creating three scenarios: (1) evaluate the impact of the current structure, (2) implementing a large dam similar to the current Rompepicos dam and (3) the inclusion of three small detention dams. These mitigation strategies are assessed in the context of a major flood event caused by the landfall of Hurricane Alex in July 2010 through a consistent application of the two modeling tools. To do so, stakeholder-relevant information on topography, soil distributions, land cover and meteorological forcing from multiple sources were assembled, quality-controlled and input into each modeling system. Independent calibration was performed for each model based on streamflow observations and maximum observed reservoir levels from the National Water Commission in Mexico. In both cases, the role of an existing reservoir in ameliorating the flood pulse was analyzed; for tRIBS through a new linear reservoir routing scheme developed as part of this effort.

Analyses from the simulations focus on the differential capability of the two models in capturing the spatial variability in rainfall, topographic conditions, soil hydraulic properties and its effect on the flood response in the presence of the different flood mitigation structures. The spatial variations are analyzed by subdividing the basin into three basic units determined by their intrinsic characteristics such as topography, land cover and presence of flood control structures. Based on the multi-model comparisons, the implementation of new hydraulic infrastructure is shown to have a positive impact on mitigating the flood peak with a more favorable reduction in the peak at the outlet from the larger dam (16.5% in tRIBS and 23% in HEC-HMS) than the collective effect from the small structures (12% in tRIBS and 10% in HEC-HMS). Furthermore, flood peak mitigation depends strongly on the number and locations of the new dam sites in relation to the spatial distribution of rainfall and flood generation. Comparison of the two modeling approaches complements the analysis of available observations for the flood event and provides a framework within which to derive a multi-model approach for stakeholder-driven solutions.

ACKNOWLEDGMENTS

This effort would not have been possible without the help and support of several people. I first want to thank my advisor Dr. Enrique Vivoni for his guidance, patience, time and great dedication towards his students. My committee members Dr. Zhihua Wang, and Dr. Larry Mays. I also greatly appreciate all the help and time provided from Dr. Giuseppe Mascaro.

I would like to thank all the members from the Hydrology group for making such a nice and fun work environment and making it a pleasure to go into the office: Nolie Pierini, Tiantian Xiang, Vivian Verduzco, Adam Schreiner, Luis Mendez, Daniel Che, Cody Anderson, Ted Bohn, Vivianna Gamez, Kristen Whitney and a special thanks to Ara Ko for her friendship and support through the stressful times and demonstrating the meaning of hard work and dedication (고마워).

Appreciation to the Decision Center for a Desert City (DCDC) for funding me and this project alongside the Ivanhoe Foundation. The Nature Conservancy (TNC), Monterrey Water Fund (FAMM), Science for Nature and People (SNAP), Dr. Dave White, Dr. Robert Pahle (DCDC-ASU), Dr. Aldo Ramírez from Tec de Monterrey and Beth Tellman (ASU) for their collaboration. The ASU Advanced Computing Center for the use of the Ocotillo cluster.

Finally the greatest appreciation to my family for all the support, encouragement love and inspiration provided to me and with which I would never have been able to complete this work.

TABLE OF CONTENTS

LIST OF TABLES

Table Page

Table Page

LIST OF FIGURES

Figure Page

Figure Page

Figure Page

Figure Page

Figure Page

CHAPTER 1

INTRODUCTION

Floods are the most relevant disasters occurring from naturally occurring phenomena with approximately 30% of the total natural disasters (Berga 2006). Significant flood events have increasingly occurred in the most recent decades and have produced considerable human losses and economic impacts (Zupka 1998; Re 2004; Berga 2006; Sakamoto and Yasuda 2009). Floods are generated from rapid increase in the water level flowing through a stream at great velocities due to extreme or uncommon meteorological events. Floods and river overflow are natural occurrences that form part of their response to high intensity events, however these are also dependent on the topography of the site, land use of the region, soil types, antecedent moisture conditions and can increase due to human interference with the natural course of the reach (Funk 2006; Ashley and Ashley 2006; Ferriño-Fierro et al. 2010). Some of the main factors playing a role in increasing flood impacts are population growth, human settlement in urban areas and flood plains, change in land cover and land use, massive urbanization, high number of residential infrastructural constructions made in flood-prone areas and unfounded sense of security in the face of flood events from the population (Berga 2006).

Unique oceanic characteristics in the Caribbean and Gulf of Mexico cause the eastern coast of Mexico to be affected by intense storm events in the second half of the year (Farfan et al. 2015). A warm pool of ocean water along the southeastern coast of Mexico (Carbosiero et al. 2009; Amador et al. 2006) combines with humid air and unstable atmospheric conditions to create frequent convective storms and rainfall (Iskenderian 1995; Cavazos 1999; Farfan et al. 2015).

Unawareness or misunderstanding of the damages caused by extreme flood events in Mexico and other countries leads to highly dense urban settlements within the flood plain areas, leaving the population susceptible to flood hazards (Ferriño-Fierro et al. 2010). The city of Monterrey, Nuevo Leon and its metropolitan area (MMA), located within the Santa Catarina River watershed, a basin with an areal extent of 1800 km^2, has developed alongside and downstream of the Santa Catarina River and has historically been affected by flood hazards due to recurring incoming tropical storms from the Gulf of Mexico (Gonzalez 1973). The MMA is the third most populated area in Mexico and has a high economic impact in the country due to its growing industrial development, foreign investment and significant manufacturing sector (Sisto and Ramírez 2015).

The MMA is located at the edge of the Sierra Madre Oriental mountain range where a number of rivers and valleys end up carrying the runoff generated in the range. The unique characteristics of the site, with its complex topographic mountain range and the city at its foot, create frequent hazardous conditions to flash floods in the populated areas by capturing the moisture generated from the tropical storms in the Atlantic Ocean (Sisto and Ramírez 2015). The region is affected by these meteorological phenomenon mostly from May to October and have higher intensities during the first half of September. Although most of the tropical storms do not reach the site in full form, they do generate intense rainfall events and flood inducing storms (Erendira 2002). The most recent major events that caused severe human losses and damages to the city's infrastructure were Hurricane Gilbert in 1988, Hurricane Emily in 2005 and Hurricane Alex in 2010.

The extreme storm event used as a base in this study is the tropical storm Alex that occurred in the period from June 30th to July 2nd 2010. Hurricane Alex was the first tropical cyclone of the season in the Atlantic for 2010 and it is registered as one of the most intense storms in the last 40 years (Hernandez and Bravo 2010).

Hurricane Alex had a maximum rainfall intensity registered of approximately 446 mm in 24-hrs and 616 mm in 60-hrs with some locations such as Estanzuela (an area in the eastern region of the basin) reporting more than 800 mm in 72-hrs (Hernandez and Bravo 2010). The runoff peak estimated at the outlet of the basin in the streamflow gauge "E.H. Cadereyta" of approximately 4300 m^3/s corresponds to a return period of approximately 200 to 300 years (Ramirez 2010).

The storm caused damages in the infrastructure of the city and residential areas destroying bridges, roads and sewer collectors with costs amounting up to $1.3 billion USD (INEGI 2014; Sisto and Ramírez 2015). Severe damages occurred to 28 miles of arterial streets in the city. Some of the main damages occurred along the Santa Catarina River where the stream path was reclaimed by the intensity of the storm (Figure 1).

The intensity of the event and increasing occurrence of these forceful events led to a collective interest by government officials, academic units, stakeholders and decision makers to address potential future flood hazards in the city of Monterrey and the surrounding metropolitan area. Through collaboration between Tec de Monterrey and Arizona State University (ASU), a participatory workshop was held with stakeholders to engage in a dynamic discussion to inform and propose viable flood mitigation strategies.

Figure 1. Photograph of the Santa Catarina River within the urban areas in Monterrey, Nuevo Leon, Mexico during the storm event of Hurricane Alex in 2010.

The series of workshops yielded a strategy of high interest to decision makers and stakeholders that will be studied more in-depth in this research: The Implementation of additional hydraulic infrastructure in the upper regions of the Santa Catarina River Basin, where most of the runoff reaching the urban areas is generated.

The structural approach has been proven to significantly reduce the impact caused by severe floods and contributed to the economic and social development of the countries developing hydraulic infrastructures. The ICOLD Committee on Dams and Floods has studied and analyzed several development plans where the construction of a dam was implemented to enhance flood controls in a region. Large flood prone areas in Japan, USA, Brazil, Korea, Spain and others have seen an impact from flood mitigation strategies between 25% and 85% reduction in the peak discharge (ICOLD 2006; Sakamoto and Yasuda 2009). However they can also negatively impact the development of a region by encouraging more occupation of the flood plain areas which are susceptible to flood risks (Berga 2006). The main role of an hydraulic infrastructure in a location such as the MMA is to (1) reduce the peak discharge and delay the flood wave by altering the routing of the streamflow before reaching the highly populated areas and (2) address the limitations in the urban design of the city (building's locations and construction specifications) (Sisto and Ramírez 2015) by reducing the amount of reconstructive efforts after each flood event, thus protecting the investment done in reconstructive projects for roadworks, urban/hydraulic infrastructure and sewage systems.

To evaluate the flood control strategy of implementing additional structures into the watershed, I propose the use of a multi-model approach in this study in favor of creating a more in-depth analysis with the advantages provided by two types of hydrological models. The first model is a semi-distributed model, a well-known and widely used in management and decision making processes Hydrologic Engineering Center – Hydrologic Modeling System (HEC-HMS) by the US Army Corps of Engineers (U.S. Army Corps of Engineers 2015). This model serves for quick assessments with readily and current available data due to its simple model representation and low computational demand. This model was developed using the 12-parameter soil moisture accounting (SMA) scheme to make use of available geospatial databases, as geographic information systems become more relevant in hydrologic modeling applications (Fleming and Neary 2004). The SMA method divides the basin model into five different storage zones to represent interception, surface depression storage, infiltration, soil storage, percolation and groundwater storage (Bennet 1998; U.S. Army Corps of Engineers 2000) and has been found to accurate replicate observed values (e.g. Bennett and Peters 2000; Bashar and Zaki 2005; McEnroe 2010; Singh and Jain 2015). Further, the reservoir routing tools in HEC-HMS are used to evaluate current and potential future hydraulic infrastructure and their impact in mitigating the peak discharges into the main urban areas by implementing dams at locations identified through a storm diagnosis. The hydrological assessment of reservoirs in water management studies involving decision makers and stakeholders has been successfully conducted using HEC-HMS and have found positive flood controls (Emerson et al. 2003; Ganoulis et al. 2008; Tingsanchali and Tanmanee 2012; Robles-Morua et al. 2015).

The second model is a physically-based fully-distributed academic research model developed in the Ralph M. Parsons Laboratory, Massachusetts Institute of Technology, the Triangulated Irregular Network (TIN)-based Real-time Integrated Basin Simulator (tRIBS; Ivanov et al. 2004a; Vivoni et al. 2007). The model's capability to capture spatially distributed characteristics of the basin provides additional output descriptors to better inform the hydrologic response of the basin and provide a scientific basis in the decision making process. The model uses a variable resolution representation of the catchment which allows to capture more precisely areas of complex topographic conditions such as those found in the Santa Catarina watershed. This is accomplished through the use of thousands of Voronoi polygons that are associated in a similar fashion as Thiessen polygons and each of the computational elements simulates the hydrological processes occurring in the watershed such as channel flow, evapotranspiration, canopy interception and infiltration. The use of a second fully-distributed model is done to complement some of the limiting capabilities of semi-distributed mathematical models. Typically, large-scale hydrological simulations were done by coarsening model resolutions and spatially distributed data that led to inevitable loss of detail in the data generated and distortion of the basin dynamics (Ivanov et al. 2004a). The increase of available computational processing power has opened the possibility to further study spatially explicit information that can be generated by these models and fully utilize novel and more complex data developed for this site. The use of the tRIBS model under different flood events and climatic settings have been successfully applied in determining flood predictions at interior locations within catchments and the impact of rainfall variability (e.g. Vivoni et al. 2006; Nikolopoulus et al. 2011; Moreno et al. 2013; Hawkins et al. 2015). Furthermore, the implementation and assessment of hydraulic infrastructure in the site is conducted using a reservoir routing code that was developed during the course of this research and has its first application within the tRIBS model.

In this study I evaluate the strategy of additional flood controls by setting three scenarios that will aid in determining the role of additional hydraulic infrastructure on flood mitigation. The first scenario considers the impact from current infrastructure in the watershed. The “Rompepicos” Dam located in the upper part of the basin is a dam structure type in which its sole purpose is to regulate the runoff generated in the mountainous regions. In this scenario the structure is removed from the simulations to assess the impact it had in this storm event. The next scenario considers the inclusion of one additional dam structure with similar characteristics as Rompepicos. The location of this dam was selected based on a storm diagnosis of the event to identify large runoff contributing areas upstream from the MMA. Finally the last scenario considers the inclusion of three small detention dams in higher upstream regions. The objective of these small dams is to regulate the stream discharge at higher regions and create a collective delay of the flow peak. This is done as an alternative to a large flood control structure which can represent a costly investment.

The objective of this thesis is to evaluate the proposed flood controls through the use of a semi-distributed and fully-distributed model, understand the hydrological response of the Santa Catarina River basin to extreme rainfall events and the hydrological controls leading to flood hazards to address the questions: (1) is the use of a simple model representation and aggregated, lumped parameters a limitation when evaluating the flood response of the catchment? (2) Can a fully-distributed model provide additional insights into the spatial hydrologic response of the basin while keeping the consistency of a simpler approach from a semi-distributed model? And (3) is the implementation of an additional large dam sufficient to contain extreme event discharges? Or are alternative flood control structures a viable option to flood mitigation? What are the limitations?

This study is organized as follows:

1. Chapter 2 describes the study site and its characteristics along with soil and land cover parameterization. A description of the hydrometeorological flood event, meteorological forcings and the two hydrological models used in this study.
2. Chapter 3 discusses the calibration of both models, the results of the flood event diagnosis, spatially-distributed characteristics of the flood event and the assessment of current and additional hydraulic infrastructure.
3. Chapter 4 presents the conclusions of this study and potential research opportunities for future work.

CHAPTER 2

METHODS

2.1 STUDY SITE AND ITS CHARACTERISTICS

The study area for this research is the Santa Catarina River basin, which is part of the Bravo-Conchos watershed located in Northeastern Mexico and encompasses part of the city of Monterrey, capital of the state of Nuevo Leon (Figure 3a). The city has a population of approximately 4 million people within its metropolitan area (INEGI 2011). The basin has a drainage area of approximately 1800 km^2 and a relief of 3260 m (Figure 3b). It is characterized by having two main contrasting areas, both in its landscape characteristics and its economic activity. The city of Monterrey, with a highly populated urban area, is found in the lower part of the basin. The city has seen an annual growth in its population of 1.3% from 1990 to 2010 (ICP 2013). Monterrey has a high economic activity and is one of the top three most influential cities (Mexico City and Guadalajara) in the economy of the country (INEGI 2009). It has 58% of the population employed in the tertiary sector. Conversely, the upper area of the watershed has predominantly rural activities where 57% of the population are employed in the primary sector. The illiteracy rate in adults 15 years or more ranges from 14 to 40% (2.6% in the urban areas) and 57% of the population have little or no access to health services (27.7% in the city) showing the high contrast in the social and economic activities found in the basin (ICP 2013). The landscape is equally distinct: the lower basin is characterized by mild slopes, low reliefs and highly impervious surfaces distinctive of densely populated cities. The upper basin on the other hand, has a vegetated, highly mountainous natural landscape with forests of pine and oak (Erendira 2002; Maqueda 2007). The watershed has a unique complex topography of folded mountain ridges in the form of a trellis pattern as seen in Figure 3b. The high slopes in the mountainous region promotes fast runoff generation, which drains directly into the city at a single point (Ramirez 2010; Ferriño-Fierro et al. 2010).

The study area has a subtropical semi-arid climate, with hot summers and occasional frosts in some winters (Navar et al. 2000) characterized by having higher loss rates (e.g. evaporation) than precipitation rates, which prevents the presence of perennial rivers in the area and their flows are dependent on the seasonality of rainfall occurrence. The mean annual temperature is of 21.5°C with a mean annual precipitation of 602 mm (SMN 2010), with most of the rainfall occurring in between the months of August and September. The Koppen climate classification shown in Figure 2 shows high semi-arid and very hot (BS1hw; BS1(h')w; BS1k(x') regions in the northwest with semi-hot humid with summer rainfall ((A)C(w1); (A)C(wo); (A)C(w2)) in the eastern regions and temperate humid (C(w1)) in the higher mountainous areas (INEGI 1990).

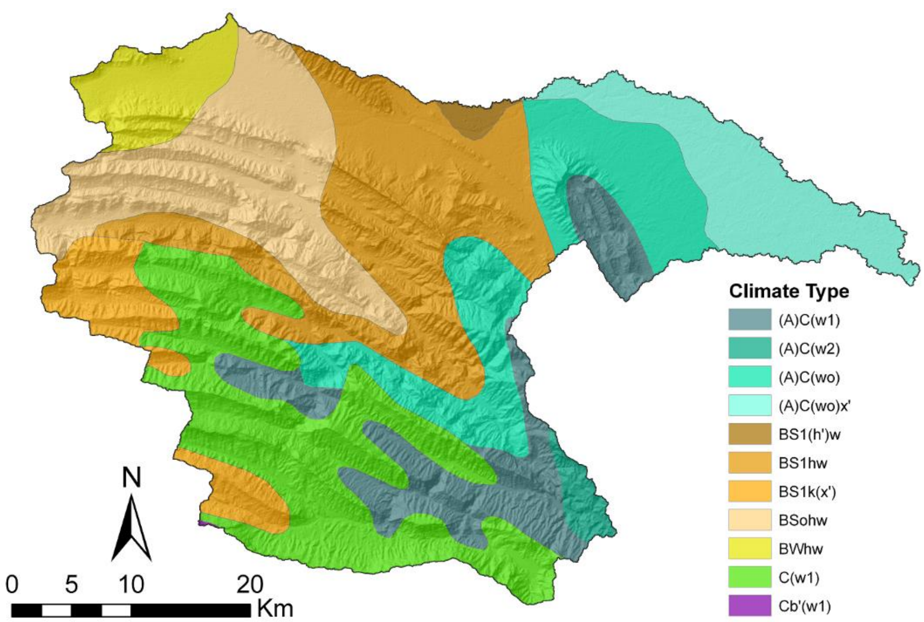

Figure 2. Koppen climate classification as adapted by Enriqueta Garcia from the Mexican National Commission for the Knowledge and use of Biodiversity (CONABIO).

11

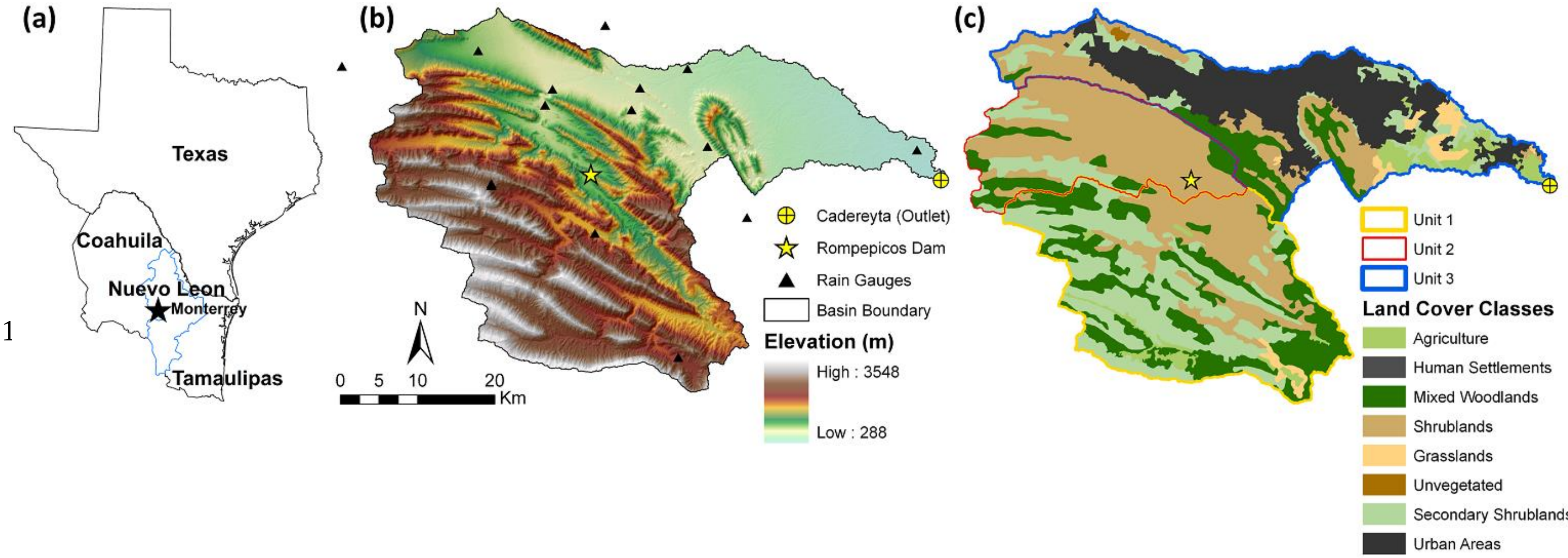

Figure 3. (a) City of Monterrey in Nuevo Leon, Mexico. (b) Santa Catarina watershed based on a 30-m Digital Elevation Model and the locations of rain gauges, current hydraulic infrastructure (Rompepicos Dam) and the stream gauge at the basin outlet (Cadereyta Station). (c) Land cover classes and the definition of basin units used in the flood event diagnosis.

2.1.1 Soil and land cover characterization

Soil and land cover characteristics are critical components in estimating the hydraulic parameters that are used in hydrological models. In this investigation, soil properties were obtained from the International Soil Reference and Information Centre (ISRIC) – World Soil Information, an independent, science-based foundation. ISRIC developed a global soil data product named SoilsGrid1km that contains spatial predictions for a selection of soil properties at six depths (ISRIC 2013). SoilsGrid1km uses global compilations of publicly available soil data (Hengl et al. 2014) in which the Mexican National soil profile database is included. The data used is the national continuum soil profile information at a scale of 1:250 000 Serie II from the Instituto Nacional de Estadística y Geografía (INEGI). This same soil profile is utilized in the ISRIC SoilsGrid1km database. The properties of interest from these data grids are sand, silt and clay fraction (% content) and bulk density (kg/m^3). Figure 5a, 5b and Figure 6a show the spatial variation of the top 5 cm for each soil class in percent content while Figure 6b displays the bulk density in kg/m^3.

The top 5 cm grids for each soil type were aggregated separately into the land cover units seen in Figure 7 by applying the Zonal Statistic tool in ArcGIS. This generated tabular values of percent clay, silt, sand and bulk density corresponding to each land cover unit. The values were organized using MS Access database following the format requirements of a sample file provided by the Pedotransfer Function Model (PFM) used. The requirements were a code ID for each type (provided by the user), a general description (e.g. “Soils_SC”) and the soil and bulk density values. An additional processing of the data was done to meet model requirements. This involved adding the percent content of clay, sand and silt in each unit and adjust uniformly so the addition of the three contents was precisely 100%, in addition to the conversion of the bulk density values from kg/m^3 to g/cm^3, as required by the model. Finally, the Pedotransfer Function Model (PFM) was executed in order to obtain parameters of interest such as the saturated hydraulic conductivity (K_s), soil moisture at saturation (θ_s) and residual soil moisture (θ_r). The model used in this research is the ROSETTA model (Kosugi 1999; Mualem 1976; Schaap et al. 1999) of the US Salinity Laboratory by the United States Department of Agriculture (USDA). This model allows for the construction of a database in which the obtained 1-km grid information on clay, sand, silt and bulk density can be used. The model relates the percent content from each soil and relates them to van Genuchten´s (1980) water retention and unsaturated hydraulic conductivity parameters through which an estimate of the saturated hydraulic conductivity can be obtained (e.g. Figure 4). Additional details on the processes and use of the ROSETTA model can be found in the USDA software download site and ROSETTA User´s Manual (USDA 1999).

2.1.2 Effects of vegetation Soil hydraulic properties have a relevant role in rainfall-runoff modeling in semi-arid regions, particularly the saturated hydraulic conductivity (K_s) (Hernandez et al. 2000). To account for the vegetation effects on the K_s, a power function suggested by Stone et al. (1992) was used to adjust the values obtained from the PFM. The power function relates increasing vegetative cover and runoff to higher infiltration rates in the form of:

$$K_{s_{veg}} = K_s e^{(0.015 * \%Vegetation\ Fraction)} \qquad (1)$$

Table 1

Watershed areal coverage for soil and land cover classifications. Note that 2.12% of the watershed area has soils classified as 'Not Available'.

Soil Class	**Coverage (%)**	**Land Cover Class**	**Coverage (%)**
Castañozem	0.44%	Agriculture	3.88%
Phaeozem	0.48%	Grasslands	2.07%
Fluvisol	0.06%	Human Settlements	6.57%
Lithosol	94.23%	Mixed Woodlands	20.83%
Luvisol	0.02%	Secondary Shrublands	23.09%
Regosol	1.07%	Shrublands	32.92%
Rendzina	0.76%	Unvegetated	0.16%
Vertisol	0.31%	Urban Areas	10.48%
Xerosol	0.51%		

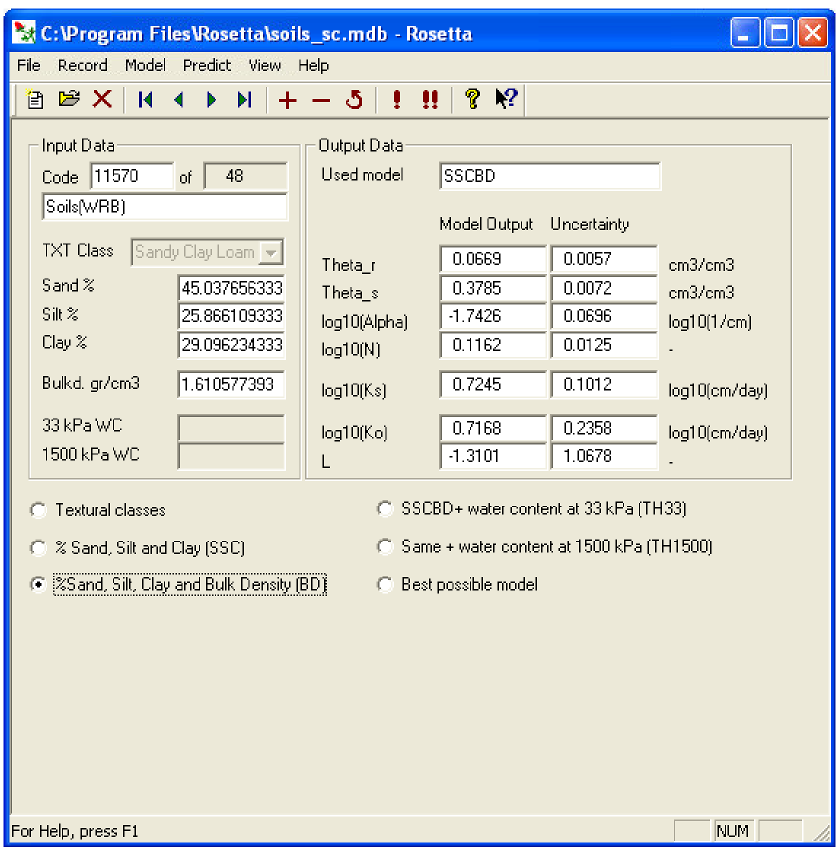

Figure 4. Input and output data generated for one of the land cover units in the Pedotransfer Function Model: ROSETTA.

Land cover properties were obtained directly from the Mexican National Database (INEGI) at a scale of 1:250 000 Serie II. Figure 7 shows the land cover spatial distribution in the basin. The areas at lower elevation mainly consist of the urban areas classified as Urban Zones (ZU) and Human Settlements (AH) which occupy 10.5% and 6.5% of the total basin area respectively. The urban metropolitan area composed of these two land cover types account for the second largest areal coverage in the basin. The main land cover type in the watershed is sub-mountainous shrub-land at 20.8% total coverage, followed by secondary shrub-land in Pine forests with 11.84% found at the higher elevations of the site. Other important land covers found are Desert shrub (9.9%), Pine forest (6.4%), Oak forest (5.8%), temporal annual agriculture (5.3%) and Oak-Pine forest (5.1%). The main land cover and soil type areal coverage is described in Table 1.

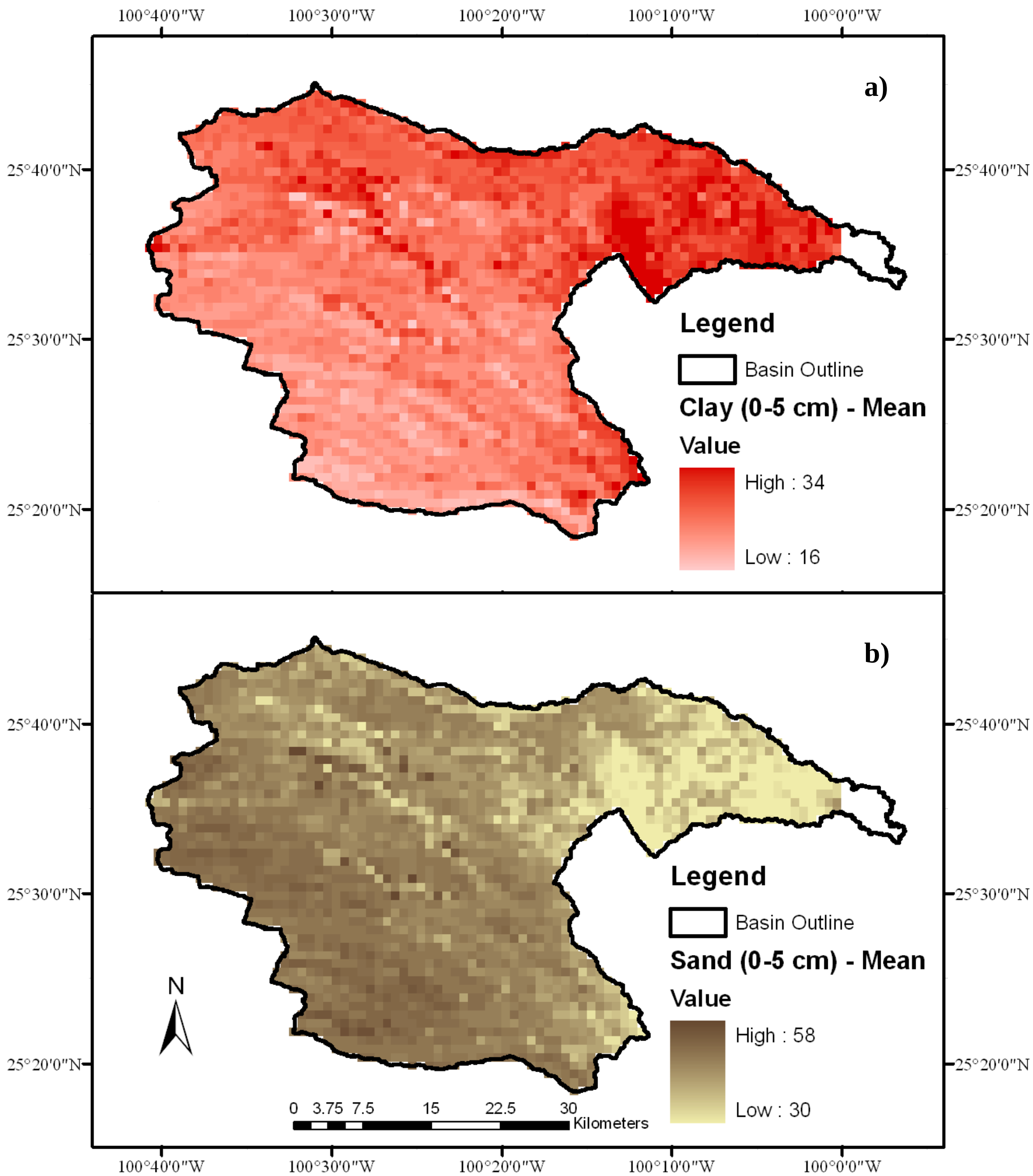

Figure 5. (a) Mean clay content and (b) sand in the top 5 cm of the basin.

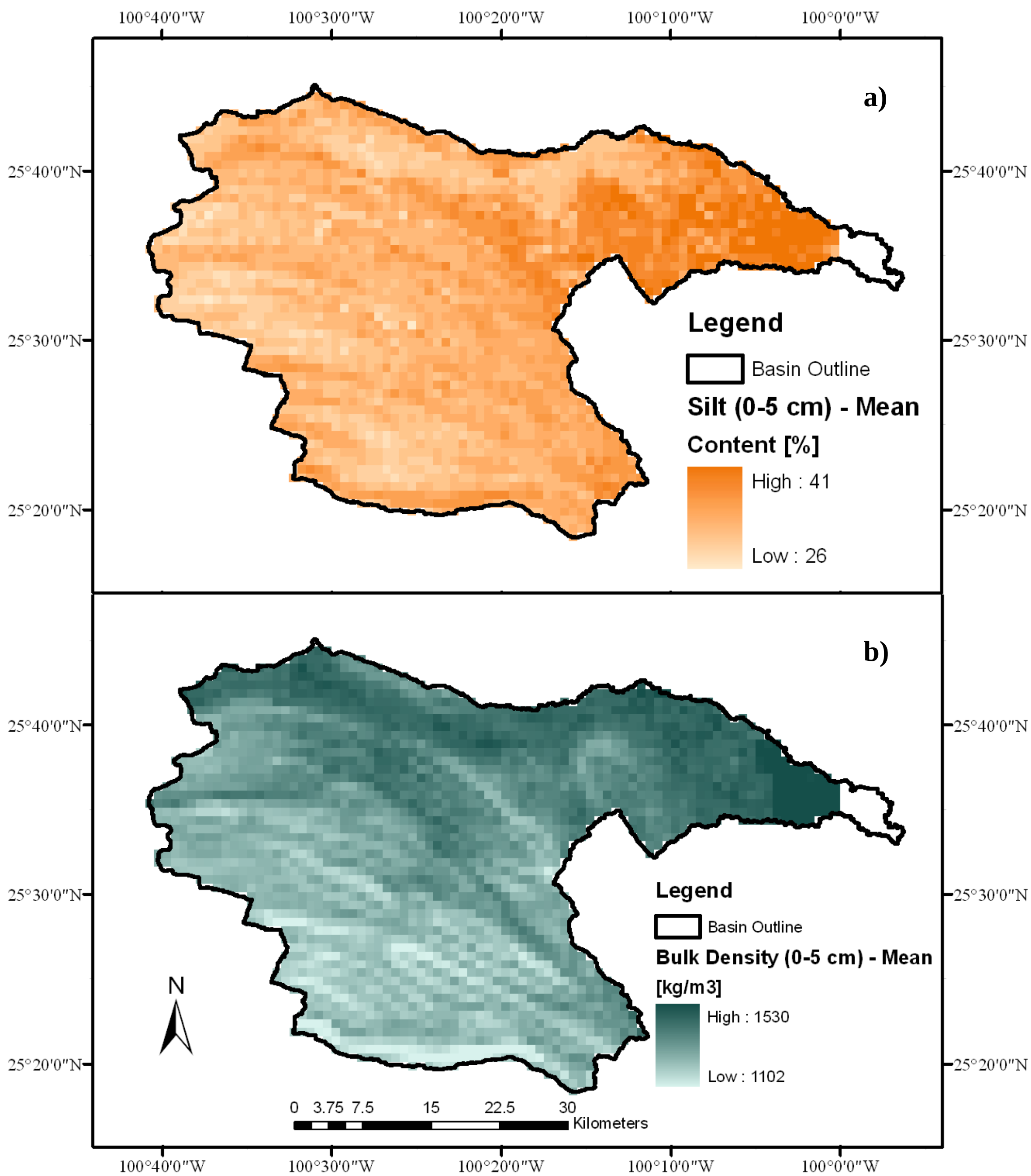

Figure 6. (a) Mean silt content and (b) bulk density in the top 5 cm of the basin.

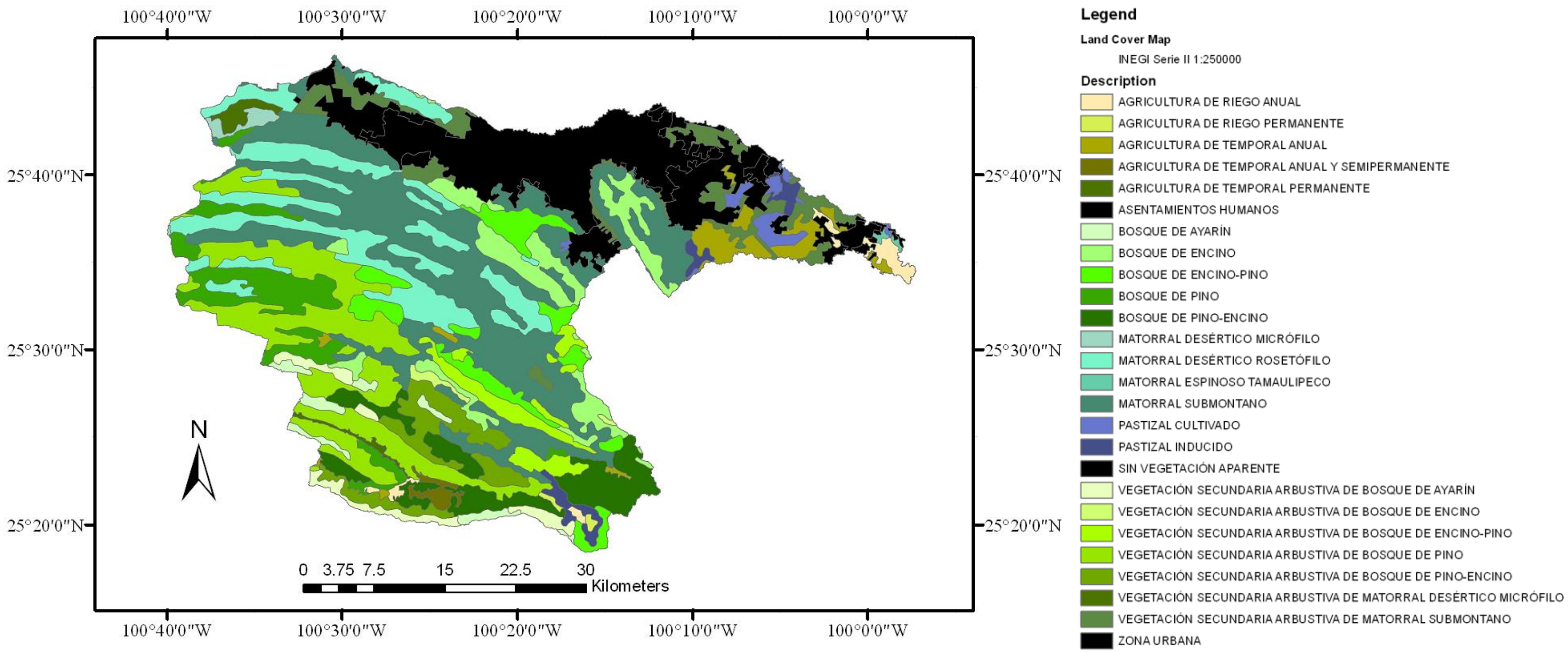

Figure 7. Series II land cover map for the Santa Catarina River Basin at a scale of 1:250 000 retrieved from INEGI.

2.1.3 Land Cover Parameterization Two main land cover parameters were obtained from vegetation indices provided by the Moderate Resolution Imaging Spectroradiometer (MODIS) through the use of its Reprojection Tool Web Interface (MRTWeb). Two datasets were obtained from MODIS, the Leaf Area Index (LAI) and the Normalized Difference Vegetation Index (NDVI). The LAI is a dimensionless parameter relating the one-sided green leaf area per unit ground area in broadleaf canopies and one-half the total needle surface area per unit ground area in coniferous canopies (Myneni et al. 2003). The data for this parameter was obtained from a 10 degrees by 10 degrees tile unit at a 1 km resolution from the MODIS/COMBINED MCD15A2 on board the Terra and Aqua satellites in an 8-day composite for June 26th 2010 (177 in Julian date) being the closest date before the occurrence of the extreme event. A scale factor of 0.1 was applied to the LAI data (LP-DAAC 2012) which was then utilized to obtain an estimate of the maximum canopy storage capacity (S) in both hydrological models based on an empirical relation from Pitman (1989) and Carlyle-Moses and Price (2007) as $S = 0.5LAI$. Further, the free-throughfall coefficient (p), a parameter accounting for the fraction of rainfall not intercepted by the vegetation was obtained following Pitman (1989) and Mendez-Barroso et al. (2014), as:

$$p = \exp(-1.5LAI) \tag{2}$$

The additional data obtained from MODIS was the NDVI, which determines the density of greenness or plant growth in a patch of land by relating the visible and near-infrared light reflected by vegetation. NDVI was collected from the MODIS Terra Vegetation Indices 16-Day L3 Global 500m SIN Grid V005 (MOD13A1) for June 2nd

2010 (153 in Julian date) being the closest available date with adequate quality data previous to the event. A scale factor of 0.0001 was applied to the dataset as indicated in the MODIS Vegetation Index User's Guide (MOD13 Series) (Solano et al. 2010). With this vegetation index it is possible to obtain an estimate of the vegetation fraction (v_f), which was computed following Carlson and Ripley (1997) as:

$$v_f = \left[\frac{NDVI - NDVI_{min}}{NDVI_{max} - NDVI_{min}}\right]^2 \qquad (3)$$

The parameters $NDVI_{min}$ = 0.06 and $NDVI_{max}$ = 0.98, were obtained from the MODIS Land Product Subsets in the Oak Ridge National Laboratory Distributed Active Archive Center (ORNL-DAAC) within a time period of 15 years (February 18, 2000 – April 23, 2015). The location for the subset created was centered on Latitude [25.637428228186394] Longitude [-100.22996873039062] and approximately 6.25 km wide and 6.25 km high (ORNL-DAAC 2014). The vegetation fraction represents the greenness or vegetation cover that can be linked to NDVI and carries out transpiration (Mendez-Barroso et al. 2014).

2.2 HYDROMETEOROLOGICAL FLOOD EVENT

2.2.1 Meteorological Forcing The meteorological forcing data used in both hydrological models consisted on data fields obtained from the North American Land Data Assimilation System (NLDAS) given the limited available meteorological forcing data in the region in addition to the improved spatial forcing it represents for the models

(Xiang et al. 2014; Robles-Morua et al. 2012, 2015) The study period encompassing the storm event is set from June 28th to July 6th 2010. Spatial meteorological fields were obtained in 1/8 degree spacing (~144 km^2) grids at a 1-hr temporal resolution (Mitchell et al. 2004). The data was obtained in the World Meteorological Organization's Gridded Binary format (WMO-GRIB) with spatial fields for wind speed (m/s), incoming short-wave and long-wave radiation (W/m^2), air temperature (°C), atmospheric pressure (Pa) and total daily precipitation (mm).

The study site contains limited data availability in the local gauging system implemented in the basin as seen in Figure 8. There are 19 rain gauges located throughout the basin with 11 of them being manual stations and having a course daily resolution in their data output while the remaining 8 stations are automatic gauges with 10-min data resolution. The name and information of the stations with areal coverage over the catchment are presented in Table 2. The automatic stations are mostly located in the lower part of the basin in the urban areas, having a limited coverage in the upper basin where the sparseness of the network is accentuated and limited to the daily output stations. To increase the spatial distribution of the meteorological data in the catchment, the high-resolution NLDAS forcing was applied in both hydrological models.

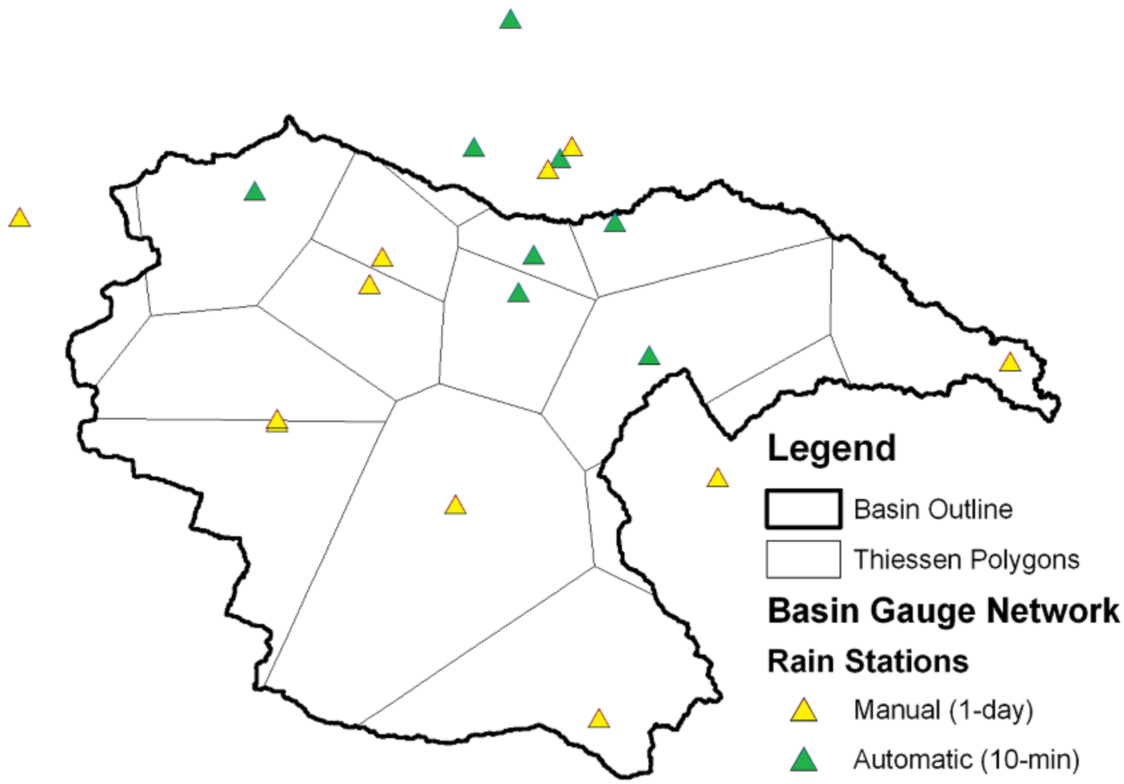

Figure 8. Local rain gauge network consisting of 19 stations. 7 automatic stations with 10-min resolution output and 11 manual stations with daily resolution output.

The raw NLDAS data obtained required additional processing in order to be used in the models. The data is presented in large tiles, therefore it is necessary to identify the location of the site in the required coordinate projection and extract only the necessary pixels. The projection used is the Universal Transverse Mercator (UTM) coordinate system and the study site is located in zone 14N (North America). The encoded WBO-GRIB data was extracted with a Matlab code in which the delimitation coordinates in UTM format were specified to extract the data. In addition to these requirements, the extracted data was converted to the required units in the models since NLDAS data has predefined units (Mitchell et al. 2004).

Table 2

Daily and sub-hourly meteorological stations with areal coverage over the basin. Retrieved from the National Water Commission's (CONAGUA) Superficial Waters National Data Compilation (BANDAS) and Ramirez (2010).

Station ID	Name	Lon.	Lat.	Elevation (m.a.s.l.)
	Daily Stations			
19002	Agua Blanca	-100.433	25.500	2690
19008	Cadereyta	-100.000	25.600	349
19015	El Cerrito	-100.183	25.517	90
19018	El Pajonal	-100.367	25.500	1531
19031	La Cruz	-100.450	25.467	445
19033	Laguna de Sanchez	-100.283	25.350	1925
19054	Rinconada	-100.717	25.700	989
19058	Santa Catarina	-100.467	25.683	113
19096	La Huastequita	-100.467	25.533	410
	Sub-hourly Stations			
MI-02	Las Mitras	-100.351	25.820	N/A
FE-04	Fierro	-100.271	25.682	N/A
OB-05	El Obispo	-100.541	25.701	N/A
AS-06	Arroyo Seco	-100.343	25.634	N/A
EZ-07	La Estanzuela	-100.245	25.592	N/A
PC-08	Proteccion Civil	-100.332	25.659	N/A

The resulting ASCII grids generated with the Matlab code can be directly utilized in the tRIBS model. For HEC-HMS, individual pixels from the ASCII grids were extracted and served as artificial rain gauges in the model. The first step was to extract the precipitation time series for each pixel using a Matlab code. Once the data for each pixel was extracted, an ASCII grid file was imported into ArcGIS and converted into a points file as seen in Figure 9. Each of the points observed represents a pixel from the precipitation time series grid of NLDAS. With the point file, the sub-basin map (Figure 9) was used to generate a data set with the weighted areal average (Thiessen polygons) for each point and its weight over each of the sub-basins.

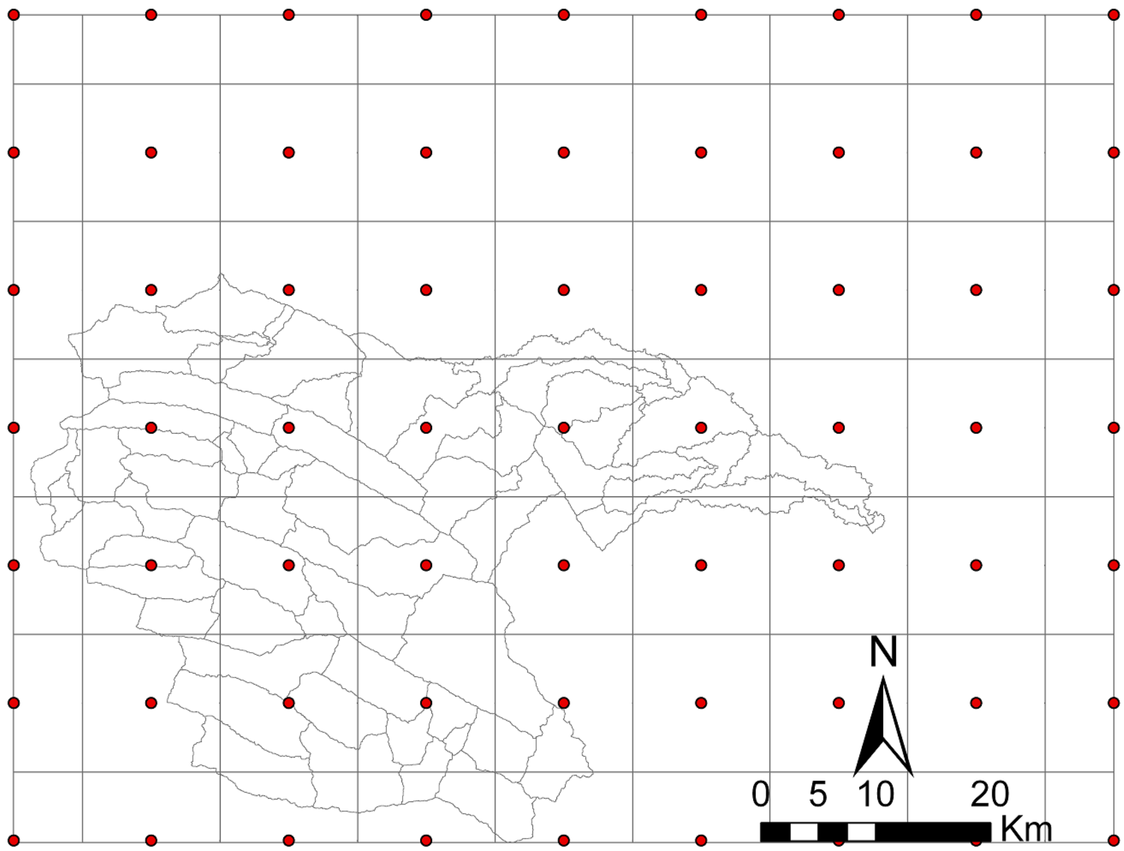

Figure 9. Visual representation of the individual NLDAS precipitation pixels converted into points and used as artificial rain gauges in HEC-HMS.

This data was then used in HEC-HMS as input for the generation of the artificial rain gauges and within the Meteorological model, the Gage Weights method was selected. For each sub-basin the pixel and corresponding depth weight was specified based on the Thiessen polygon analysis. This method in the rainfall input simplifies data management within the model without having to deal with a more complex gridded precipitation management in HEC-HMS. This method has also been utilized in Robles-Morua et al. (2015).

2.2.2 Mean Field Bias Correction A comparison was done between the ground rainfall data from the gauge network and each corresponding pixel in the NLDAS grids. The comparison exhibited an underestimation by the original NLDAS data series as seen in Figure 10 and Figure 11a. To account for this difference in the data a correction factor was applied to the NLDAS data with the Ratio of Means (RM) multiplicative factor of Steiner et al. (1999) and applied in Robles-Morua et al. (2012). The Mean Field Bias correction was evaluated at a daily scale due to the limitations in the temporal resolution and spatial distribution found in the gauging network. The RM bias correction factor was obtained at daily time steps (j) for the months containing the storm event (June-July 2010) using

$$RM(j) = \frac{\sum_{i=1}^{N} g_i(j)}{\sum_{i=1}^{N} p_i(j)} \qquad (4)$$

where N is the number of gauges (i) and corresponding number of pixels from NLDAS (N = 19), and $g_i(j)$ and $p_i(j)$ are daily rainfall values obtained from the gauges and the grid pixels respectively. To indicate the fitness of the values in the correction the bias was used as

$$B = \frac{1}{N}\sum_{i=1}^{N} \frac{P_i}{G_i} \qquad (5)$$

where G_i and P_i are the cumulative total rainfall for the entire study period for the rain gauges and the NLDAS pixels respectively. The adjusted precipitation for NLDAS was obtained by applying uniformly the Ratio of Means multiplicative factor over the entire watershed.

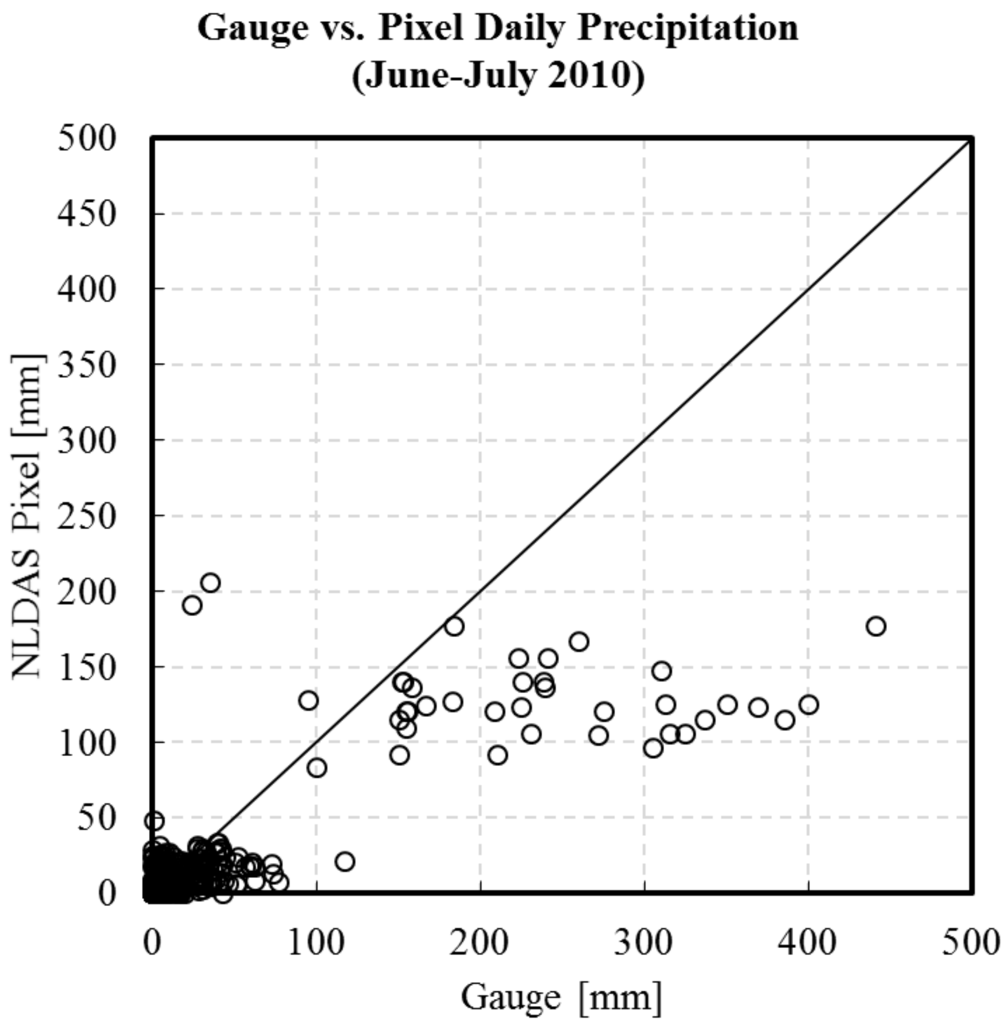

Figure 10. Comparison between the ground observations and remote sensing precipitation grids from NLDAS revealed an underestimation from the satellite product.

Given the sparseness in the ground observations as seen in Figure 11b it is expected that certain pixels without a corresponding gauge to be adjusted will result in overestimation or underestimation of the rainfall values, especially in the southern region where there are more regions without an available station (Robles-Morua et al. 2012). The results of the NLDAS bias-corrected product can be seen in Figure 11c.

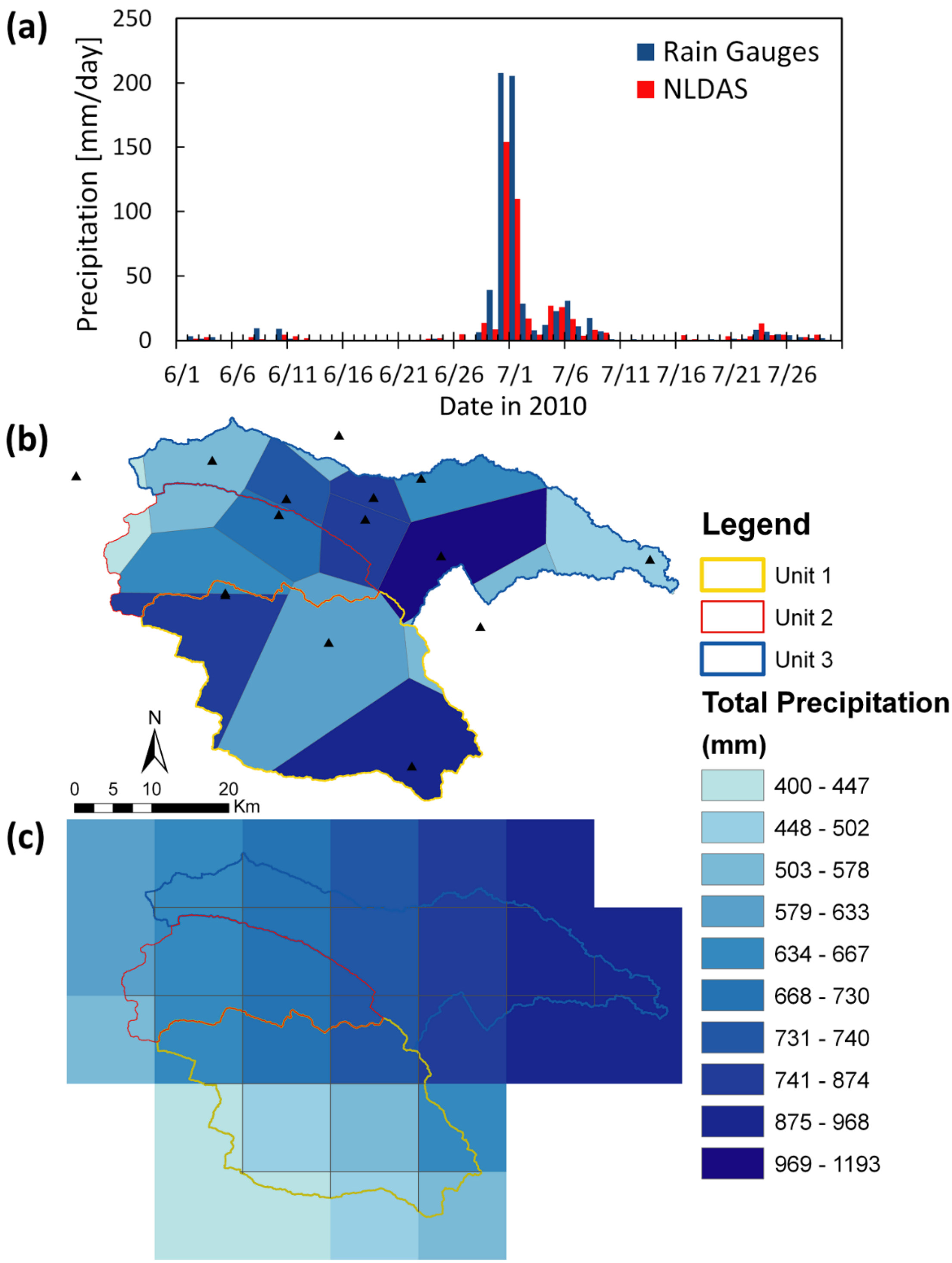

Figure 11. (a) Time series of the basin-averaged daily precipitation (mm/day) from the rain gauge network and the original NLDAS product (12-km, 1-hr resolution). Spatial distribution of total precipitation (mm) for June and July 2010 obtained from (b) rain gauges using a Thiessen polygon interpolation and (c) bias-corrected NLDAS product.

2.3 MULTI-MODAL APPROACH FOR FLOOD DIAGNOSIS

2.3.1 Hydrologic Engineering Center – Hydrologic Modeling System (HEC-HMS)

HEC-HMS is a semi-distributed numerical mathematical model developed by the US Army Corps of Engineers that can be used for several hydrological simulations. HEC-HMS has several applications in the hydrologic engineering area such as planning and designing new flood-damage reduction facilities, evaluating existing hydraulic-conveyance and water-control facilities, flood response, environment restoration, etc. (U.S. Army Corps of Engineers 2015).

The model has three basic capabilities for conducting the hydrological simulations. First is the watershed physical description through the use of a basin model. In this model, each of the elements or sub-basins are connected in a dendritic network that simulates runoff processes (U.S. Army Corps of Engineers 2010). In this way it is possible to obtain runoff hydrographs for each of the elements in which the basin was discretized. Second is the meteorology description, in here the meteorological data is analyzed through a meteorological model that includes precipitation and evapotranspiration. Finally there is the simulation run, where all of the control specifications are determined (e.g. duration of the simulation) and combines with the basin and meteorological model to create the hydrologic simulation.

2.3.1.1 Soil Moisture Accounting The soil moisture accounting (SMA) loss method represents the watershed through three layers that simulate the dynamics of water movement in the soil (U.S. Army Corps of Engineers 2010). The method is typically coupled with a canopy and surface method. Water is stored in the canopy, surface depressions, soil profile and up to two groundwater layers. The storage in the canopy represents initial abstractions, a storage that has to be filled before rainfall reaches the surface (e.g. trees, shrubs and grasses). Any precipitation that cannot be infiltrated into the soil profile is stored in the surface depressions. If the depression storage is exceeded this is then converted into runoff. Losses in the canopy are accounted through evaporation while water stored in the surface depressions is removed through evaporation and infiltration (McEnroe 2010). A conceptual diagram of the method retrieved from the HEC-HMS Technical Reference Manual (2000) is presented in Figure 12. The SMA was selected for this study over more practical and traditional methods such as the Curve Number (CN) approach. Although the SCS-CN approach offers a simple, stable and predictable conceptual method in estimating direct runoff, along with well-documented environmental inputs (Ponce and Hawkins 1996) it comes with a series of limitations and disadvantages that are important to consider (Garen and Moore 2005; Chu and Steinman 2009). The method was developed and originally intended for use in agricultural areas and has been documented to perform poorly in applications to forests sites (Hawkins 1984, 1993), as found in the Santa Catarina Basin. Its application to basins larger than 250 km^2 are not recommended or are suggested to exercise caution (Ponce and Hawkins 1996).

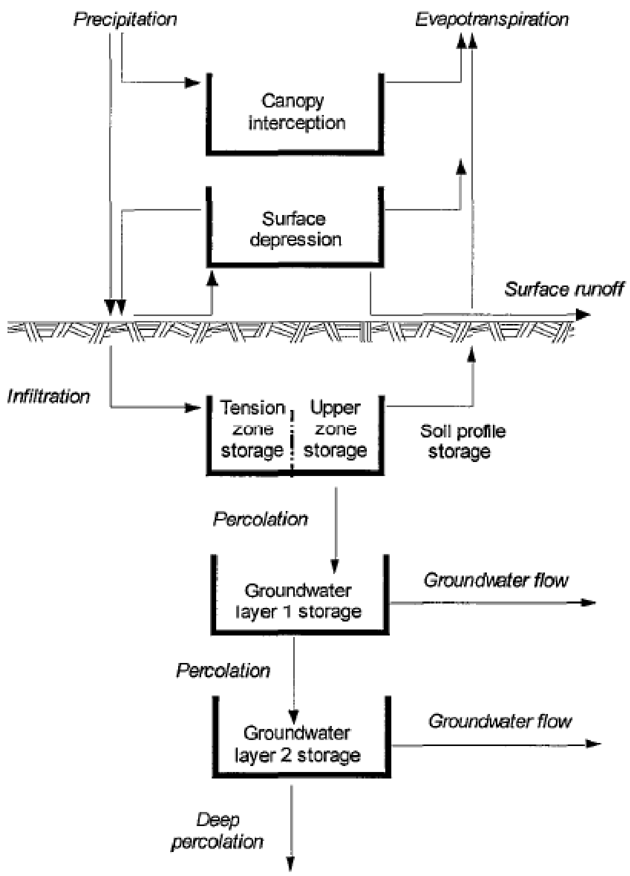

Figure 12. Conceptual diagram of the Soil Moisture Accounting scheme retrieved from the Technical Reference Manual (2000).

The SMA method simulates movement of water through the canopy and surface, the soil profile, and two groundwater storages (Bennett and Peters 2000) using separate inputs for each layer allows the use of available spatial data sets and Geographical Information Systems (GIS).

2.3.1.2 Routing Schematic The routing schematic utilized in this research is the Kinematic Wave model. This method is used for both the overland-flow model and channel routing in the watershed. The Kinematic Wave model conceptualizes the watershed as a two plane surfaces in which water flows down into the reaches as seen in Figure 13. Overland planes are treated as a very wide open channel draining into the reaches and then water is routed into the outlet of the basin (U.S. Army Corps of Engineers 2010). The basic equations upon which the Kinematic Wave model is based on the one-dimensional momentum equation (1) as:

$$S_f = S_0 - \frac{\partial y}{\partial x} - \frac{V}{g}\frac{\partial V}{\partial x} - \frac{1}{g}\frac{\partial V}{\partial t} \tag{6}$$

where S_f = energy gradient (friction slope); S_0 = bottom slope; V = velocity; y = hydraulic depth; x = distance along flow path, t = time; g = acceleration due to gravity; $\frac{\partial y}{\partial x} =$ pressure gradient; $\frac{V}{g}\frac{\partial V}{\partial x} =$ convective acceleration; and $\frac{1}{g}\frac{\partial V}{\partial t} =$ local acceleration. In addition, the one-dimensional continuity equation (2) as:

$$A\frac{\partial V}{\partial x} + VB\frac{\partial y}{\partial x} + B\frac{\partial y}{\partial t} = q \tag{7}$$

where B = water surface depth; q = lateral inflow per unit length of channel; $A\frac{\partial V}{\partial x} =$ prism storage; $VB\frac{\partial y}{\partial x} =$ wedge storage; and $B\frac{\partial y}{\partial t} =$ rate of rise. Further details and concepts of this method can be found in Chow (1959) and Chaudhry (1993).

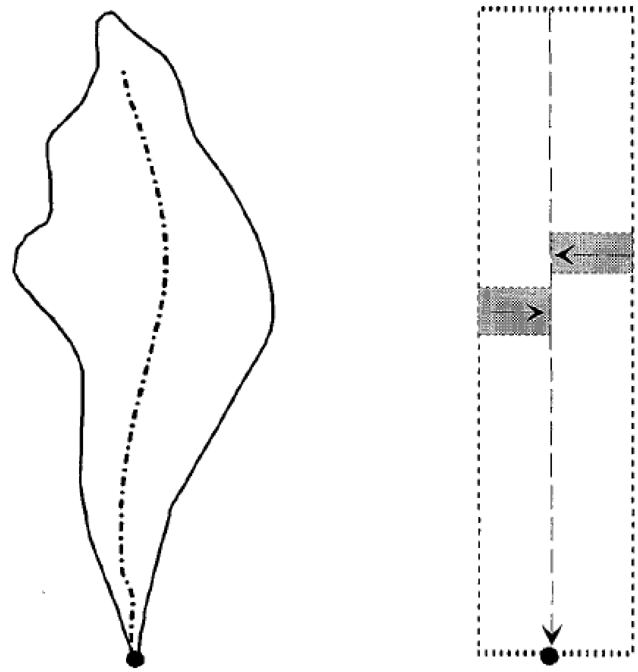

Figure 13. Simple watershed representation through the kinematic-wave model as described in the HEC-HMS Technical Reference Manual (2000).

2.3.1.3 HEC-HMS Model Setup Watershed and sub-basin boundaries along with the river network were delineated utilizing a 30-m resolution Digital Elevation Model (DEM) from the Advance Spaceborne Thermal Emission and Reflection Radiometer (ASTER). Processing of the DEM was done using the Geographical Information System (ArcGIS) extension Geospatial Hydrological Modeling (HEC-geoHMS) that enables exporting the basin processing project into HEC-HMS. The DEM obtained was composed of two larger tiles that were merged using the Mosaic to New Raster tool in ArcGIS. The resulting larger DEM was used to delineate the basin and process the data into a compatible format for the models. The initial basic processing step of the DEM is to fill the sinks of the data. This is done to avoid any discontinuities in the drainage network and ensure proper pour points. Once the filled DEM was obtained, the file was processed to determine flow direction, flow accumulation, stream definition, catchment grid delineation, catchment polygon processing, drainage line processing and adjoint catchment processing as indicated by the HEC-geoHMS manual. Further details and an overview of the steps in setting up the basin model through ArcGIS can be found in the HEC-geoHMS User's Manual (2010) and Appendix [B] in this document.

The initialization of the model requires twelve parameters and five initial conditions to represent the selected methods in the canopy, surface, soil and groundwater storage units (McEnroe 2010). The range of parameters used in the model resulting from the calibration efforts can be seen in Table 3. Calibration adjustments of the soil hydraulic properties and routing parameters were done to match streamflow registered in the Cadereyta outlet streamflow gauge and the maximum water surface elevation reported by the national water commission at the hydraulic structure located within the watershed.

To determine the most sensitive parameters in the calibration process, one parameter at a time was varied and evaluated while keeping all other parameters constant. Initial parameters were established from literature and other studies that apply the SMA approach. Subsequently the values were varied and the output results were compared to the initial estimates. The most sensitive soil hydraulic properties were found to be the soil storage, tension storage and the maximum infiltration. The first two parameters are connected through the potential infiltration equation used in the SMA method. The volume of infiltration at a given time interval will be a function of the water available to infiltrate, the current storage in the soil profile and the maximum infiltration rate (U.S. Army Corps of Engineers 2000) in the form of:

$$PotSoilInfil = MaxSoilInfil - \frac{CurSoilStore}{MaxSoilStore} MaxSoilInfil \qquad (8)$$

where *MaxSoilInfil* = the maximum infiltration rate; *CurSoilStore* = the volume in the soil storage at the beginning of the time step; and *MaxSoilStore* = the maximum volume of the soil storage. The actual infiltration rate is the minimum of the *PotSoilInfil* = potential infiltration volume and volume of water available for infiltration (U.S. Army Corps of Engineers 2000). The resulting analysis showed that the peak discharge at the outlet was less sensitive to changes in the soil storage than at the interior location at the dam. Since higher infiltration values are found in the upper part of the basin, given the natural landscape characteristics of the area, changes in these areas were more sensitive. The maximum infiltration parameters were adapted from the saturated hydraulic conductivity (K_s) values (Singh and Jain 2015) obtained from the ISRIC grids.

Moderately sensitive parameters were the channel roughness coefficients adapted from Mays (2010). A different set of ranges were established given the contrasting characteristics of the site. In the lower basin the roughness was considered to be streams on plains while the higher upper basin can be considered as mostly mountain streams (with cobbles and large boulders). Similarly to the hydraulic parameters, the target observations to match were the peak discharge at the outlet and the water surface elevation at the dam structure.

Table 3

The HEC-HMS Model Parameter Ranges and Source Used in the Santa Catarina Simulations

Parameter Symbol	Description	Units	Parameter Range	Source
		Vegetation Properties		
C	canopy maximum storage	mm	0.01 - 2.5	remote sensing
D	depression maximum storage	mm	0.176 - 2.36	literature
		Soil Hydraulic Properties		
K	maximum infiltration	mm/h	0.01 - 13.57	literature
S_s	soil storage	mm	50 - 150	calibration
T_s	tension storage	mm	25 - 50	calibration
GW_s	groundwater storage	mm	50 - 150	calibration
S_p	soil percolation	mm/h	1.27 - 5.4	literature
GW_p	groundwater percolation	mm/h	1 - 5.4	calibration
GW_c	groundwater coefficient	hr	100	calibration
		Routing Parameters		
n	Manning's channel roughness		0.35	calibration
n_f	flow plane roughness		0.1 - 0.32	literature
c_l	channel losses	%	0.02 - 0.1	calibration

2.3.2 TIN-based Real-time Integrated Basin Simulator (tRIBS) tRIBS is a physically-based fully-distributed numerical model developed at the Ralph M. Parsons Laboratory at the Massachusetts Institute of Technology (MIT). This hydrological model represents the basin through a Triangulated Irregular Network (TIN) that captures elevation, stream network and boundary delimitations at multiple resolutions. A variable resolution representation of the catchment allows to model more precisely areas of complex topographic conditions while minimizing computational demand by reducing the number of nodes required to represent low-varying regions (Vivoni et al. 2004).

The rainfall-runoff scheme in the model is determined by infiltration fronts, variable water table and lateral soil moisture fluxes in the soil profile (Robles-Morua et al. 2012). Depending on the moisture state of the soil profile, four potential runoff generation mechanisms can be considered: 1) Infiltration excess, 2) Saturation excess, 3) Groundwater exfiltration and 4) Perched subsurface stormflow (Ivanov et al. 2004a).

The computational elements are defined through the use of Voronoi polygons that are associated in a similar fashion as Thiessen polygons to the mesh nodes from the TIN to have a finite volume used to estimate the state of the dynamic variables in the basin (Ivanov et al. 2004a). The topographic representation through the use of the TIN's provide significant reductions in the computational demand required for the simulations, particularly in basins greater than 1000 km^2 (Hawkins et al. 2015). The fully-distributed approach offers the possibility of generating detailed spatial representation of hydrological processes such as runoff generation occurrence, soil moisture and dynamic water table depth (Ivanov et al. 2004a). Each of the computational elements simulates the hydrological processes occurring in the watershed such as channel flow, evapotranspiration, canopy interception and infiltration. Distributed modeling applications from tRIBS in similar sized basins as the one under study are available from Ivanov et al. (2004b) and Vivoni et al. (2005a, b).

2.3.2.1 Hillslope and channel flow routing The representation of the overland runoff generation is simulated through individual hillslope node elements. Unlike the semi-distributed model, where the overland flow routed into the reaches is represented by long

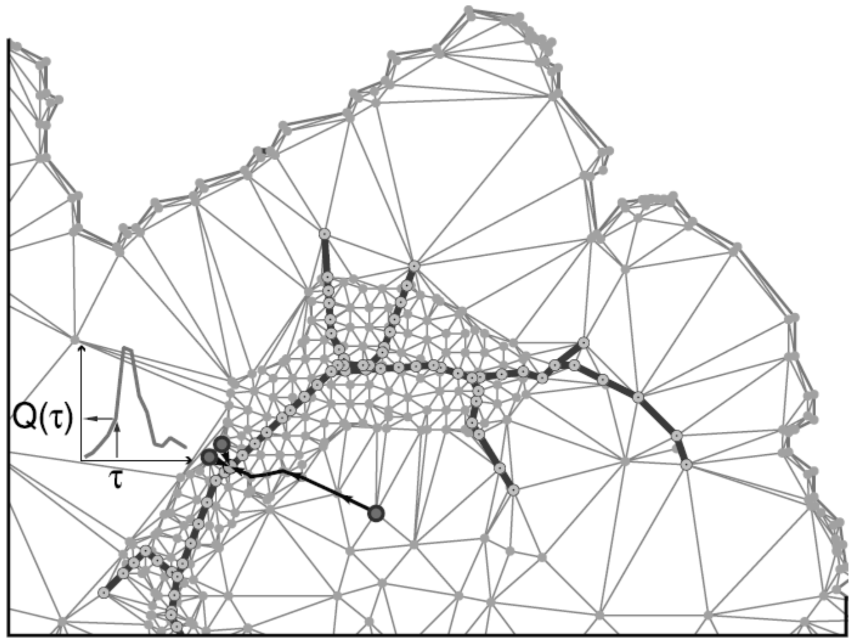

Figure 14. Runoff generated at each hillslope node is routed through the edges of the TIN network into its corresponding outlet stream node (circles with dots inside). Figure retrieved from Ivanov et al. (2004).

planes, tRIBS simulates lateral inflow into the channels through incremental responses of the hillslope nodes. Each hillslope node is assigned an outlet node at the stream an runoff generated is routed through the edges of the TIN network as seen in Figure 14 retrieved from Ivanov et al. (2004a). Lateral inflow into the channels is then routed using the Kinematic wave model described previously.

2.3.2.2 tRIBS Model Setup The boundary delimitations and TIN delineation for the Santa Catarina River Watershed was done using an ASTER-DEM with a 30 m resolution that resulted in the generation of 580434 Voronoi polygons or computational nodes to represent the catchment's complex terrain as seen in Figure 15. Such a high resolution dataset can create extensive computational demands given the large size of the basin (1800 km^2). To have a reasonable computational performance in these large watersheds, and efficient coarsening of the domain's topographic data is required (Vazquez et al. 2002; Hawkins et al. 2015). Variable resolution in the topographic representation of the model is achieved through the use of triangular irregular networks where high complexity areas of the terrain (e.g. rugged, mountainous areas) is prioritized to have more accurate (finer resolution) elements while low relief areas can be coarsened to preserve computational efficiency. This process removes DEM nodes based on the relief of the topographic model, resulting in a TIN network with less computational nodes. The coarsening of the basin's topographic representation will vary based on the intrinsic characteristics of each site, however the degree of aggregation in the TIN model can be established with the horizontal point density (*d*) metric (Vivoni et al. 2005) as:

$$d = \frac{n_t}{n_g} \tag{9}$$

where n_t is the number of TIN nodes and n_g is the number of DEM nodes. A higher horizontal point density (i.e. closer to 1) represents lower losses of nodes, a higher resolution representation while a ratio closer to 0 has a high degree of aggregation, or coarser resolution. The horizontal point density for the study site is d = 0.277, with n_t = 580434 and n_g = 2094908. This represents a moderately fine resolution, the preservation of elevation nodes is expected given the complex terrain found on the site. Additionally, an effective resolution or "equivalent" cell size (r_e) metric can be defined to interpret the resulting spatial aggregation of the TIN network into a length scale of the average grid spacing of points in a TIN (Vivoni et al. 2005a; Tucker et al. 2001):

$$r_e = \sqrt{\frac{A}{n_t}} \qquad (10)$$

where A is the basin area defined as $A = n_g r^2$, where r is the DEM cell length. An r_e = 56.17 m was defined for the study site, which is consistent with the horizontal point density (d). The reader can refer to Vivoni et al. (2004) for a detailed description of the TIN generation within the tRIBS model.

The simulation period established in the model started on June 28th 2010 and had 225 simulation hours (ending on July 7th 2010) to capture the duration of the storm and the recession period following it. Due to a higher computational demand, simulations were done in parallel by distributing computations over several cores in the Ocotillo cluster administered by the ASU Advanced Computing Center. In the model simulations, the Message Passing Interface (MPI) (Gropp et al. 1996) is used to communicate the different processors in a parallel computing platform. The MPI protocol allows processors to send and receive messages between them. The hydrologic elements (reaches and junctions) are organized from upstream to downstream direction. The parallelized model operations are organized according to the channel reaches, therefore the information on fluxes and basin states are passed between sub-basins and processors in a sequential order for each time step (Vivoni et al. 2011). For tRIBS, the data passed between the sub-basins are: (1) lateral surface fluxes through the channel network; and (2) lateral subsurface fluxes between Voronoi polygons located on shared boundaries between sub-basins (Vivoni et al. 2011).

Parameterization of the model consisted of input for soil and land cover/land use parameters in reclassification tables read by the model. Soil parameters included the hydraulic properties of saturated hydraulic conductivity (K_s), soil moisture at saturation (θ_s) and residual soil moisture (θ_r) obtained through the use of pedotransfer functions described in previous sections. Land cover parameters for the basin that were obtained through remote sensing products included the Canopy storage capacity (S), vegetation fraction (v_f) and Leaf Area Index described in the land cover parameterization section. Similarly to the HEC-HMS model, the soil hydraulic properties and routing variables in the tRIBS model were varied one at a time to establish a sensitivity of the parameters on the hydrologic response of the basin. Similarly, the parameters were aggregated into the land cover units seen in Figure 7. Since soil texture classification data available shows a homogeneous spatial distribution, the vegetation and land use classes were utilized as an alternative representation of the soils spatial variability as in Ivanov et al. (2004a).

As described before, the target observations for both models were the peak discharge registered at outlet of the basin for the Cadereyta streamflow gauge and the maximum water surface elevation (related through the peak discharge) at the flood control structure "Rompepicos", an interior location in the basin. Table 4 presents the range of values obtained through the manual calibration for the Santa Catarina River Watershed. Calibration efforts were performed on a limited number of parameters to which the model was most sensitive (Ivanov et al. 2004a). Parameters that were not available for the study site were obtained from previous model studies from Vivoni et al. (2005a) and Ivanov et al. (2004a) which are based from the literature.

Land use parameters can describe the physical characteristic of the land cover: The amount of precipitation held (free throughfall coefficient), the storage capacity (canopy storage) and drainage rate properties of each land cover. Additionally, land use parameters can describe the energy fluxes and evapotranspiration such as: albedo (a), vegetation height (H_v), optical transmission coefficient (K_t), canopy stomatal resistance (r_s) and vegetation fraction (v).

Soil parameters on the other hand, describe the rainfall infiltration characteristics in the vertical profile and the lateral moisture redistribution. The most sensitive parameters used for calibration were the anisotropy ratio (a_r), defined as the ratio between the saturated conductivities in the parallel and normal directions to the soil surface. The conductivity decay parameter (f), which controls the surface saturated conductivity and its exponential decrease with depth at a rate f. The routing parameters were also found to have a high sensitivity on the hydrologic response of the basin. Manning's channel roughness, obtained from Mays (2010), was kept consistent with the HEC-HMS model. The hillslope velocity coefficient (c_v) was the most sensitive parameter found in the calibration process. The hillslope velocity coefficient is part of the hydrologic routing process, influencing the travel time of runoff between a hillslope node and an outlet node. The travel time t_r of runoff between these two points is defined as:

$$t_r = \frac{l_h}{v_h(\tau)} \tag{11}$$

where l_h is a hillslope fraction and $v_h(\tau)$ is the hillslope velocity at time τ. The velocity varies in space and time as (Ivanov et al. 2004a):

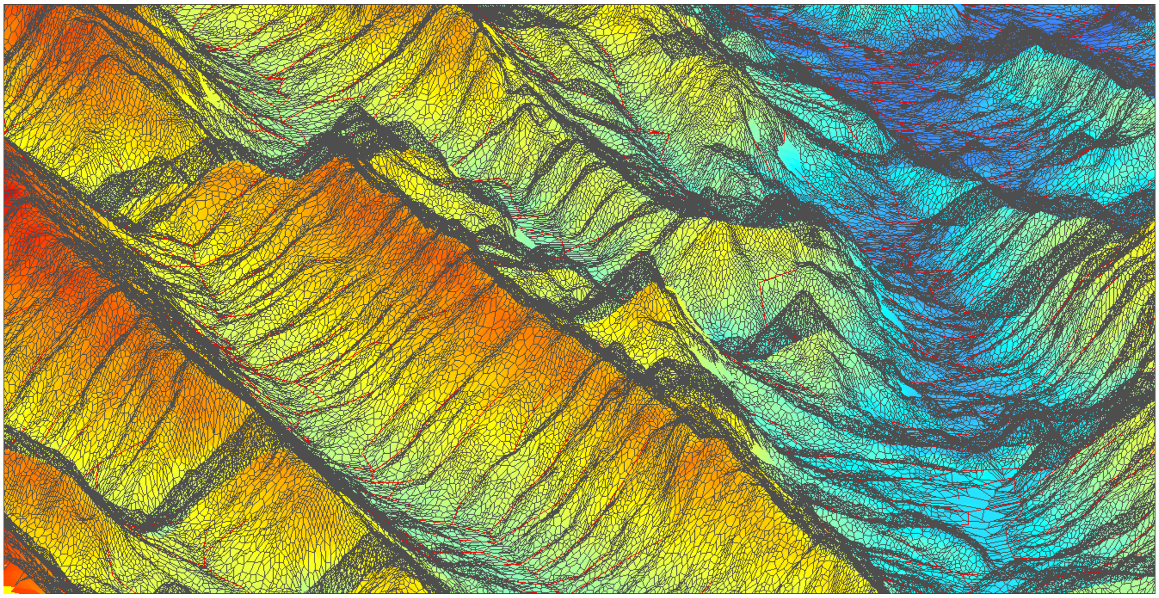

Figure 15. The Voronoi mesh generated for the Santa Catarina River watershed is able to capture the high variability of the complex terrain found in the site.

$$v_h(\tau) = c_v \left[\frac{Q(\tau)}{A_c}\right]^r \tag{12}$$

where $Q(\tau)$ is the discharge at the outlet stream node at time τ, A_c is the contributing area of the outlet stream node (not the basin outlet) and r is the hillslope velocity exponent.

Table 4

The tRIBS Model Parameter Ranges and Source Used in the Santa Catarina Simulations

Parameter Symbol	Description	Units	Parameter Range	Source
	Land Use Properties			
p	free throughfall coefficient		0.3 - 0.65	literature
S	canopy capacity	mm	0.01 - 2.5	remote sensing
K	canopy drainage rate coefficient	mm/h	0.1 - 0.2	literature
g	canopy drainage exponent	mm-1	3.7 - 4	literature
a	surface albedo		0.105 - 0.3	remote sensing
Hv	vegetation height	m	0.1 - 20	literature
Kt	optical transmission coefficient		0.45 - 0.95	literature
rs	average canopy stomatal resistance	s/m	20 - 135	literature
v	vegetation fraction		0.103 - 0.7	remote sensing
LAI	canopy leaf area index		0.01 - 6	remote sensing
	Soil Hydraulic Properties			
K_s	saturated hydraulic conductivity	mm/h	0.01 - 34.74	literature
θ_s	saturated soil moisture content		0.4 - 0.44	literature
θ_r	residual soil moisture content		0.06 - 0.07	literature
λ_0	pore distribution index		0.165 - 0.277	literature
Ψ_b	air entry bubbling pressure	m	1.5 to 0.12	literature
f	conductivity decay parameter	mm-1	0.0008 - 0.011	calibration
a_r	anisotropy ratio		25 - 90	calibration
N	total porosity		0.44 - 0.49	literature
k_s	volumetric heat conductivity	J/m s K	1.33	literature
C_s	soil heat capacity	J/m^3 K	2,400,000	literature
	Routing Parameters			
n	Manning's channel roughness		0.35	calibration
α_B	channel width-area coefficient		2	calibration
β_B	channel width-area exponent		0.5	calibration
c_v	hillslope velocity coefficient		2.45	calibration
r	hillslope velocity exponent		0.4	calibration

2.3.3 Accounting for Impervious Areas and Depression Storage The simple surface method applied in HEC-HMS considers the volume of rainfall that can be intercepted at the surface and must be filled before runoff can occur. This type of storage is typically considered the initial abstractions or losses due to surface ponding and wetting. Tabular estimates from Urban Drainage and Flood Control District (2008) were used for pervious surfaces whereas a relationship for depression storage and basin slope developed by Kidd (1978) was applied for impervious surfaces as:

$$D_p = 0.0303\, S^{-0.49(C_c)} \tag{13}$$

where D_p is the depression storage (in.), C_c is the correlation coefficient (0.85) and S is the slope (%). The impervious surfaces considered in the models were based on the land cover map retrieved from INEGI. In the classification, the land cover map contains two categories that were considered as impervious surfaces: urban areas and human settlements. Given the fully distributed capabilities of the tRIBS model, these impervious areas can be directly captured by the model. In HEC-HMS, a semi-distributed model, it was necessary to obtain a percent of impervious area found within each of the sub-basins. To obtain these percentages the land cover map, the sub-basin delineation map and the Zonal Statistics as Table tool in ArcGIS were used. With the Zonal Statistics tool, the amount of pixels corresponding to urban areas or human settlements were found for each sub-basin. The total amount of pixel count considering all types of land cover was also found, with this count, the fraction of total impervious areas within each sub-basin could be estimated. The Kinematic Wave transform method used in HEC-HMS has the option to utilize two separate planes for each single sub-basin. For example, if no impervious areas are found within sub-basin W770, then W770 (Plane 1) will have 100% of the area, meaning that only parameters held for Plane 1 will be used by the model. If in sub-basin W710 the user specified 57% area for Plane 1 and 43% area for Plane 2, then 43% of that sub-basin contains impervious surfaces and a representative amount of the parameters will be used by the model for each Plane. In this study, Plane 2 was utilized as the impervious plane.

2.4 HYDRAULIC INFRASTRUCTURE

Currently there is only one main hydraulic structure within the basin. The structure is located at a site called Corral de Palmas for which the dam was named, but is better known as the Rompepicos dam (Figure 16). The dam began its planning stages in 1997 and was concluded in 2004 after some interruptions to the project as political administrations changed over the time of its construction. The cost of the project was nearly 530 million pesos (approximately 53 million USD). The geographical location of the dam is at 25° 33’ 23’’ latitude and 100° 23’ 51’’ longitude (Ramirez 2010). The dam has a gravity curtain composed of roller compacted concrete. An elevation of 70 m and a maximum length of 240 m. The structure has two outlet structures: A secondary rectangular opening of 6 m x 6 m at the base of the dam with a capacity of 838 m^3/s when the water elevation reaches the maximum design point, and a main Creager spillway with a crest length of 60 m and a capacity of 3376 m^3/s at the maximum design elevation (Ramirez 2011). The elevation-storage-discharge relationships for the dam are shown in Figure 17 and Figure 18. This structure receives runoff generated in the uppermost region of the basin and discharges close into the entry to the city. The structure has already served its flood control functions in two extreme rainfall events: Hurricane Emily in July 2005 and Hurricane Alex in June-July 2010.

Figure 16. Rompepicos Dam at the “Corral de Palmas” site operating during Hurricane Alex storm event in 2010. (Source: Movimet)

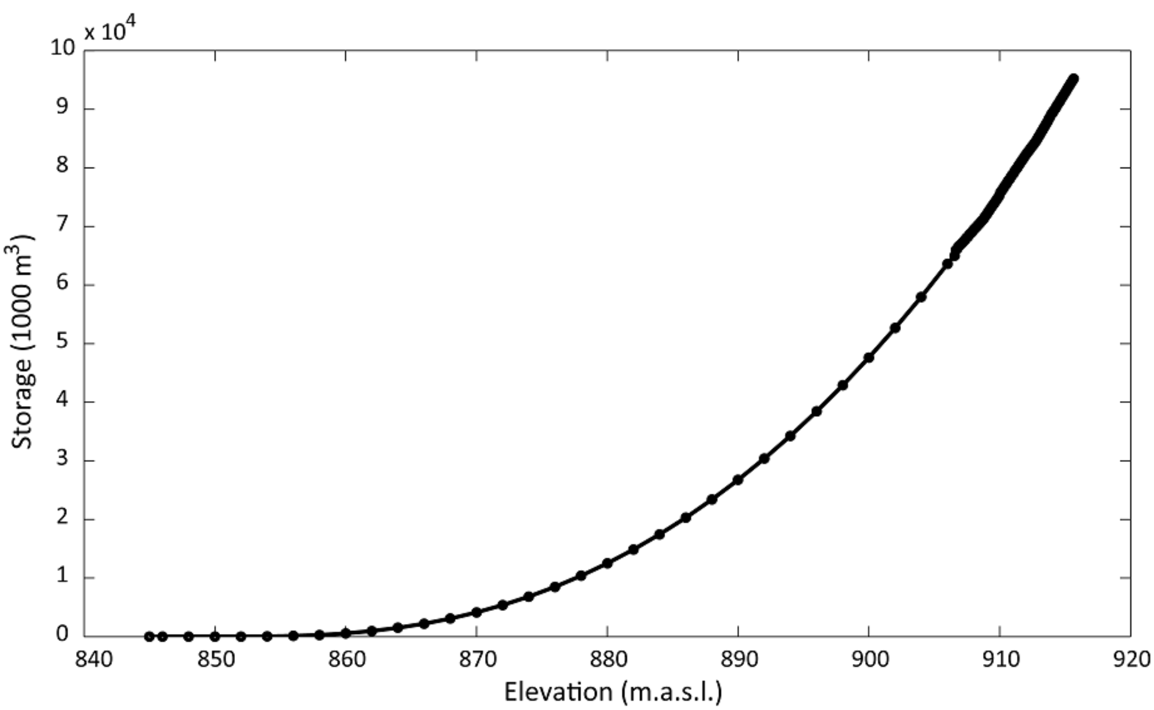

Figure 17. Storage-elevation function of the flood control structure Rompepicos.

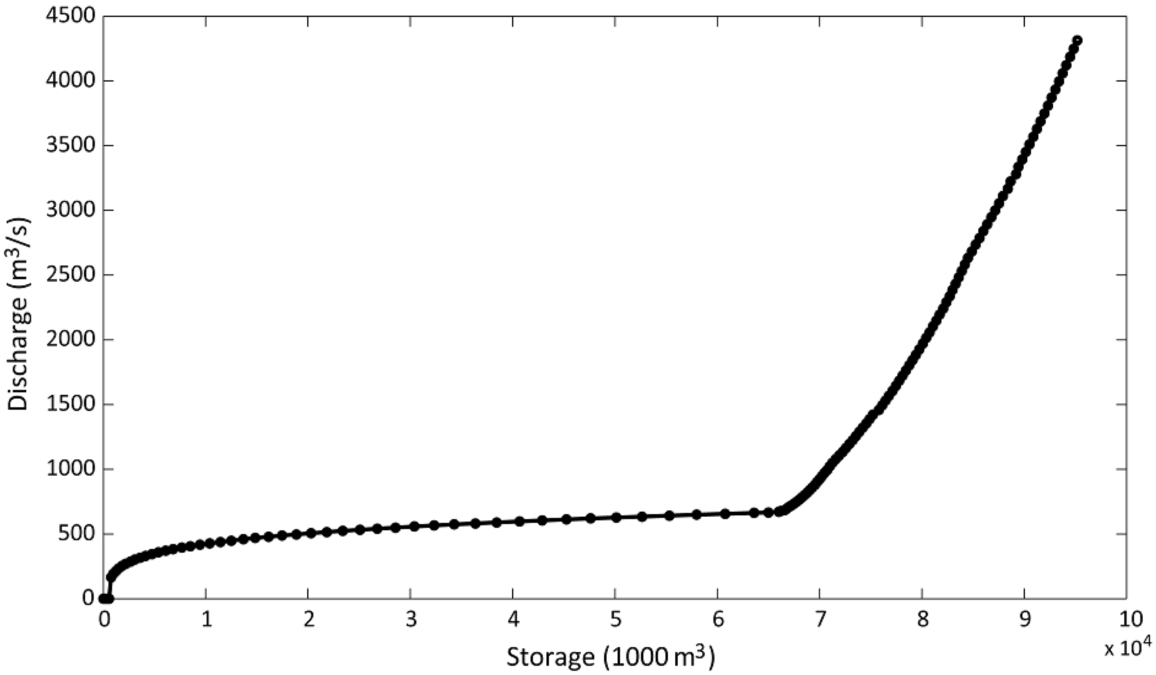

Figure 18. Discharge-storage function of the flood control structure Rompepicos.

CHAPTER 3

RESULTS AND DISCUSSION

This section is divided into 3 parts: First, the model calibration outcomes from both models and the confidence built upon these results. The calibration will then serve as a base case upon which a storm diagnosis will be carried out to evaluate the basin's response to the extreme event and distinguish the possible impacts that the inherent features of a semi or fully distributed model may have. Next, the intrinsic characteristics of the watershed are evaluated through the generation of spatially distributed state variables of the system such as runoff occurrence and soil moisture. Finally, an analysis of current and proposed additional hydraulic infrastructure and their impact on the peak discharge of the basin is presented to understand how they contribute to flood control.

3.1 MODEL CALIBRATION AND CONFIDENCE BUILDING

The calibration of the model was done using the limited information available from the basin's outlet and reported estimates by the National Water Commission (CONAGUA) at the Rompepicos Dam. The first point of calibration is the hydrological station Cadereyta II at the basin´s outlet. The data from this station is sparse and does not have a defined temporal output resolution, discharge estimates can vary from 1-hr up to 6-hrs in resolution. An important calibration value was the peak discharge at outlet given the uncertainty in the temporal resolution for inter-storm discharge values. A peak discharge of 4300 m^3/s was registered in the station. Given the size of the basin (>1800 km^2) it is preferred to have streamflow information at the interior of the basin. Due to the extreme nature of the event, streamflow gauges available were either destroyed or not operating adequately during the storm event, thus limiting the available options for interior calibration. Such is the case for the streamflow station Monterrey II located within the urban areas in the northern part of the watershed. The only other resource for calibration at an interior point of the basin is the water surface elevation at the Rompepicos Dam. CONAGUA reports indicated that the level at the reservoir reached approximately 904.05 MASL, 2.5 m below the crest of the spillway (Ramirez 2010). Using the elevation-discharge curve for the reservoir described in the methods section of this work, the maximum elevation reported corresponds to a peak discharge of 650 m^3/s.

Figure 19 shows the results of the manual calibration for both models at the outlet of the basin during the period of June 28^{th} to July 7^{th} 2010. It is evident at first look how there is an early peak in both the HEC-HMS and tRIBS as compared to the observed data. However this temporal lag can be attributed to the uncertainties had within the precipitation data. As described in the methods section for the Mean Field Bias Correction, the multiplicative factor was applied at a daily scale, which allowed the use of all available rain gauges in the basin, producing a more spatially representative data set. The mean areal precipitation from NLDAS was plotted in Figure 15 alongside an average rainfall time series from some of the automatic sub-hourly gauges to show the discrepancy in the rainfall products. An early spike can be seen for the NLDAS time series on June 30^{th} while the first high intensity rainfall from the automatic gauges is observed 14 hours later. The time difference between the observed peak discharge and the simulated peak discharges from both models is of 15 hrs.

Figure 20 shows the simulated results at the second point of calibration, the Rompepicos Dam at the site known as Corral de Palmas. It can be seen that both models follow similar trends in their response to the event reaching an incoming peak discharge of almost 1500 m^3/s. This amount of inflow translates into 650 m^3/s as outgoing discharge from the reservoir, which strongly agrees with official reports from the National Water Commission. Additionally, Figure 21 shows the cumulative discharge at the outlet for both models and the observed streamflow gauge at Cadereyta. It can be seen that there is a general good agreement in the simulations in terms of discharge volume, particularly in the tRIBS model. Table 5 outlines the statistical metrics of the two models compared to the measured streamflow at Cadereyta to assess model performance. The peak error (m^3/s) quantifies the difference between observed and simulated peak discharges. Consistent results were found in HEC-HMS with an error of 35.94 m^3/s and a slightly higher error in tRIBS with 251 m^3/s. However, the overall mean error (m^3/s), which represents the error between observed and simulated discharges over the entire period, was higher in HEC-HMS with 260 m^3/s and 103 m^3/s for tRIBS. This is expected as the tRIBS recession limb was longer as observed in Figure 19 and the cumulative discharge follows more closely as seen in Figure 21. The dimensionless correlation coefficient (*CC*) measures the linear relation of observed and simulated discharges and varies from -1 to 1, where *CC* = 0 would indicate no correlation. Correlation coefficients of 0.84 and 0.7 were computed for tRIBS and HEC-HMS respectively, this reveals the temporal shift discussed above cause by the uncertainty in the precipitation time series and further shown in the root mean square error (*RMSE*).

Table 5

Model performance metrics for simulations as compared to the observed discharge at the Cadereyta station. Metrics are defined following Vivoni et al. (2006). Peak Error [m^3/s] is the error between observed and simulated peak discharges, Mean Error [m^3/s] is the error between observed and simulated mean discharge over the entire period, CC [dimensionless] is the correlation coefficient, B [dimensionless] is the bias between the simulated and observed total runoff volume for the entire simulation, and RMSE [m^3/s] is the Root Mean Square Error.

Metric [unit]	**tRIBS**	**HEC-HMS**
Peak Error [m^3/s]	251.72	35.94
Mean Error [m^3/s]	103.15	260.73
CC [-]	0.84	0.70
B [-]	0.99	0.80
RMSE [m^3/s]	747.51	1011.06

The *RMSE* is measured in units of discharge and measures, on average, the closeness of a data point to a fitted line. Finally, the bias (*B*) is computed to show the correspondence between the mean observed and simulated runoff volume for the entire simulation where we see excellent agreement of 0.99 in tRIBS and a slight underestimation for HEC-HMS, as was shown in Figure 21.

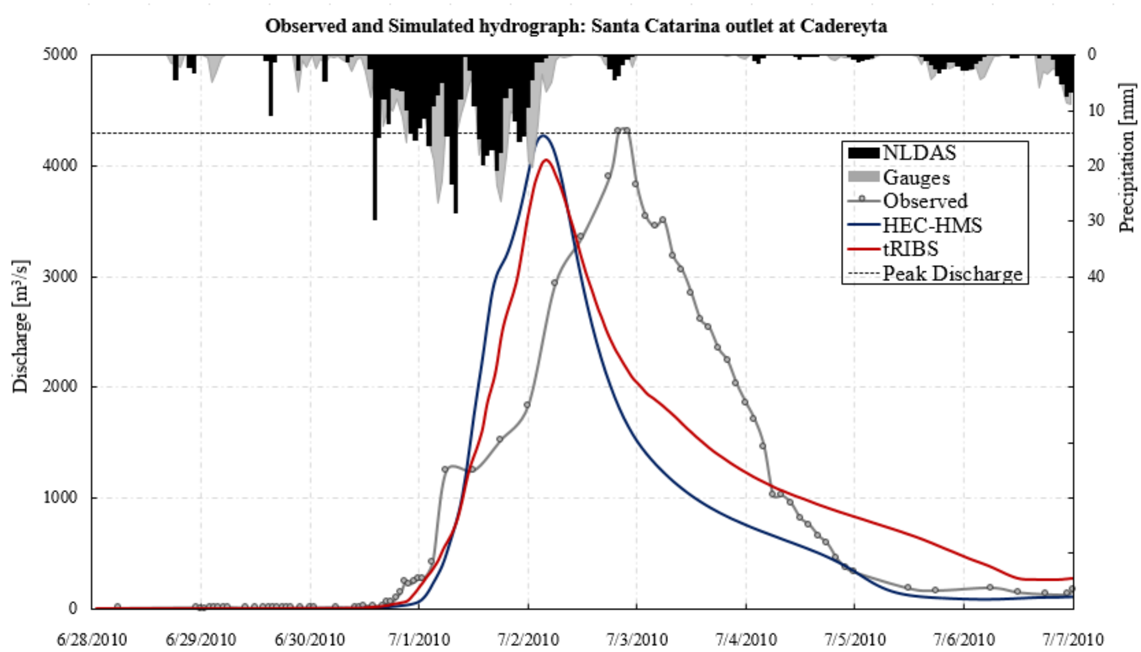

Figure 19. Results from the manual calibration showing the simulated and observed hydrographs at the first point of calibration: Cadereyta.

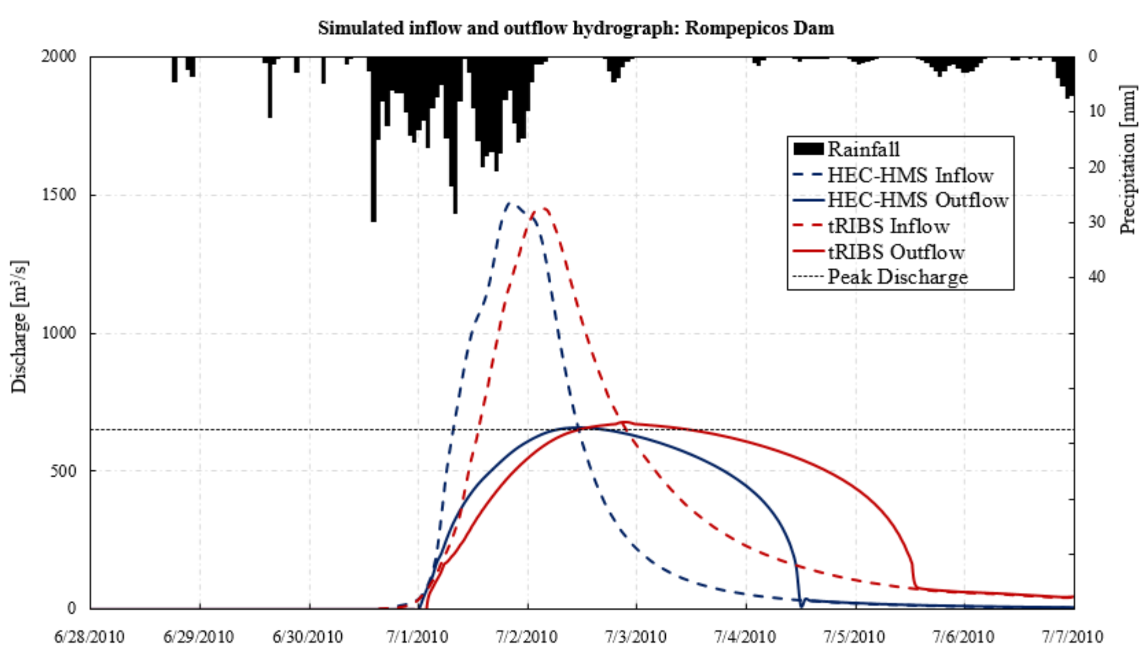

Figure 20. Results from the manual calibration showing the simulated and observed hydrographs at the second point of calibration: Rompepicos Dam.

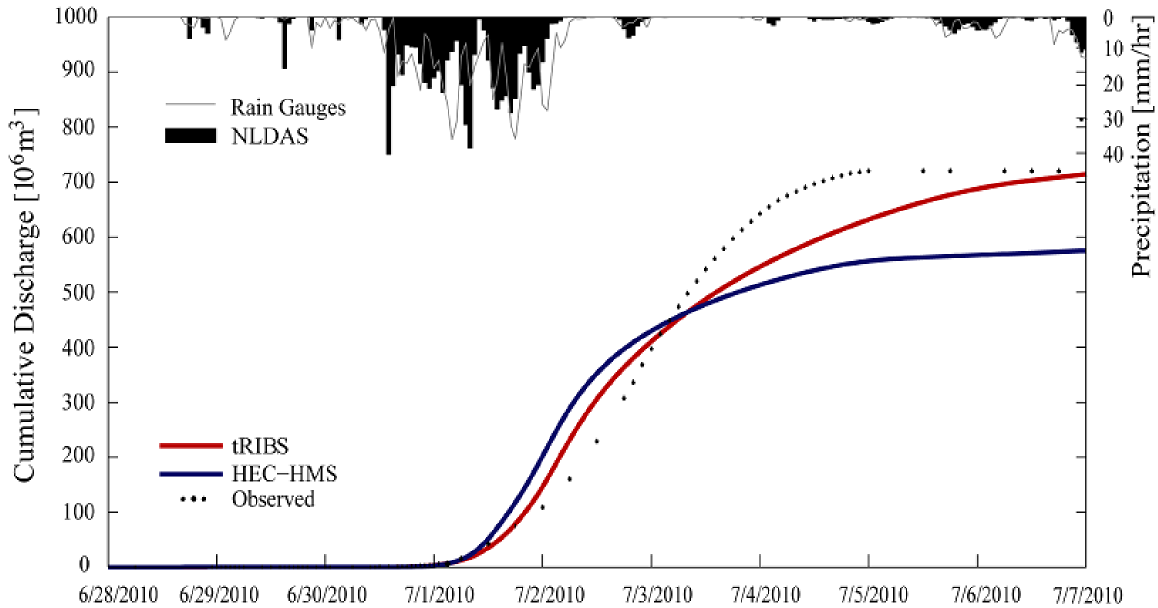

Figure 21. Cumulative discharge at the basin outlet (Cadereyta Station, in 10^6 m^3) from observations and model simulations along with the basin-averaged precipitation from rain gauges and the bias-corrected NLDAS fields.

An advantage of using a multi-model approach is the additional confidence obtained in the model results with the general good agreement between the two simulated discharge series. The agreement from both models in the response of the basin for the storm event adds value to the models' physical description of the landscape characteristics and soil properties, isolating the uncertainty introduced by the sparse rainfall gauging network. Table 3 contains the parameters for HEC-HMS used in the calibration of the Soil Moisture Accounting scheme and its corresponding routing and transformation methods. Likewise, Table 4 lists all of the parameters used for the calibration of the tRIBS model and their corresponding ranges for soil textures, land use, vegetation and routing values in the Santa Catarina Basin.

3.2 FLOOD EVENT DIAOGNOSIS

In order to determine the hydrological response of the basin to this extreme rainfall event, outflow hydrographs were generated at several points within the watershed. These points correspond to the junctions in the HEC-HMS model. These points were selected for comparison purposes. It is in these locations where it is possible to have discharge hydrographs from both models. In these points, the corresponding node from the Voronoi polygons at each location was selected to generate the discharge time series from the tRIBS model. In this way it is possible to see the evolution of the flood wave and determine the areas that contribute the most to runoff generation. There are a total of 31 Junctions, given this large amount of comparison points, the basin was divided into 3 large sub-units based on shared characteristics from the sub-basins as shown in Figure 22 and Figure 23. The first unit is determined by the hydraulic flood control structure Rompepicos. All contributing areas upstream from Rompepicos will be considered part of Unit 1 (yellow). The second unit (red) is determined by the areas upstream from the Entry to the City location. These areas are still dominated by natural landscape and high slopes as in the first unit, with the difference that runoff generated in this unit is uncontrolled discharge, meaning there is no flood control structure to regulate the flood wave. Finally the third unit (blue) will consider all areas downstream from the Entry to the City point. These areas encompass the urban impervious surfaces and the natural areas found here have milder slopes as compared to the rugged folded terrain found in the higher mountainous regions. The properties and land cover characteristics are presented for each unit in Table 6.

Table 6

Terrain properties and land cover characteristics for three units (Unit 1, 2 and 3).

Parameter [unit]		**Unit 1**	**Unit 2**	**Unit 3**
Area [km^2]		732	397	702
Elevation [m]	Mean	2108	1617	720
	Std. Dev	492	521	345
Slope [degrees]	Mean	26.94	26.51	11.42
	Std. Dev	12.59	13.82	12.73
Impervious Area [%]		0	0	44.6
Forested Area [%]		32.2	15.5	11.2
Hydraulic infrastructure		1	0	0

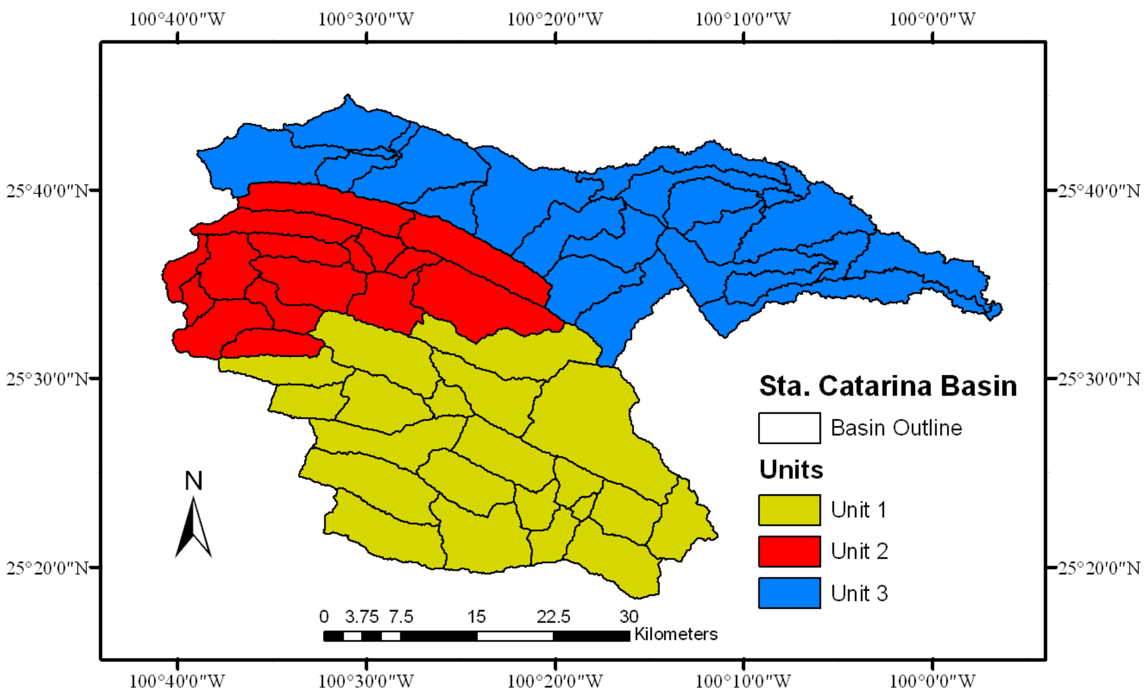

Figure 22. Colored Unit descriptors used to evaluate the response of the watershed.

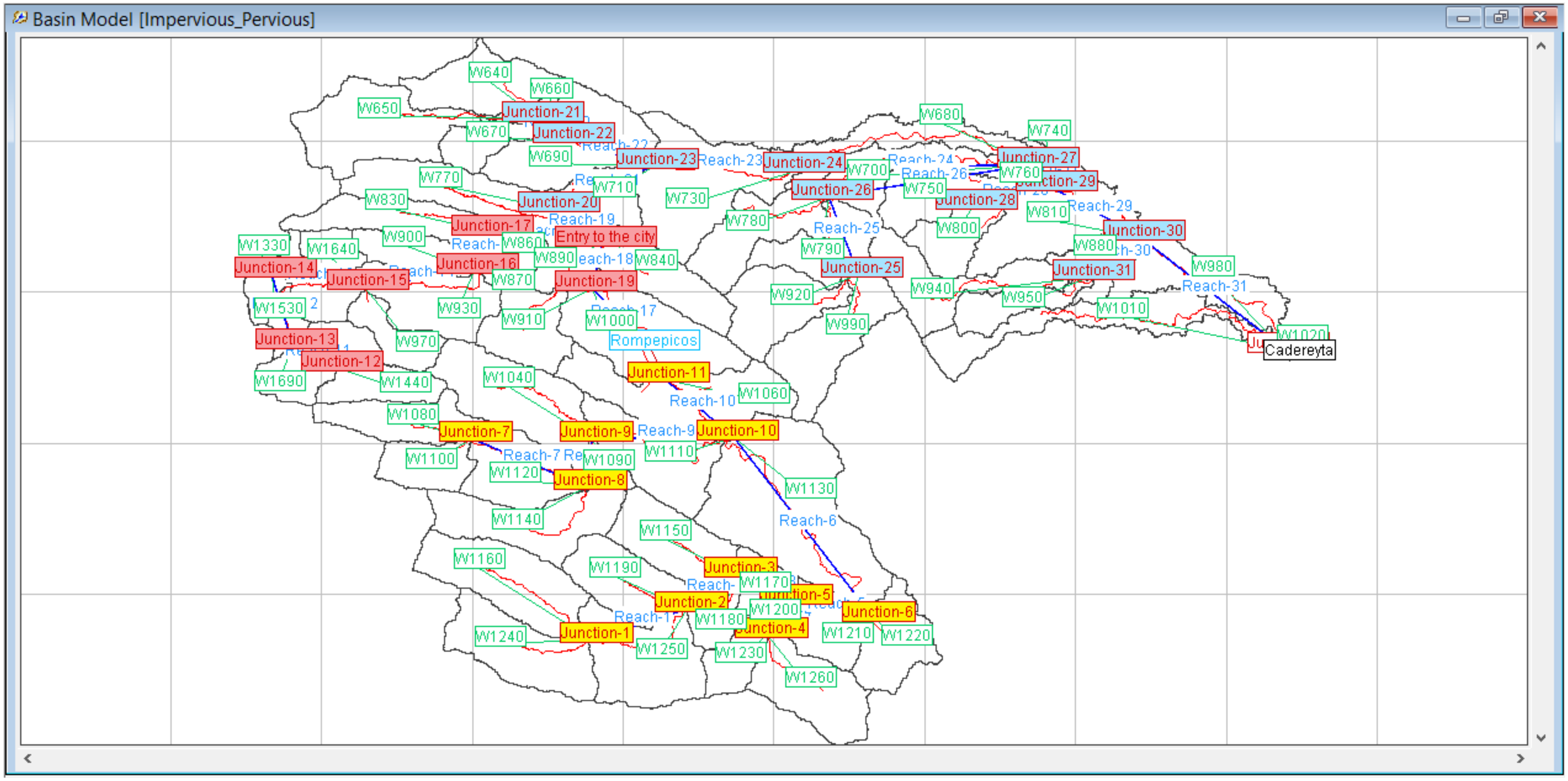

Figure 23. HEC-HMS model setup displaying the Junction and Sub-basin names to evaluate and their corresponding unit color.

Unit 1 contains Junctions 1 through 11 (hereafter referred to as J-1, J-2, etc.), with this last one being the last junction before reaching Rompepicos Dam. Figure 25a shows the discharge hydrograph from J-1. The contributing areas to this points are mainly composed of secondary shrub vegetation around Pine and Oak forest, characteristic vegetation of the highest points within the basin. The elevation of this point is the highest at approximately 3500 m above sea level. It has a contributing area of 98.54 km^2 (5.4% of the total area) from sub-basins W1160 and W1240, and corresponds to node 573872 in the voronoi polygon mesh. The HEC-HMS simulation shows a faster hydrological response with a quicker rise and higher peak discharge at approximately 200 m^3/s but with a fast recession as well. The tRIBS model shows a lower peak at 110 m^3/s but has a more prolonged recession. At J-2 (Figure 25b) HEC-HMS exhibits a similar response as in J-1 with a pronounced peak reaching discharges of 380 m^3/s while tRIBS starts to show some increase in the runoff contributions and still shows that same long recession tail as in the previous location. This is expected as the characteristics of the additional contributing areas to J-2 have the same secondary scrub vegetation for Pine-Oak forests. J-3 and J-5 (Figures 25c and 25e) have almost identical responses. The fast rise in HEC-HMS becomes more evident in these locations as the contributing area increases and more runoff is generated, while in the tRIBS simulations we can see the proportional growth in the recession limb. J-3 has a contributing area of 223 km^2 and J-5 has 293 km^2. At J-4, shown in Figure 25d, we find a similar case is in J-1, this hydrograph is a product of two small sub-basins and has a small contributing area of 52.8 km^2. Here we do not see the pronounced peak from HEC-HMS but this can be attributed to the small area and a lower slope in sub-basin W1260 which decreases quick runoff production. Further downstream J-6 (Figure 25f) can be found with a contributing area of 347 km^2 (19% of the total basin area). This junction can be considered a sub-unit of Unit 1 since it encompasses all areas in the most south-upper regions with very similar vegetation covers in the sub-basins upstream from J-6 and has not yet merged with contributions from Junctions 7-9, which contain different dominant vegetation covers in some of the sub-basins. J-6 summarizes well what was exhibited upstream, high, fast rises from HEC-HMS and prolonged recession limbs from tRIBS. Discharges are quickly becoming relevant in contributing for a flood hazard given that this area is only 19% of the total and from the cumulative precipitation map we know these areas were subjected to overall lower rainfall. Peak outflows area reaching approximately 550 to 700 m^3/s for tRIBS and HEC-HMS respectively.

At this point is important to remember the underlying equations in the rainfall-runoff transformation method for each model described in the Methods section, as they play a key role in the differences exhibited in the discharge hydrographs. Although both models share the same hydraulic routing method for channels in the form of the Kinematic Wave, the hydrological routing, or flow discharging into the stream network is distinct for each model. HEC-HMS uses the Kinematic Wave transform method. In this method the slope has an important role in the momentum equation within the overland-flow model and directly impacts flow generation.

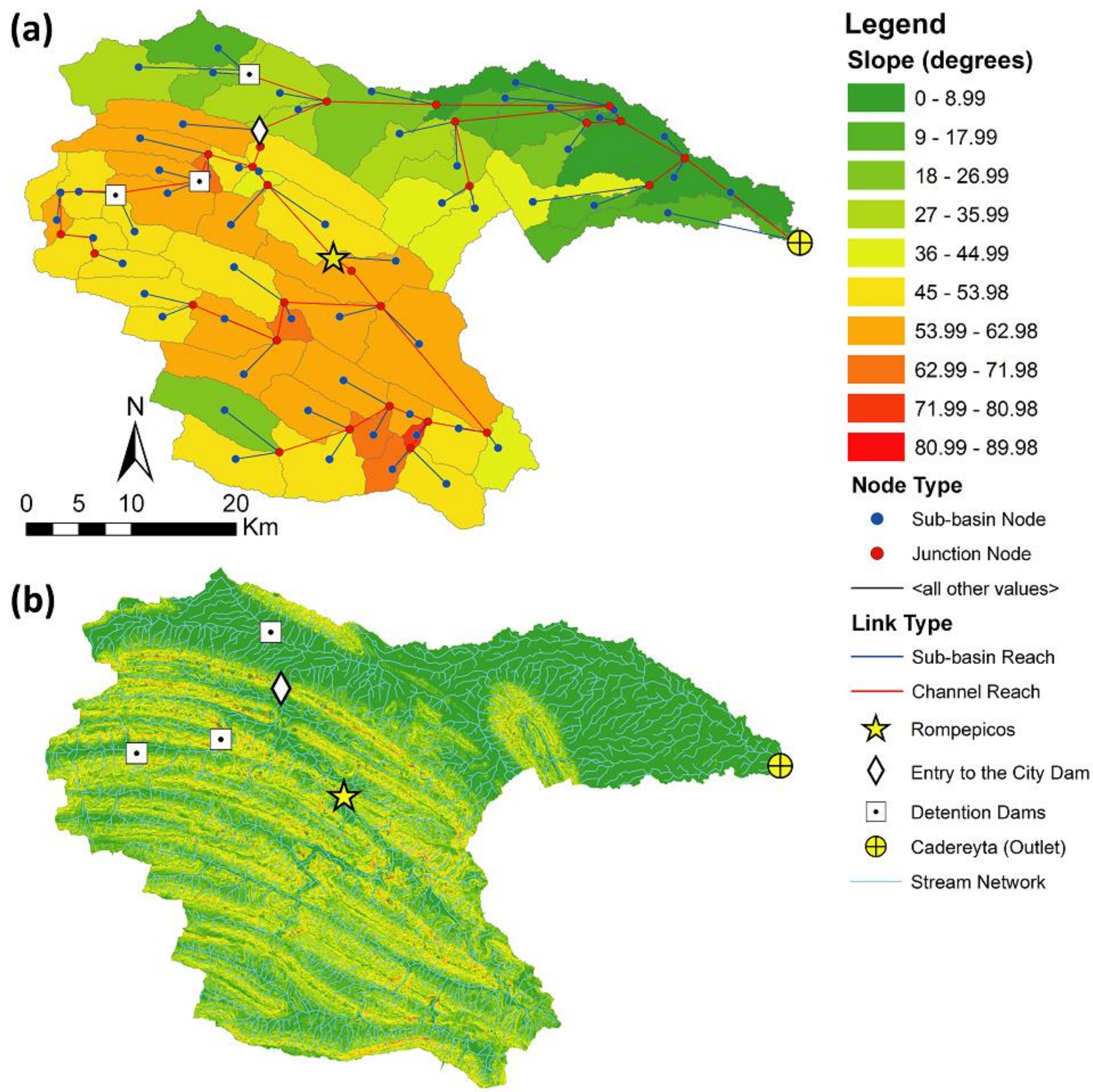

Figure 24. (a) HEC-HMS sub-basin definition with the mean aggregated slope for each sub-basin and schematic network representation. (b) tRIBS Voronoi polygon network with the slope field and the stream network captured in the model. Hydraulic infrastructure used in the simulations (Rompepicos Dam, Entry to the City Dam, Detention Dams) and the stream gauge at the basin outlet (Cadereyta Station) are displayed in each model representation

This region of the watershed has the most complex terrain with very high slopes, and given the lumped sub-basin properties within HEC-HMS, the slope is immediately susceptible to high discharges, thus the high peaks and fast recession seen in the HEC-HMS simulations. The spatial variation of the slope, derived from the DEM, represented in both models has a clear distinction as seen in Figure 24. The aggregated slope values over large areas or subbasins in HEC-HMS (Figure 24a) results in uniform high slope values that are used in the computations for the hydrological routing. Contrastingly, the representation of the basin through the thousands of Voronoi polygons assigns an individual slope value to each node and results in a more complete depiction of the conditions at the site (Figure 24b).

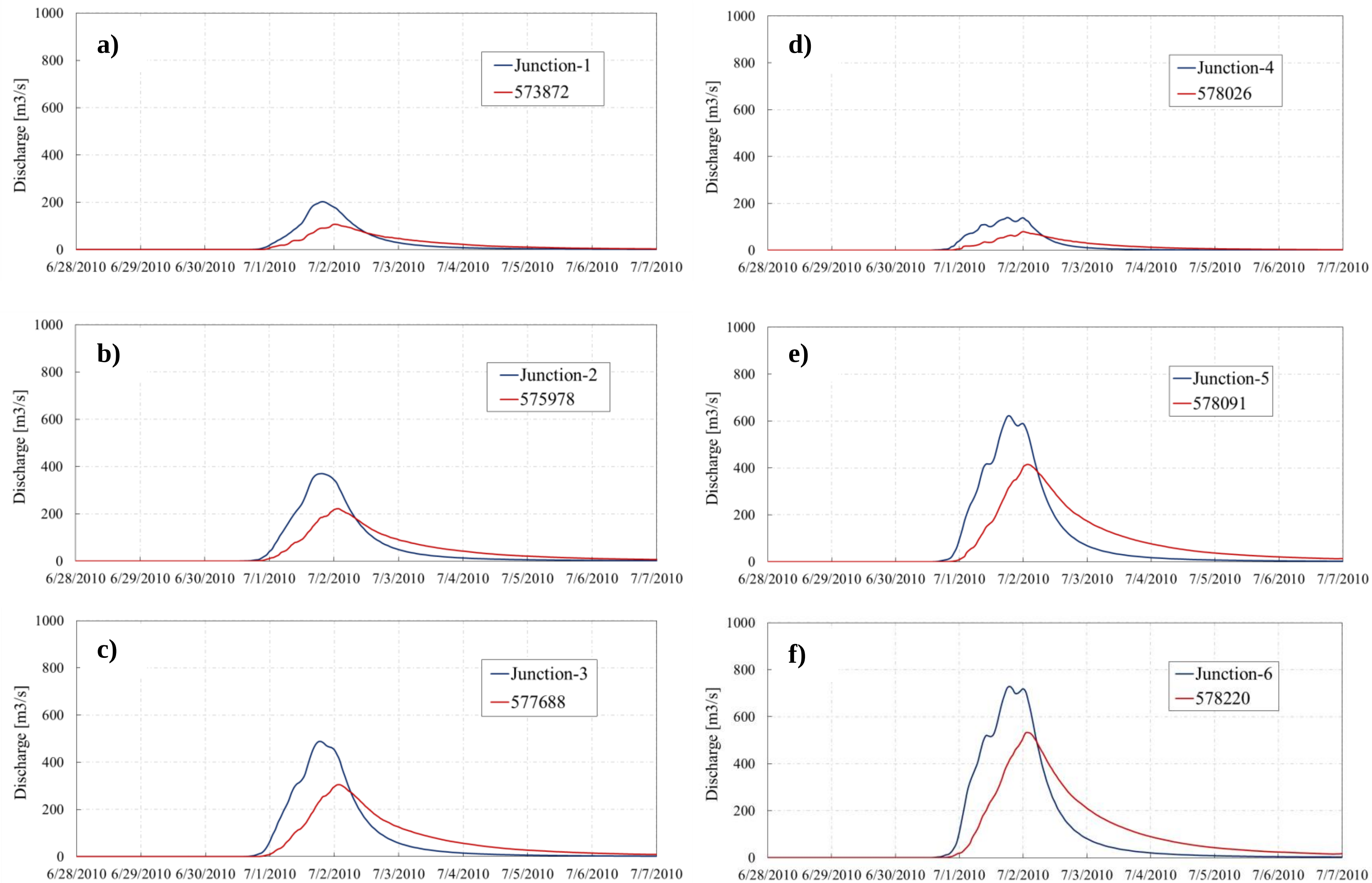

Figure 25. (a-f) Discharge hydrographs from HEC-HMS Junctions 1-6 (blue) and its corresponding node in tRIBS (red).

On the other hand we have a hillslope method in the tRIBS model that applies at a node scale, rather than at the sub-basin scale. As explained previously, this method determines the travel time of runoff between the hillslope node and an assigned outlet node with the hillslope velocity (Ivanov et al. 2004a). One of the sensitive parameters in the tRIBS model is the hillslope velocity coefficient (c_v), which is part of the velocity equation varying in space and time and determined through calibration. The averaged uniform high slope values might not be representative of the basin's response as slope is changing and decreasing as it reaches the channel, a property captured by the routing method in tRIBS, where each node has an elevation value representative of its location in the basin. The impact from these high slope values found in the upper HEC-HMS sub-basins will become more evident as further downstream units are evaluated.

Next we have what can be considered the second sub-unit within Unit 1 and begins at Junction-7 shown in Figure 26a. This location is the beginning of the second largest contributing area into the Rompepicos Dam. J-7 receives discharge from W1080 and W1100, sub-basins with very similar dominating vegetation as areas upstream from J-6, secondary pine forest shrubbery and pine forest. The contributing area for this location is 47.7 km^2. Although the runoff contributions are small at this point, we can see a better overall agreement between the two simulations while still maintaining similar characteristics discussed in previous locations: a slightly faster rise in HEC-HMS and longer recession limb in tRIBS. J-8 and J-9 showed in Figures 26b and 26c continue to have good agreement between the models with similar responses to the event. J-9, with a contributing area of 185 km^2 is the last junction before both sub-units from Unit 1 merge and is the first junction at which a different vegetative cover starts to be more dominant as lower elevations are reached. The dominant land cover in W1090, just upstream of J-9, is sub-mountainous shrubs. This vegetative cover is the most commonly found in the basin, and is also dominant in sub-basins W1130 and W1110 within Unit 1. The next location is J-10 (Figure 26d), an important location where streamflow from the two sub-units described above merge and serves as a close prelude to the amount of discharge going into the flood control structure. It can be seen that J-10 mirrors well the features from upstream hydrographs. J-1 to J-6 were characterized by sharp rises and higher peaks from HEC-HMS simulations while J-7 to J-9 had higher recession limbs from the tRIBS simulations and the peak discharges had better approximates between the models. This is reflected in J-10, where there is a fairly good agreement in the discharge hydrographs with a slightly higher peak discharge from HEC-HMS carried over from the higher sub-basins. Finally J-11, shown in Figure 26e, displays the discharge going into the Dam and with a contributing area of 732 km^2 (40% of the total basin area), it has a peak inflow into the reservoir of almost 1500 m^3/s. This amount of runoff generated in the higher regions of the basin is significant and the impact the Dam had in controlling this flood wave will be evaluated in next section. Unit 1 was characterized by quick rises in runoff generation that can become hazardous in a short amount of time if they continue uncontrolled due to the complex physical characteristics of the higher regions.

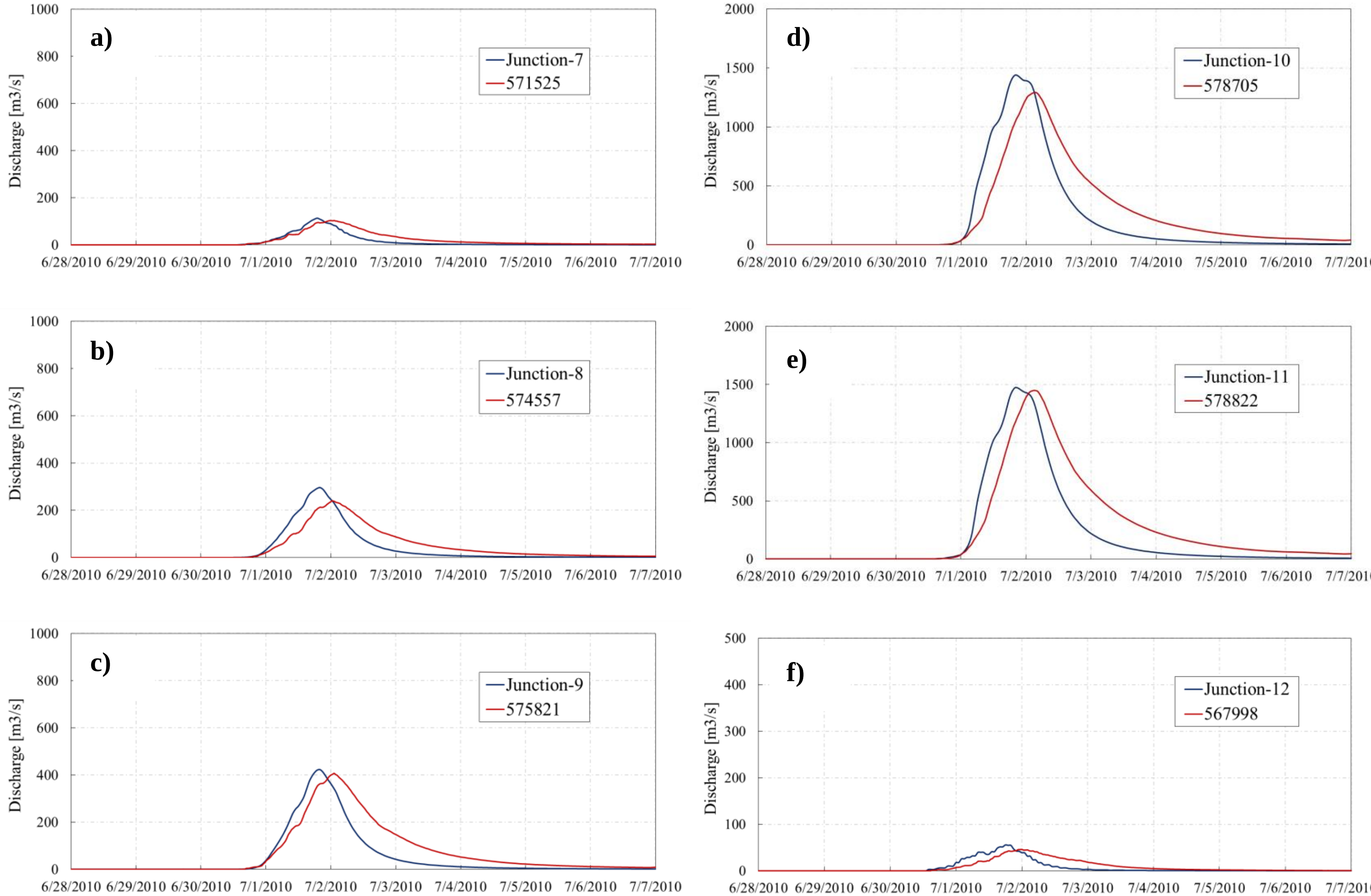

Figure 26. (a-f) Discharge hydrographs from HEC-HMS Junctions 7-12 (blue) and its corresponding node in tRIBS (red).

The next group of locations assessed categorized into Unit 2, share the characteristic of having the natural landscape in the mountainous region, but unlike Unit 1, the runoff generation from these sub-basins runs uncontrolled into the Entrance to the City. The assessment of this location becomes highly relevant to this research as the implementation of additional hydraulic infrastructure is part of the objectives and identifying the areas with higher discharge will aid in determining locations for these structures.

Unit 2 begins in the most western side of the watershed with the contributions from sub-basin W1440 into J-12 shown in Figure 26f. J-12 has the lowest contributing area receiving discharge from only one sub-basin with 20 km^2 (1.07% of the total area). This region is at a high elevation (> 2500 m) where it is common to find forested areas and the dominant cover here is pine forest. The hydrograph at J-12 has a very similar response to what is seen in J-7, and it is expected given their shared physical characteristics in elevation, slope and vegetative cover. The response pattern observed in Unit 1 continues to be observed in subsequent junctions in Unit 2. Figures 27a and 27b show the response for J-13 and J-14 with a faster rising limb from HEC-HMS and a slightly slower response but with a longer recession limb from tRIBS due to the previously discussed transformation method characteristics in each of the models. The response is very similar to what is observed in J-8 with peak discharges between 100 to 200 m^3/s. The evolution of the flood wave from J-15 to J-17 (Figures 27c, 27d and 27e) has the expected response to the rainfall event. Since these sub-basins are located within the upper mountainous region they can be compared to the areas with similar characteristics found in Unit 1 and observing the same pattern of response reinforces the discussion on the impact the different methods have in the hydrograph shape. A key location in Unit 2 is the Entrance to the City (E-C), located at Lon. -100.45, Lat. 25.648 at an elevation of 701 MASL. As the names suggests, the runoff at this point will go directly into the urban areas, where it is desired to have lower discharges to mitigate damages in the residential areas and transportation infrastructure (e.g. roads, bridges, etc.). The discharge hydrograph at this point, shown in Figure 27f, indicates a significant amount of runoff incoming from the mountainous regions. The peak discharge is comparable to what is received at the Rompepicos Dam with almost 1500 m^3/s with the critical difference that this amount of runoff will go on uncontrolled into the urban areas, making this site a potential candidate for a flood control structure.

The last set of locations evaluated belongs to Unit 3. It is expected to see a significant change in the response of the hydrographs given the drastic change in the physical landscape properties. The areas within this unit are located in the lower elevations, outside of the natural-mountainous landscape and have flatter open spaces with the urban cover having a significant presence in the region. Unit 3 carries, for the most part, discharges from Units 1 and 2 but there are still significant independent areas that contribute to runoff generation. When described as independent, it should be noted that this refers to the area as not having the main flood wave passing through the sub-basin or channel, but rather having their runoff merge downstream into the main path of the flood wave.

67

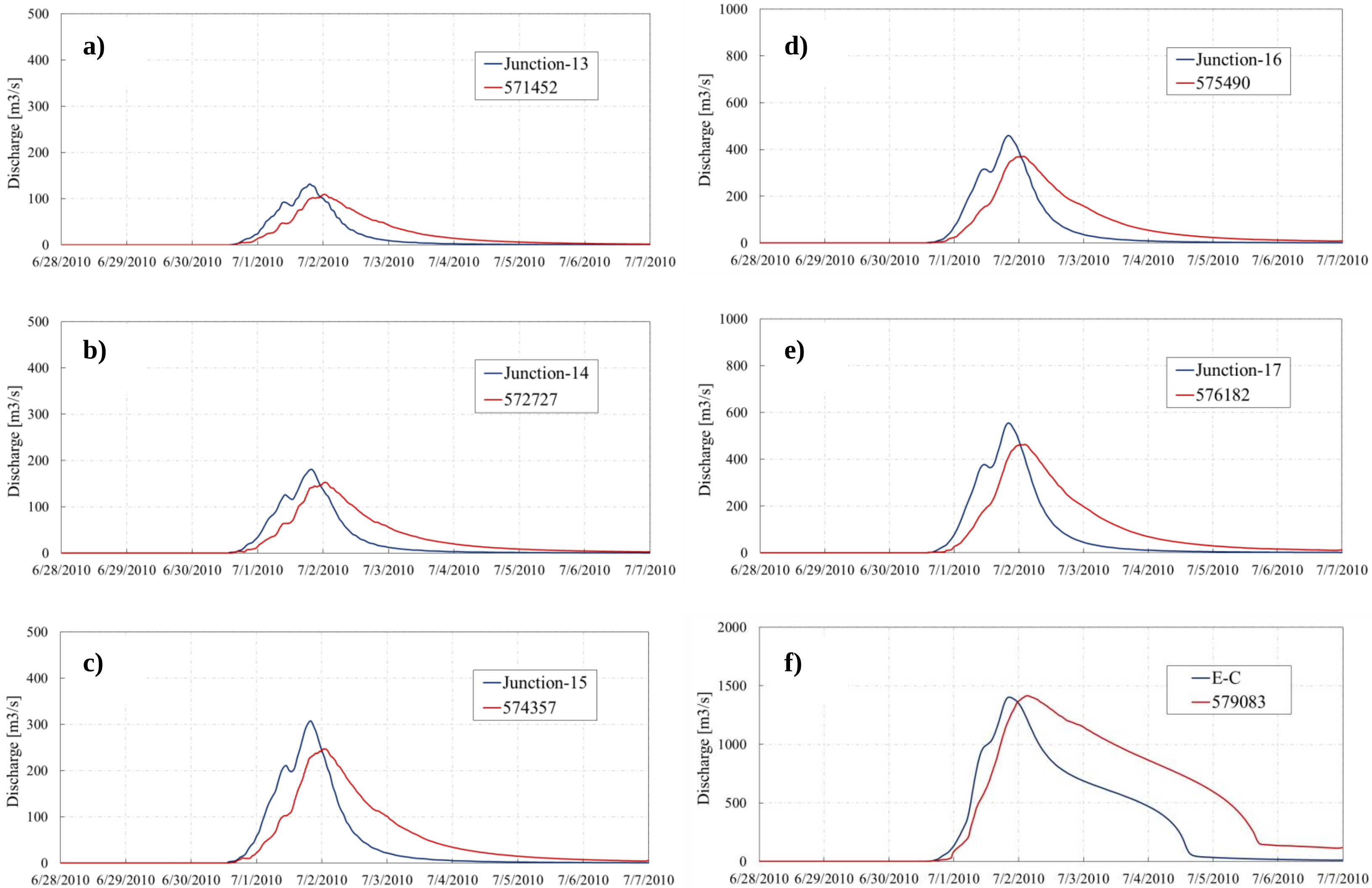

Figure 27. (a-f) Discharge hydrographs from HEC-HMS Junctions 13-17 and E-C (blue) and its corresponding node in tRIBS (red).

The first area with these characteristics can be found in the most north-western side of the basin. The area draining into J-22 shown in Figure 28d has almost identical responses from both models. The contributing area is significant with 106 km^2. The low slopes found within this region support the argument that the lumped slope values in HEC-HMS led to sharp rises in the hydrographs, as slopes become milder the response from the basin is seen to greatly agree between both models.

Moving further downstream into J-23 (Figure 28e) the discharges from Units 1 and 2 are present once again and merge with discharges from J-22. This point can be considered the division from the natural pervious surfaces into the highly dense urban areas with impervious surfaces. Although the E-C location divides the upper mountainous region from the lower planes, contributions from J-22 still contain dominant surfaces such as sub-mountainous shrubs and secondary shrubbery. It is at J-23 where the impervious surfaces become the main type of cover. The impacts from the milder slopes in the lower areas reflect a subtle difference in J-23 and J-24 (Figure 28f) as compared to what is observed at the E-C junction. The main contributions into J-23 and J-24 come from E-C, but the contributions coming from J-22 and sub-basin W690 show a good agreement between the simulations of both models, particularly in the recession limb and this had a positive, although slight, impact in both J-23 and J-24.

The second set of independent contributing areas can be found in the mid-east region of the basin upstream from J-25 and J-26, shown in Figures 29a and 29b. Sub-basins W920 and W990, contributing into J-25 have a natural landscape with mostly sub-mountainous shrub vegetation as most of the areas fall outside the urban delimitations.

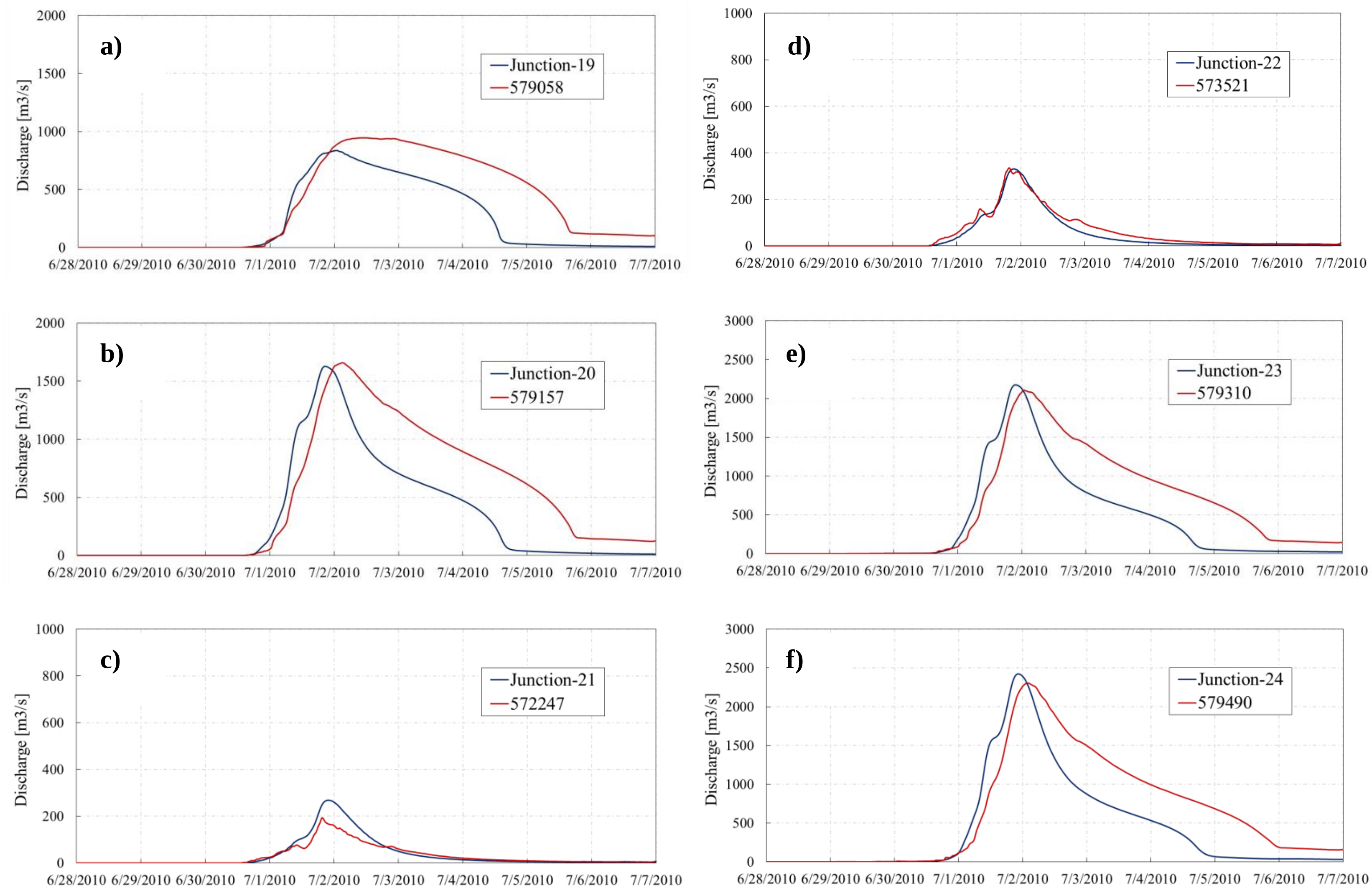

Figure 28. (a-f) Discharge hydrographs from HEC-HMS Junctions 19-24 (blue) and its corresponding node in tRIBS (red).

There is very good agreement found between both simulations with peak discharges of approximately 300 m^3/s. This good agreement in the discharge hydrographs is carried onto J-26 where the additional contributing sub-basins W780 and W790 have dominant impervious surfaces. The upstream contributing area from J-26 is of 139 km^2 (7.6% of the total area) but has a significant contribution with peak discharges at almost 600 m^3/s. This peak is significantly larger as compared to other areas with similar areal extension. Such cases include J-8 (124 km^2), J-2 (172 km^2) and J-16 (170 km^2) but none of these go above 500 m^3/s. As the flood wave travels downstream into J-27 (Figure 29c), J-29 (Figure 29e) and J-30 (Figure 29f) the similarity in the response from both models increases. The greatest change in the hydrograph comes in the notable increase in the peak discharge. The difference in contributing area from J-24 to J-30 is less than 300 km^2 but such increases in runoff is mainly attributed to the contributions from the urbanized areas and highly impervious surfaces. In this path the peak discharge increases almost 1500 m^3/s from approximately 2500 m^3/s at J-24 to almost 4000 m^3/s at J-30. This represents a growth of 22% in contributing area but an increase of approximately 60% in runoff. Finally the last areas contributing to runoff generation before reaching the basin outlet are sub-basins W940 and W950, draining into J-31, displayed in Figure 30. Sub-basin W940 has dominant sub-mountainous shrub vegetation, but sub-basin W950 is the only area where temporal annual agricultural lands are the dominant land cover. The discharge hydrographs from this location show very good agreement, as has been the case for areas in the lower region and mild slopes.

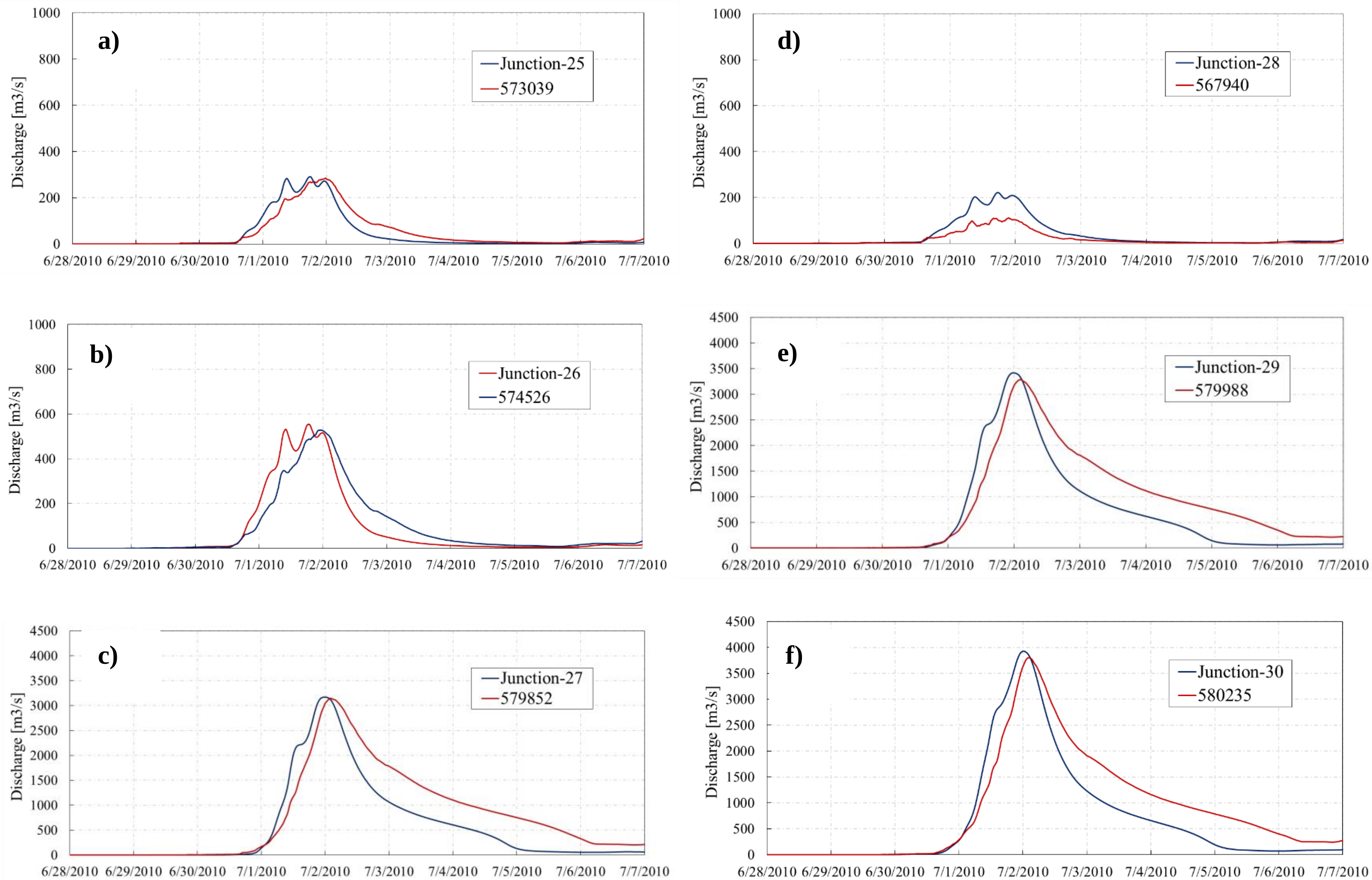

Figure 29. (a-f) Discharge hydrographs from HEC-HMS Junctions 25-30 (blue) and its corresponding node in tRIBS (red).

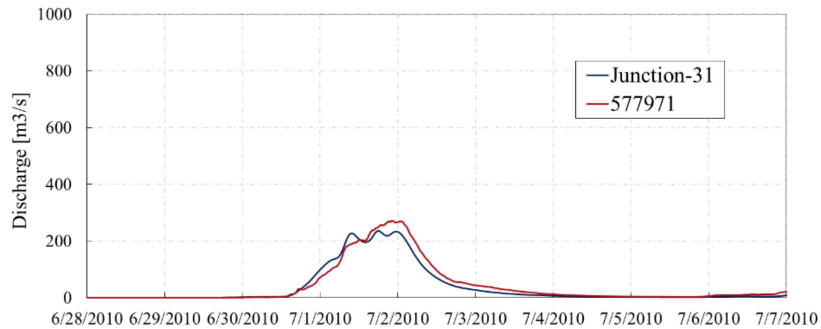

Figure 30. Discharge hydrograph from HEC-HMS Junction 31 (blue) and its corresponding node in tRIBS (red).

The patterns and model responses within each unit are summarized in Figure 31 and Table 7. The sharp increases in HEC-HMS due to higher aggregated slope values and longer recession in tRIBS can be observed at Site I in Unit 1 (Figure 31b) and reflected in the streamflow characteristics with a peak discharge of 533 m^3/s in tRIBS and 728 m^3/s for HEC-HMS. These differences in response can also be exposed by their time lag (hr), defined as the time between the centroid (50% accumulation time of rainfall for the main event) and the flood peak time. At Site I, HEC-HMS had 10.92 hrs. lag while tRIBS had 17.92 hrs. Similar responses are observed at Site II within Unit 2 (Figure 31c) where the natural landscape is still dominant and high slopes within the mountainous regions are a common feature. Finally, Unit 3 was shown to have higher similarities between the simulations due to the milder slopes found here as seen at Site III (Figure 31d) and supported by their similar lag times (12.92 hrs. and 11.49) and peak discharges (330.6 m^3/s and 335.4 m^3/s) for HEC-HMS and tRIBS respectively.

Table 7.

Streamflow characteristics at locations for interior sites, along the main channel and the basin outlet.

Location	Model	Peak Discharge [m^3/s]	Time Lag [hr]	Volume [10^6 m^3]
Interior Sites				
Site I	tRIBS	533	17.42	75.49
	HEC-HMS	728.9	10.92	77.16
Site II	tRIBS	247	17.30	34.54
	HEC-HMS	307.4	11.92	27.41
Site III	tRIBS	335.4	11.49	39.61
	HEC-HMS	330.6	12.92	32.16
Main Channel				
Site A	tRIBS	1449	18.86	202.87
	HEC-HMS	1473	11.92	154.89
Site B	tRIBS	1415	19.11	360.51
	HEC-HMS	1401	12.92	231.16
Site C	tRIBS	2104	16.86	457.29
	HEC-HMS	2174	13.92	308.03
Site D	tRIBS	3803	18.11	685.16
	HEC-HMS	3927	15.92	530.94
Outlet	tRIBS	4059	18.92	714.60
	HEC-HMS	4274	16.92	575.06

The significant contribution from the urban areas in the increase of the peak discharge can also be observed in Figure 32 and Table 7 where the hydrological response at different locations along the main channel reveal the considerable change in runoff after the urban areas at Site D (J-30). It is also to notice the changes in time lag along the main channel and how they become closer in both models as they approach the outlet.

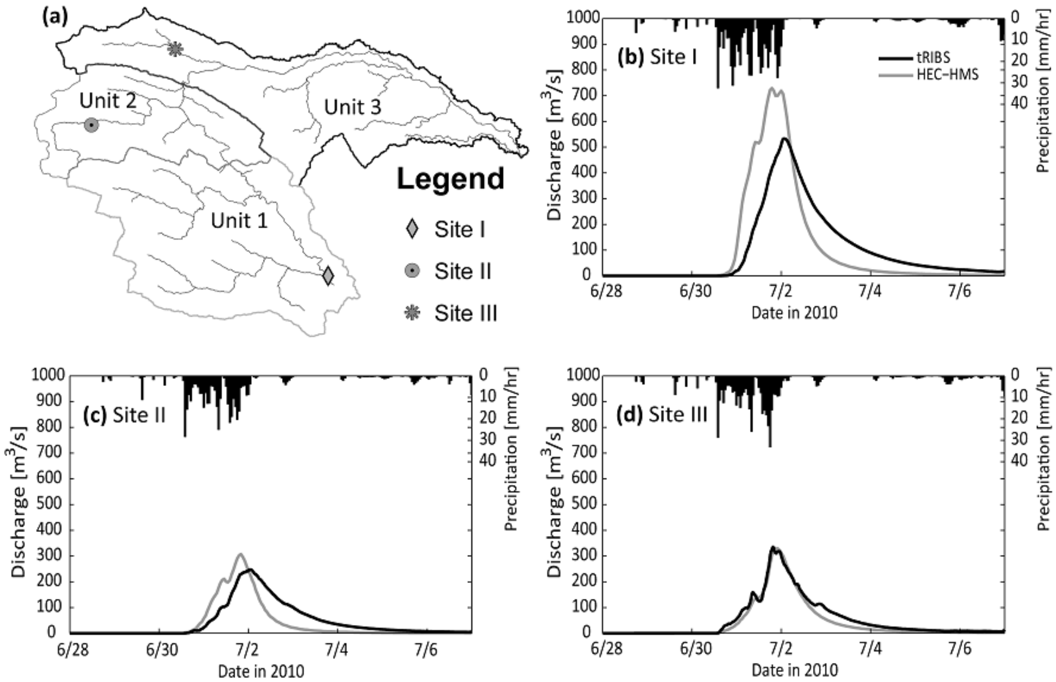

Figure 31. Comparison of the hydrologic responses from HEC-HMS and tRIBS at the three internal sites shown in (a) along with hourly precipitation upstream of each location: (b) Site I located in Unit 1, (c) Site II located in Unit 2, and (d) Site III in Unit 3.

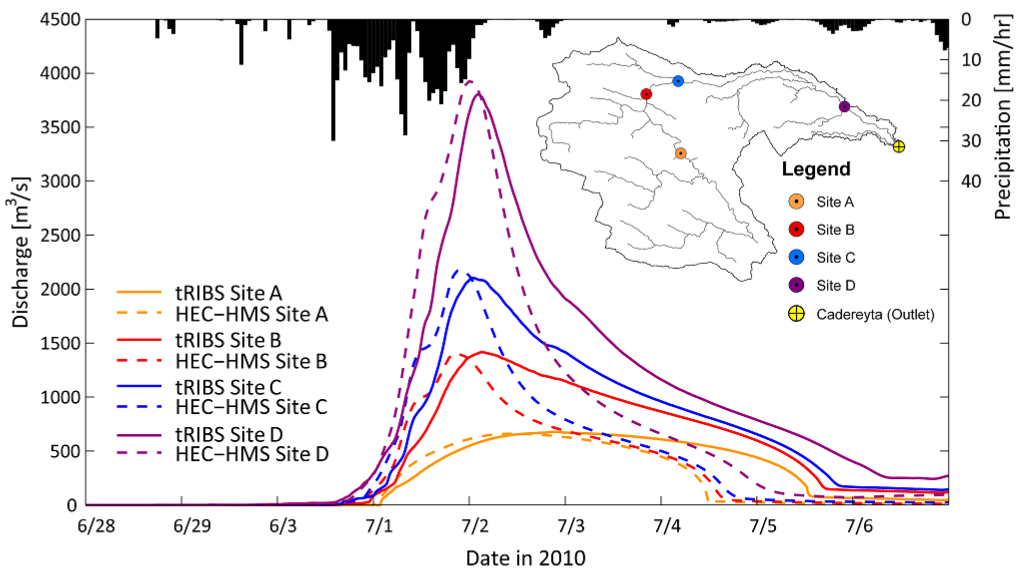

Figure 32. Comparison of the hydrologic responses from HEC-HMS and tRIBS at the four locations along the main channel as shown in the inset along with hourly basin-averaged precipitation. Site A is the outflow from Rompepicos Dam, Site B is at the Entry to the City, Site C is upstream of the urban area and Site D is downstream of the urban area.

3.3 SPATIAL DISTRIBUTION OF THE FLOOD EVENT

Hornberger and Boyer (1995) have emphasized the need to consider spatial variability and scaling in hydrology, an important advantage of using fully-distributed models is the possibility to display internal basin dynamics and obtain spatial fields of the state variables of the system (Ivanov et al. 2004a). Physical characteristics of the basin such as topographic features and soil properties determine the hydrological response of the catchment to rainfall events. Parameters and hydrological processes within models that control the watershed response operate at different space and timescales (Singh and Woolhiser 2002). It is important to understand this response in order to identify the main driving factors in runoff contribution and areas of high wetness. Time-integrated basin state variables can serve as a useful representation of the intrinsic features of the catchment (Ivanov et al. 2004b). As it has been described previously, the Santa Catarina River basin has a complex topographic setting. The occurrence and frequency of runoff generation on such complex terrains relies on the meteorological variables like climate and rainfall in addition to its own physical descriptors (e.g. basin topography and soils) (Vivoni et al. 2007). On such variable topography, small-scale topographic changes can affect groundwater recharge and streamflow. Similarly, spatial variations in vegetation can affect infiltration and surface runoff (Seyfried and Wilcox 1995; Milly and Eagleson 1988). This does not mean a simplified method in hydrological modeling is not sufficient, model simplification is justified as long as essential performance is retained (Morel-Seytoux 1988).

The total runoff production from the event can be observed in Figure 33a for HEC-HMS and in Figure 33b for tRIBS. Similar patterns are observed on both simulations with an explicit representation of the spatial distribution of runoff production from the fully-distributed model. The variations in soil properties will invariably cause the discrepancies in runoff generation as more variability in the catchments infiltration properties are captured in tRIBS. This is supported with studies by Smith and Hebbert (1979) , Sivapalan and Wood (1986) and Woolhiser and Goodrich (1988) where spatially variable soil properties, as opposed to lumped or averaged properties revealed differences in the infiltration rate, therefore on runoff production. The higher runoff generation rates occur in the north-east areas where the higher precipitation totals occurred. We can see the critical difference in evaluating spatial output from a fully-distributed model and a semi-distributed one. Coarsening of catchment data leads to an unavoidable loss of information and spatially detailed hydrological dynamics are limited in their interpretation (Ivanov et al. 2004a). The use of the spatially explicit information generated from the fully-distributed model can serve to inform coarser models to identify controls on runoff generation and identify wet areas within a catchment. This research uses the spatial basin dynamics generated from tRIBS in combination with the storm diagnosis to identify potential locations for additional infrastructure to be implemented in both models.

Figure 33d displays a high-resolution map of the spatially distributed runoff occurrence due to saturation excess conditions. The percent occurrence is based on the frequency over the total run time of 225 hours (9 days). This state suggests that the bottom wetting front in the soil profile has reached the water table level and the top moisture front is located at the surface. The infiltration capacity when this state is reached becomes null and additional incoming precipitation is directly converted into runoff. The saturation excess runoff occurrence in Figure 33d is directly related to its intrinsic properties. The highest frequency areas correspond to mildly sloped regions in the north where lateral redistribution of soil moisture is less efficient. Further, these areas hold significant infiltration rates that promote a faster saturation of the soil profile. With less frequency, although with relevance in understanding the response from the basin, it is shown that the topographic attributes contribute to the generation of saturation runoff. This is evident in the junctions of topographic forms found in the higher south regions. The low saturation occurrence in the mountainous region is expected as the high slopes promote lateral soil moisture redistribution efficiently, inhibiting the saturation of the soil profile (Ivanov et al. 2004a). It is also important to note the good representation of the urban areas in northern areas of the catchment. The very low infiltration rates from urban surfaces prevent the saturation of the subsurface.

The next runoff mechanism considered is the Hortonian runoff type, also referred to as infiltration excess runoff (Ivanov et al. 2004a). This runoff mechanism is characterized by having the infiltration rate capacity of the top surface layer exceeded by the rainfall intensity or an immediate saturation of top of the soil profile caused by insufficient redistribution of moisture. The frequency of infiltration excess runoff in the basin can be seen in Figure 33c. As expected, the urban areas in the north yield the highest occurrence of infiltration excess due to their highly impermeable surfaces that prevent adequate redistribution of moisture. The mountainous regions in the south, characterized by the dominant steep slopes, contain significant occurrence of this type of runoff mechanism. It is also evident the impact of the rainfall distribution in the watershed. Lower rainfall rates were perceived in the south-west regions of the basin and are reflected in the frequency of runoff occurrence. Even at small scales, spatial variability of rainfall can have significant impact on simulated infiltration excess runoff (Faurés et al. 1995).

The results from these runoff mechanisms are consistent with what can be observed in the time-averaged saturation fraction in HEC-HMS (Figure 34a) and the soil moisture profiles in the root zone layer of 1 m shown in Figure 34b where higher moisture in the areas susceptible to saturated conditions is observed. It is important to note that HEC-HMS computes a saturation fraction, which indicates how much of the soil layers capacity has been occupied, this is solely based on the soil storage capacity in the soil moisture accounting method and is specified as a calibration parameter. Conversely, tRIBS displays soil moisture based on the 1 m soil profile, a profile uniform in depth but varying according to the topography. Soil moisture distribution can also be observed to vary according to topographic and land cover properties. Flatter areas within what was described as Unit 3 have the highest moisture contents due to the inefficient moisture distribution in low sloped areas. However, urbanized conditions within this region cause some of the lowest soil moisture values due to the impervious surfaces. This is consistent with what was revealed in the storm diagnosis, where urban areas significantly increased the runoff production, despite having relatively small increase in contributing area.

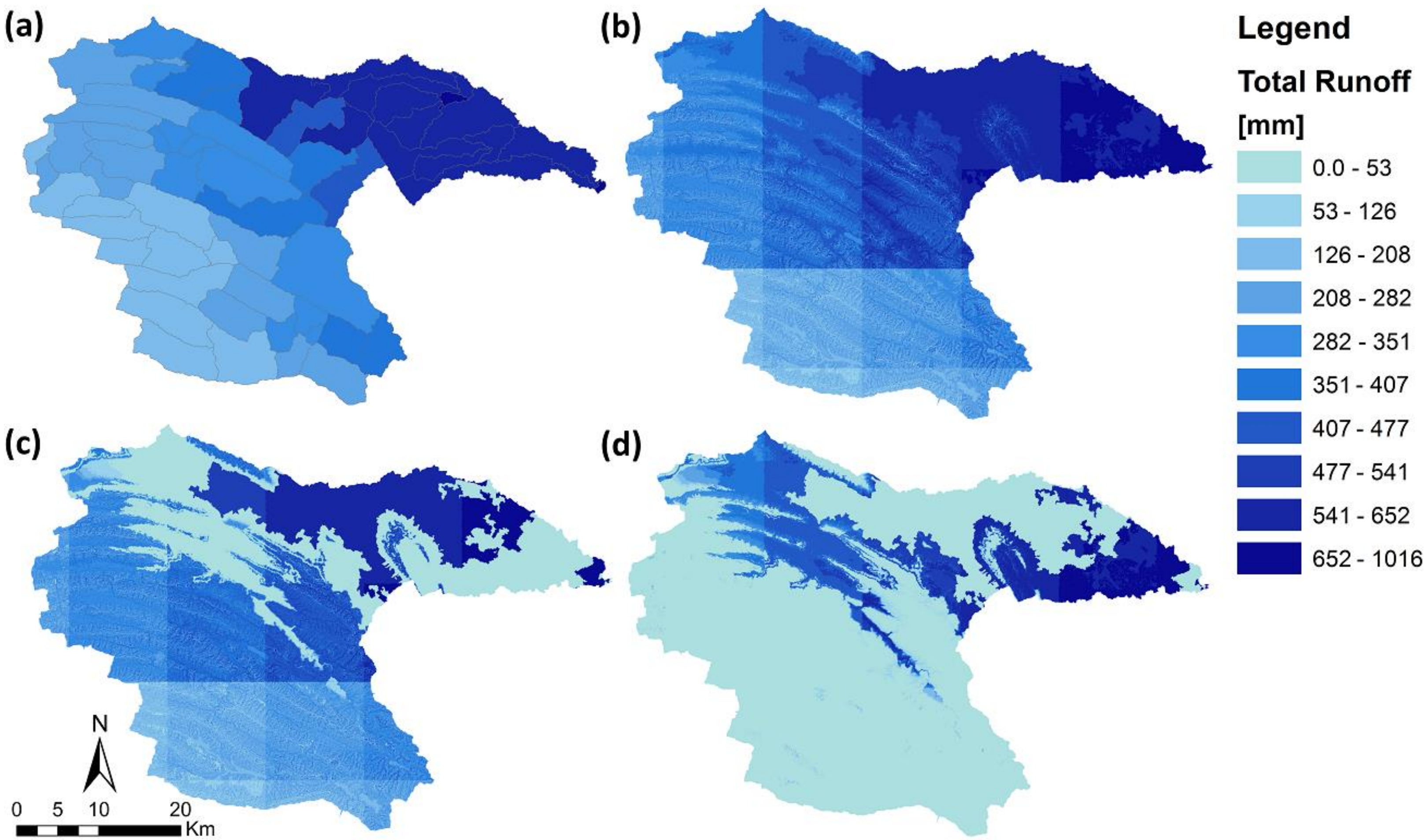

Figure 33. Spatial distribution of the total runoff (mm) generated during the simulation period from (a) HEC-HMS and (b) tRIBS. Spatial distribution of the runoff (mm) generated from the infiltration-excess (c) and the saturation-excess (d) mechanisms simulated in tRIBS.

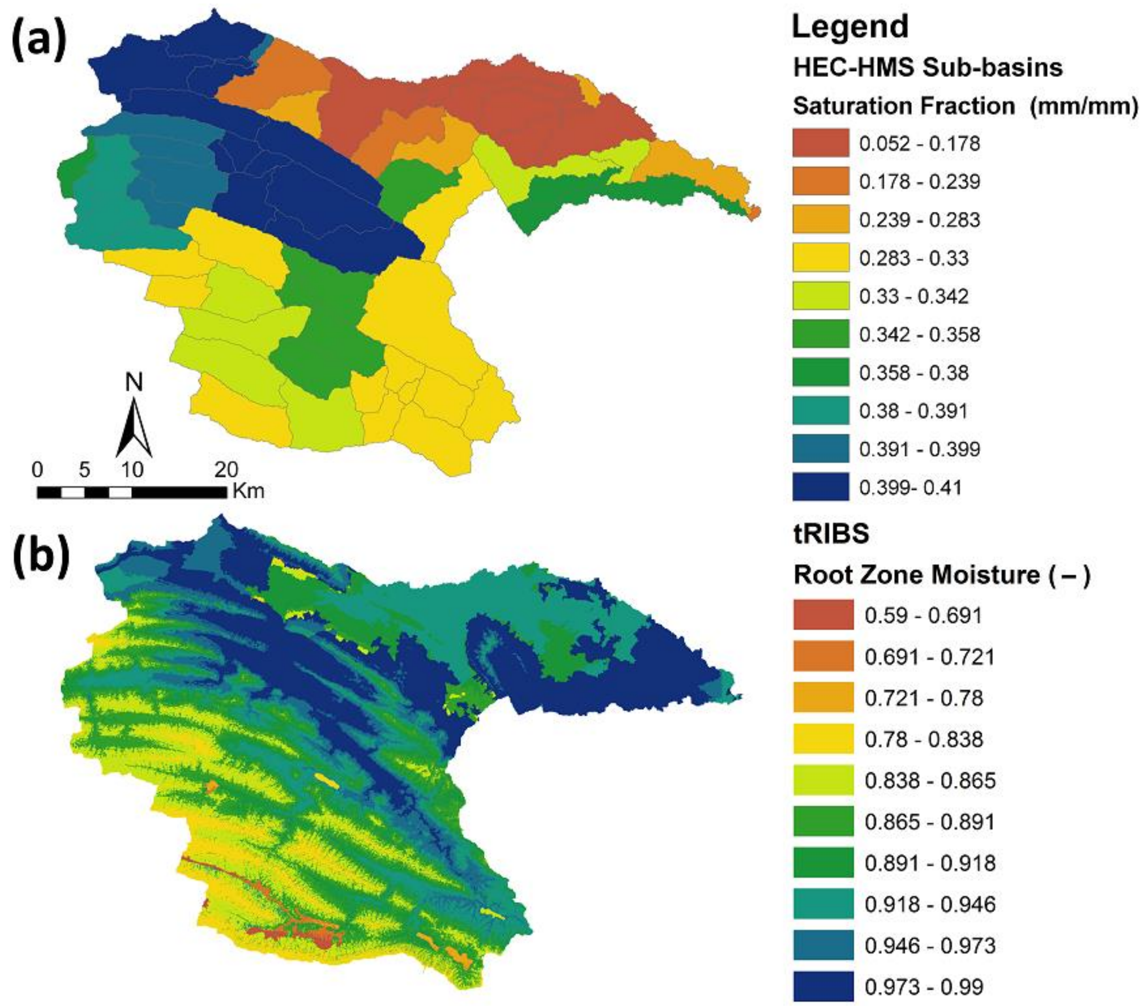

Figure 34. (a) Time-averaged saturation fraction distribution in the watershed for HEC-HMS. (b) Time-average Root Zone Moisture spatial distribution in the top 1 m for tRIBS.

3.4 HYDRAULIC INFRASTRUCTURE SCENARIOS

This section of the study aims to assess the hydrological impact of current and potential hydraulic infrastructure implemented in the watershed by determining peak discharge mitigation at key locations within the basin. The analysis is divided into 3 main categories: 1) Evaluation of current structures (i.e. Rompepicos Dam), 2) inclusion of an additional Dam at the Entry to the City Junction and 3) inclusion of three small detention basins at locations producing uncontrolled discharge (i.e. discharges not passing through Rompepicos).

3.4.1 Current infrastructure The Rompepicos Dam (Figure 35) is often locally misunderstood in its purpose as a flood control structure given the ephemeral nature of the channels going through it and can be seen non-operational most of the time, frequently leading to question the value of its construction. It is in extreme events like Hurricane Alex where the reservoir can exhibit its role and significance as a flood hazard control. The scenario to assess the impact of the existing infrastructure consisted of removing the dam from both models. In HEC-HMS the stream network was disconnected from the reservoir and reaches discharging into the Junction upstream from Rompepicos were directly routed into the next connecting sub-basin. In the tRIBS model the Reservoir Routing option was disabled so any nodes assigned with reservoir characteristics are now ignored and routed normally.

In this analysis all locations upstream from the structure will not be considered as all discharges generated in the upper basin remain unchanged regardless of the structures present. These areas include all Junctions within Unit 1 described in the storm diagnosis section. The locations of interest will include points downstream through which the flood wave passing through the location of the dam can be tracked until it reaches the outlet point of the basin. The first point corresponds to the dam's location, now removed from the simulations. The simulated hydrograph from both models shown in Figure 36a is very similar to the manual calibration in Figure 20 but with an important difference: the discharge of almost 1500 m^3/s is now outflow from this point rather than inflow into the reservoir. The impact from the structure is observed immediately here as now a flood wave with a peak discharge 230% larger than the previous 650 m^3/s is flowing downstream into the city. As expected, the impact is reflected at downstream locations, such as J-19 in Figure 36b just before reaching the Entry to the City. It is at the Entry to the City (E-C) shown in Figure 36c where Rompepicos exhibits its mitigation effect during the storm event. With the structure in place there was still a considerable amount of discharge incoming into the city with a peak at ~1400 m^3/s but without it a potential discharge of almost 2300 m^3/s could have carried devastating effects into the urban areas. This peak is further increased up to almost 3000 m^3/s at Junction-23 shown in Figure 36d, where the density of urban areas is intensified and marks a partition between the city and the natural landscape. Moving further downstream into J-30 the effects of the reservoir can still be observed in the simulated hydrographs shown in Figure 36e, although contributions from the impervious surfaces in the city at this point slightly dissipate the

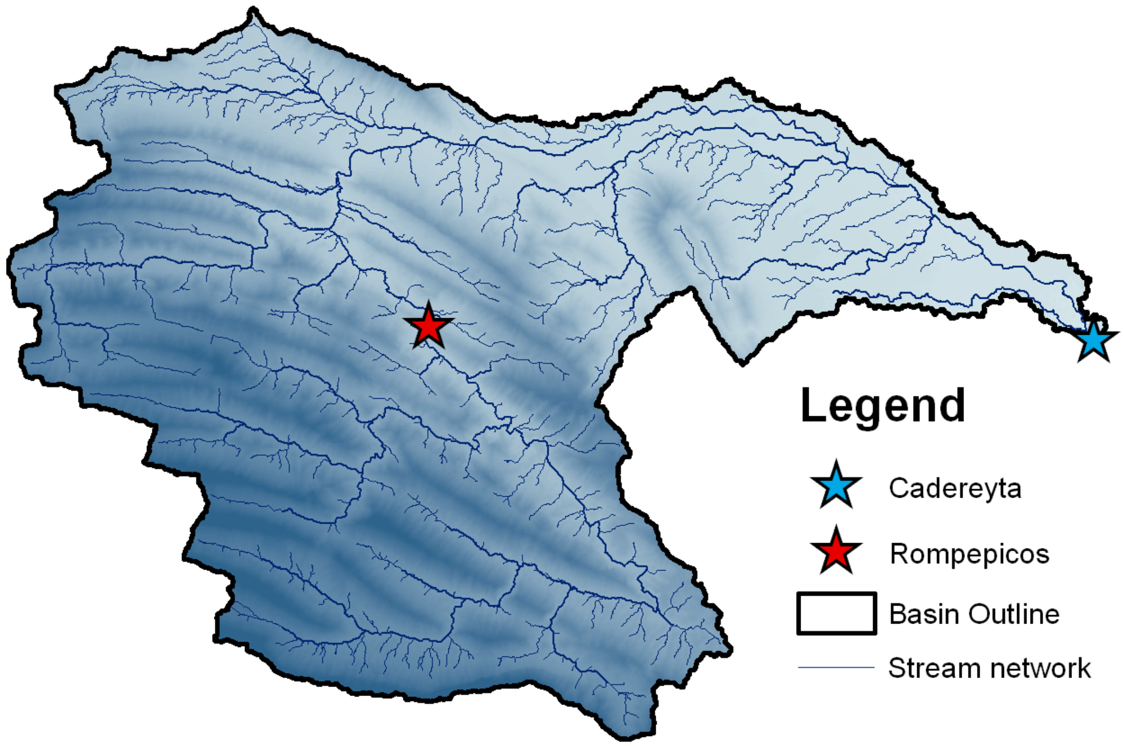

Figure 35. Location of the Rompepicos Dam within the Santa Catarina Watershed.

dramatic contrast in peaks observed at other locations. Finally, the outlet hydrograph shown in Figure 36f displays the significant role the Rompepicos Dam had in this event, reducing the peak by approximately 650 m^3/s in tRIBS and 700 m^3/s in the HEC-HMS simulation. This reduction represents a 13.7% (tRIBS) and 15% (HEC-HMS) peak mitigation from the current structure at the outlet. The significance of the structure during this storm event is more evident in locations upstream from the urban areas. Despite having a considerable mitigation impact the discharges into the Entrance to the City and Junction-23 still remain a considerable threat to the city and highlight the importance of additional flood controls in the basin.

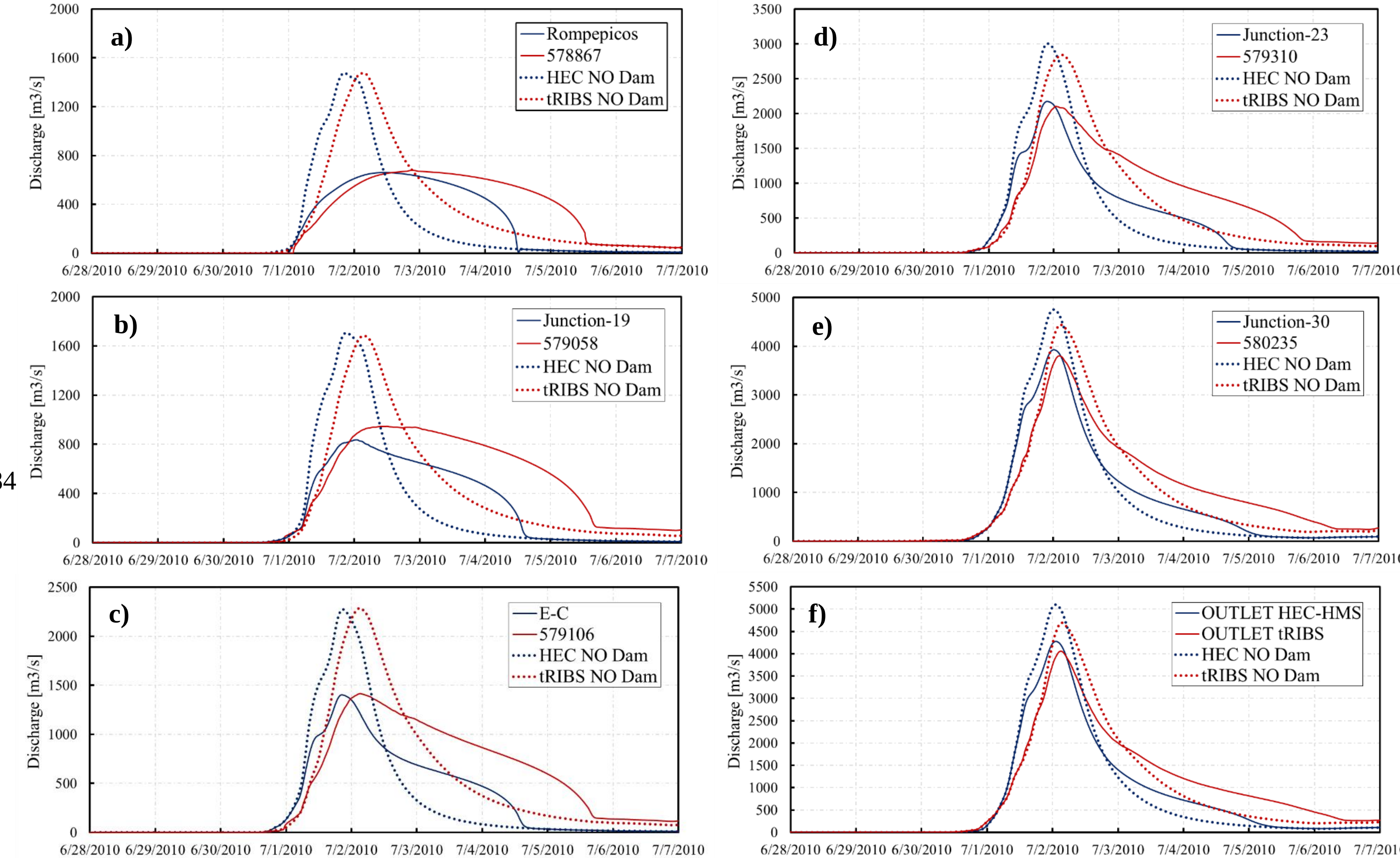

Figure 36. (a-f) Discharge hydrographs from HEC-HMS (blue) and tRIBS (red) evaluating the impact of the current Dam.

3.4.2 Additional Dam at the Entry to the City The storm diagnosis and spatial output generated from the models has served to identify important areas that contribute to the runoff generation in the watershed. The two main locations being: the Entry to the City and Junction-23. The importance of E-C lies in its contributing area, both in extension and characteristics. At 1129 km^2 it is represents 61.6% of the total area but also all of the upstream extent from this point consists of the steeped sloped mountainous landscape, where rapid infiltration excess runoff generation frequently occurs. A single point receiving streamflow from the entire upper basin in such proximity to the city makes E-C a potential candidate for the inclusion of a flood control structure. This site was also identified as a significant point in the Santa Catarina River's Sustainable Development Master Plan presented by the government of the state of Nuevo Leon (CERN 2010).

The additional dam simulated at this location (Figure 37) shares the design features of the Rompepicos Dam given the similarities in the physical characteristics of the site and the magnitude of the discharges going through this point. The same elevation-discharge-storage functions presented for the Rompepicos dam in the methods section are utilized for this new artificial structure. The locations of interest for this case will be similar to those used in the evaluation of Rompepicos. The locations considered will be the Entry to the City, Junction-23, Junction-30 and the outlet of the basin.

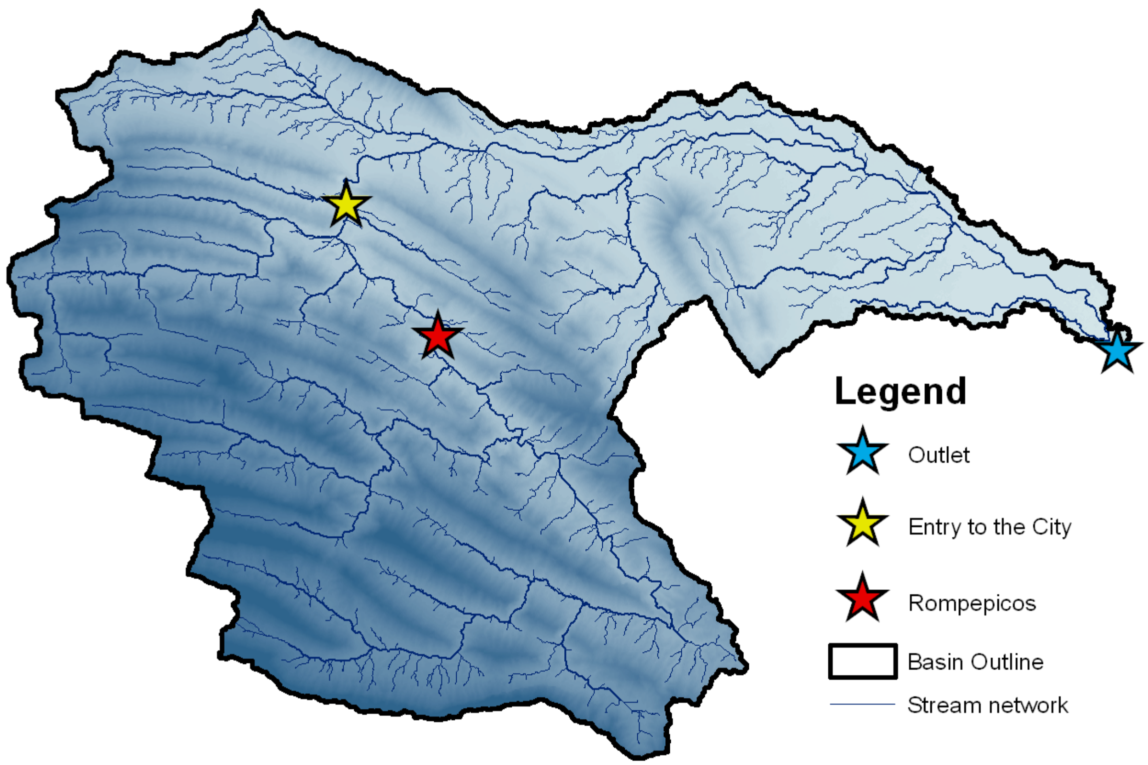

Figure 37. An additional hydraulic infrastructure is implemented at the Entry to the City in both hydrological models.

The effect of the structure at the E-C site can be seen in Figure 38a. An important difference can be observed in the operation of the dam as compared to Rompepicos. Although both dams receive similar inflow peaks, the new Reservoir at E-C is receiving longer, more prolonged high discharges while Rompepicos has a quicker recession in the incoming flow. This difference is reflected in the simulated outflow from both models where the initial steady rise in the hydrograph has a sudden increase. This increase is caused by the water elevation at the site, meaning that discharges are now going over the spillway structure and discharging at a higher rate, whereas at Rompepicos the flows are solely from the secondary outlet structure at the base. The peak reduction at E-C is not very significant but there is a very important function the structure is carrying out at this location that magnifies its relevance at downstream locations. This function is to delay the peak discharge that arrives to the city, preventing incoming flows generated from the north-west areas to magnify the flood wave. This effect can be seen at the next location downstream in Junction-23 shown in Figure 38b. The delayed effect considerably increases the mitigation impact from the structure at a location of converging streams that caused discharges of considerable risk.

At J-30 (Figure 38c) the peak reduction due to the delay is further accentuated and is extended onto the outlet of the basin shown in Figure 38d. The hydrograph's single peak discharge from the storm event is now transformed into two separate peaks caused by the second reservoir structure and is most noticeable in the tRIBS simulation. The inclusion of the second flood control structure at the E-C site created a favorable delay in the peak from runoff produced in units 1 and 2 and a reduction of the peak discharge at the outlet of the basin by 16.5% in tRIBS with a peak of 3343 m^3/s while HEC-HMS had a 23% reduction at 3262 m^3/s.

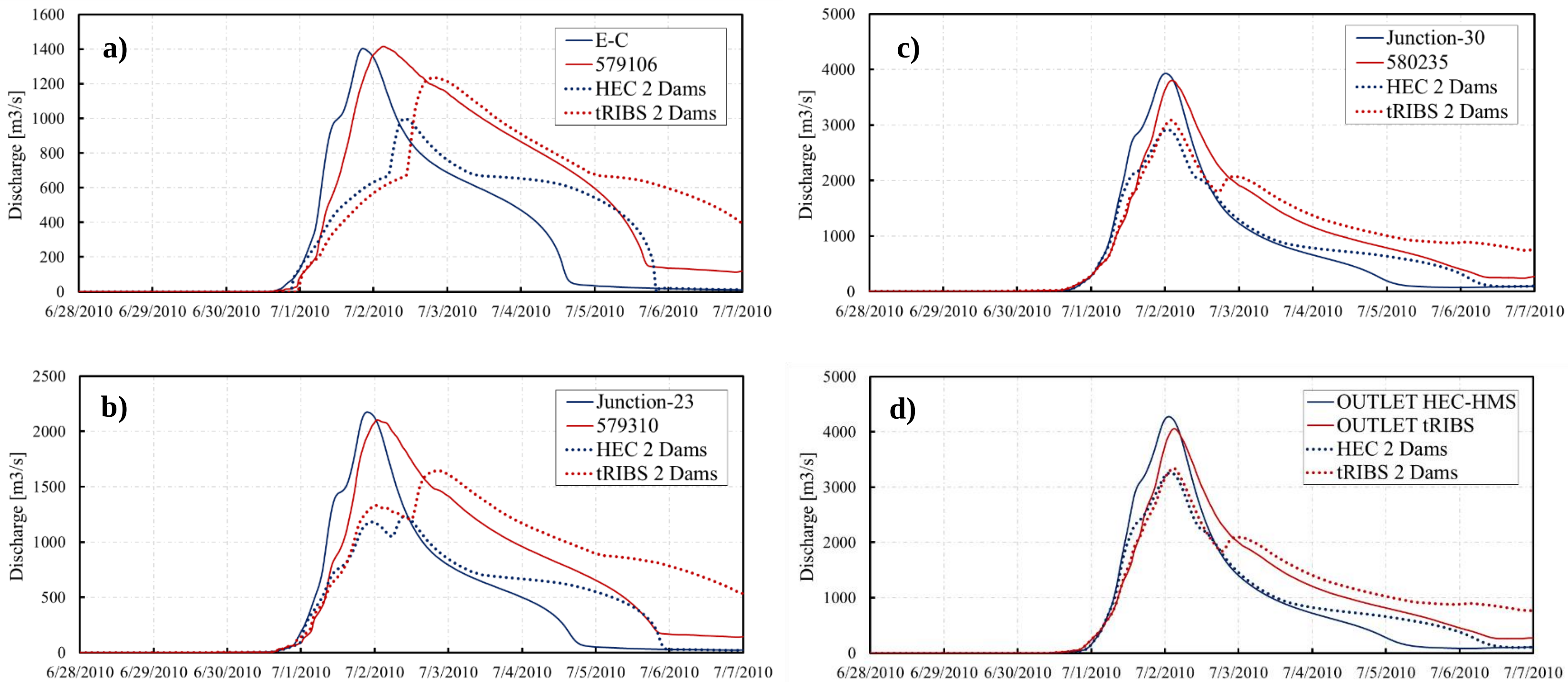

Figure 38. (a-d) Discharge hydrographs from HEC-HMS (blue) and tRIBS (red) evaluating the impact of one large additional hydraulic structure located at the Entry to the City.

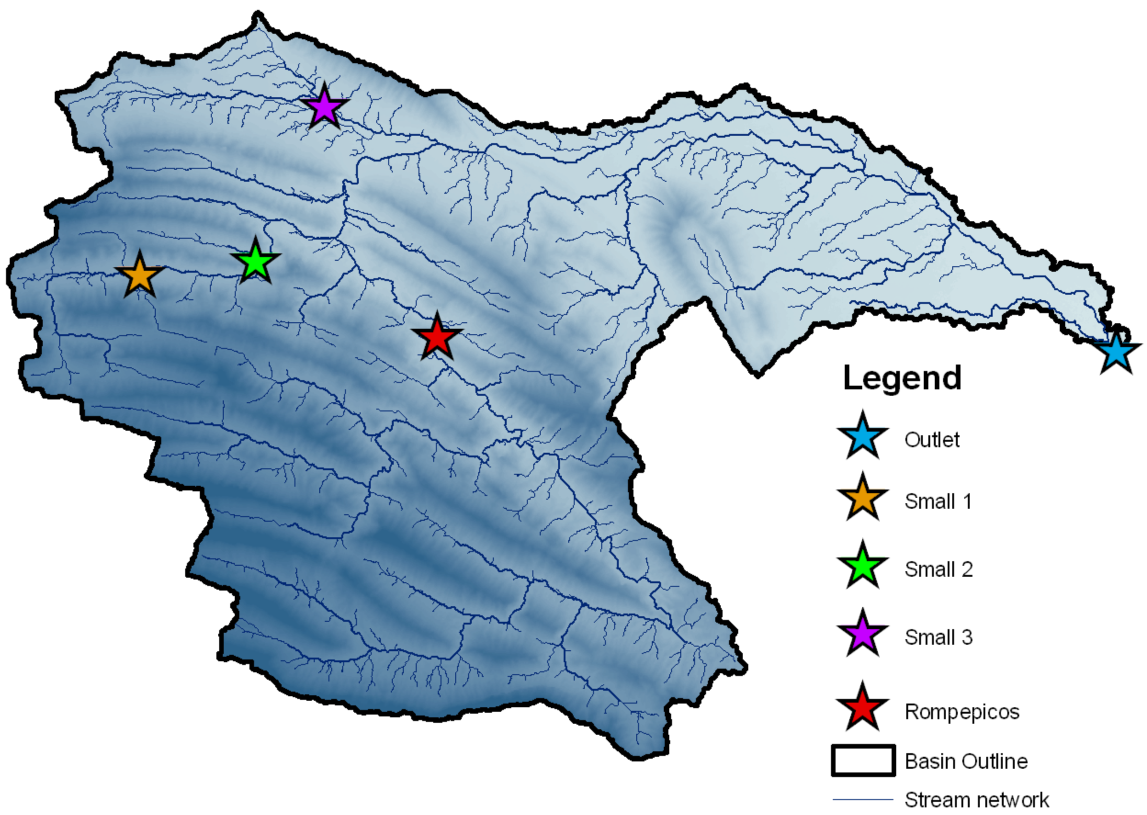

Figure 39. The location of the three small detention dams was done based on the storm diagnosis where significant runoff generation was identified.

3.4.3 Detention Basins The construction of an additional hydraulic structure such as Rompepicos represents an important and costly investment, so alternative flood control structures are also explored through the implementation of strategically placed small dams with the main purpose of delaying the discharges from relevant smaller contributing areas. By controlling the runoff at several higher upstream points (Figure 39) in the channel network a collective delay of the flood wave from the main runoff generating areas could create alleviation in the final hydrograph and at the Entry to the City location.

In this study the placement of 3 small dams are evaluated in locations with considerable runoff generation. The criteria for selecting the locations were based on the analysis of the storm event presented in the diagnosis section. As it was established before, two main locations were identified as relevant contributing areas: Uncontrolled runoff from the western side of the basin upstream from E-C and the confluence at J-23 receiving runoff from the north-western region and discharges from the upper basin. To create these artificial small detention dams, the original streamflow discharges and water surface elevations at these location were studied to have an established base discharge-elevation function similar to that of the Rompepicos dam. The topographic conditions of each location were also taken into consideration to have reasonable heights for each detention dam. Based on the topography, an elevation for the dam was established, and using the storm event discharges form the diagnosis section, the elevation-discharge function will contain initial discharges until the elevation of the small dam is reached and runoff begins to overflow the small structure. This is a limitation to consider when interpreting the results as these detention dams serve as artificial representations of an alternative proposition for flood control. Further studies on the feasibility and design of actual structures to be implemented in the site represent an opportunity on future development of alternative flood mitigation strategies.

Runoff generated in the western region (Unit 2) has a considerable contributing area of approximately 205 km^2 upstream from J-17. Due to this large area it was decided to place 2 small dams upstream from this location. This first dam is placed in Junction-15 (Node 574354) and has an area of 114 km^2 where significant contributions were observed in the simulated hydrograph with peaks between 250-300 m^3/s. The second small dam was placed downstream from J-15 at Junction-16 with a total area of 170 km^2. Finally the third dam was implemented at Junction-22, the second contributor to the confluence at J-23 (the first being E-C). The total area upstream from J-22 is of 106 km^2, this is a similar area as the one considered for the first small dam. The peak discharges here were also found to be significant with values above 300 m^3/s. The selection of these sites is expected to ameliorate small peaks upstream that can create a combined effect in the flood wave arriving at the city. An integrated map of all the existing and additional flood control structures considered in the study is shown in Figure 40 with a delineation of the corresponding contributing area of each structure presented in the context of the HEC-HMS model structure and tRIBS stream network.

The simulated hydrograph at the location of the first small dam is shown in Figure 41a. The resulting outflow hydrograph shows a promising outcome from both simulations by displaying a smoothed out peak and a longer recession limb. The small dams are not expected to contain large discharges from the upper regions but rather contain only the initial runoff generated at the early stages of the storm. The second location at J-16 also exhibits the same response from implementing the small dam although it should be noted that the effect seen in Figure 41b is not solely due to the second structure since the first dam at J-15 is located upstream. Figure 41c shows the simulated outflow from J-17, the last point before reaching the confluence at the E-C junction where additional runoff coming from Rompepicos is combined. The resulting effect at the point of interest in E-C and at J-20 shows a favorable reduction in the peak of the flow in both simulations

(Figure 41d and 41e) with approximately 13% reduction in tRIBS and 17% in HEC-HMS. J-20 is the last point before the runoff generated from the upper basin combines with the runoff generated from the north-western region. The combination of these flows generated a peak discharge of approximately 2100 m^3/s before reaching the urban areas.

The third small dam is located at J-22 receiving runoff from 4 sub-basins upstream adding a total contributing area of 106 km^2. This region differs from the other two locations in having overall milder slopes. These conditions prevent to some extent quick sharp rises as those seen in the mountainous areas. The resulting outflow from this site shown in Figure 42a reflect these conditions, with a very smooth outflow from this small dam where originally the simulated discharge had a moderate rising and recession limb. The first combined effect of the hindered discharges from all 3 dams is produced at the J-23 location as seen in Figure 42b. The reduction in the peak at this location for tRIBS was of 16.3% while HEC-HMS showed a 21.2% reduction. The effect is propagated downstream and at J-30 (Figure 42c) and the outlet (Figure 42d) the results show a favorable amelioration of the flood wave. It is interesting to see that at the outlet tRIBS had an 11.6% reduction of the peak while HEC-HMS had 10.9%.

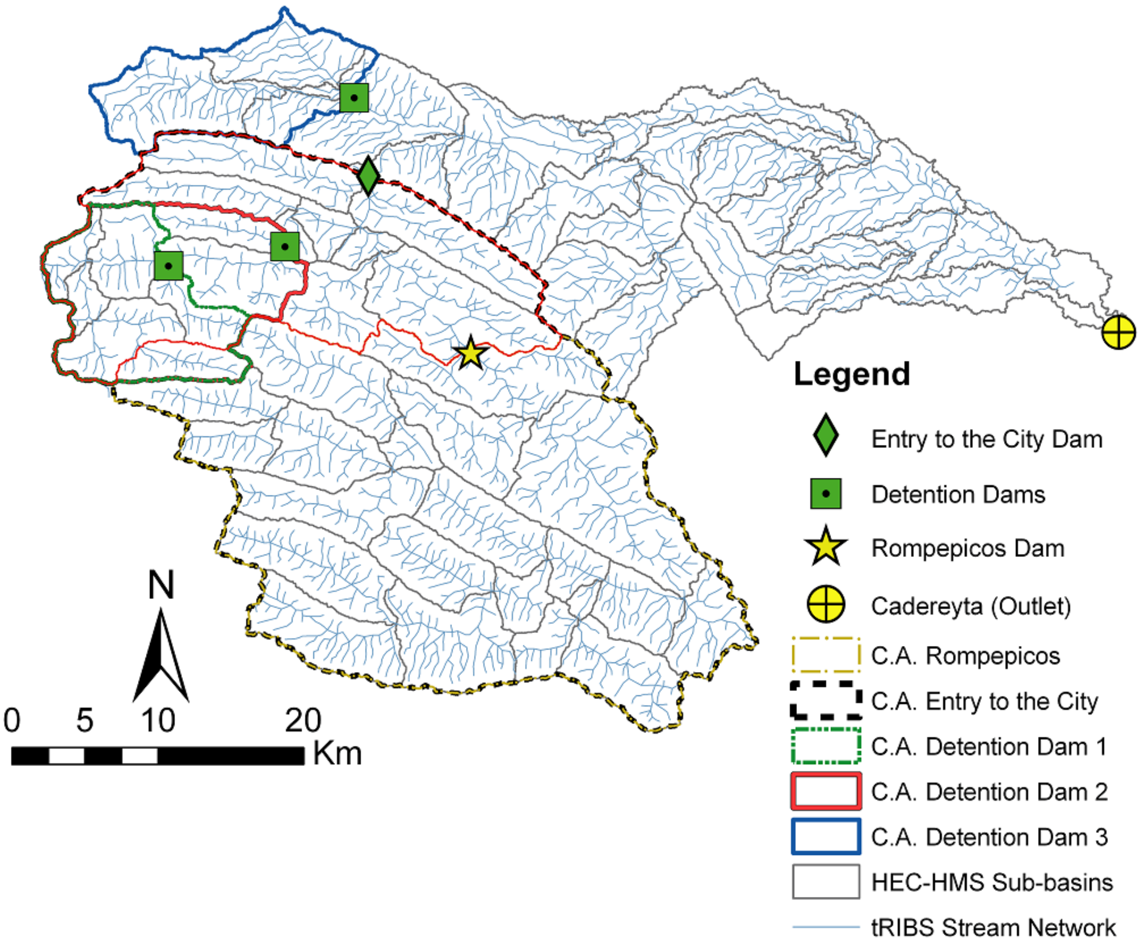

Figure 40. Location of Rompepicos Dam and the hydraulic infrastructure scenarios with a large dam at the Entry to the City ('Large Dam') and three detention dams ('Detention Dams'). For each site, the contributing area (C.A.) is shown within the context of the HEC-HMS sub-basins and tRIBS stream network

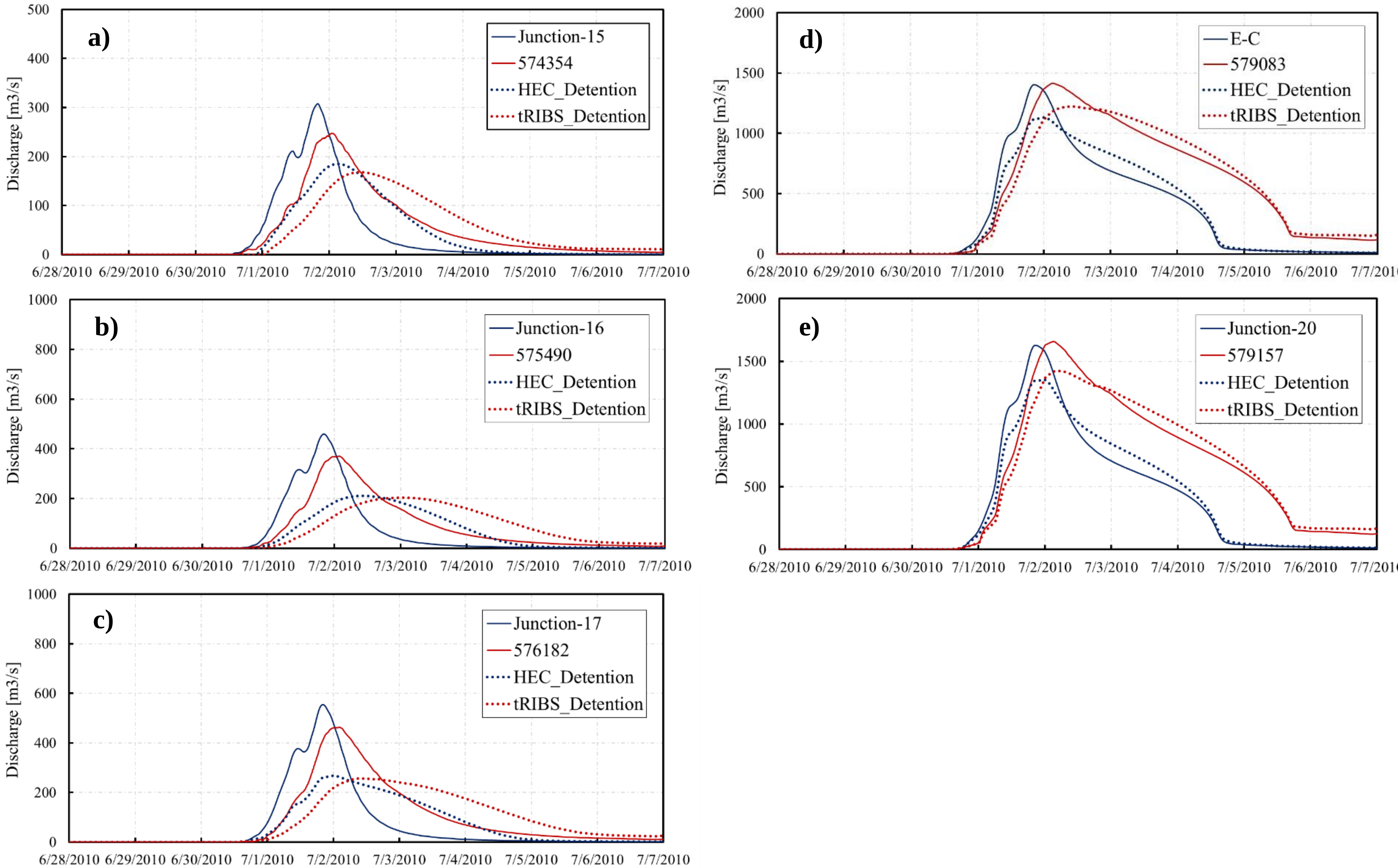

Figure 41. (a-e) Discharge hydrographs from HEC-HMS (blue) and tRIBS (red) for the first two small basins at J-15 and J-16 and locations downstream of these structures including the Entrance to the City (E-C).

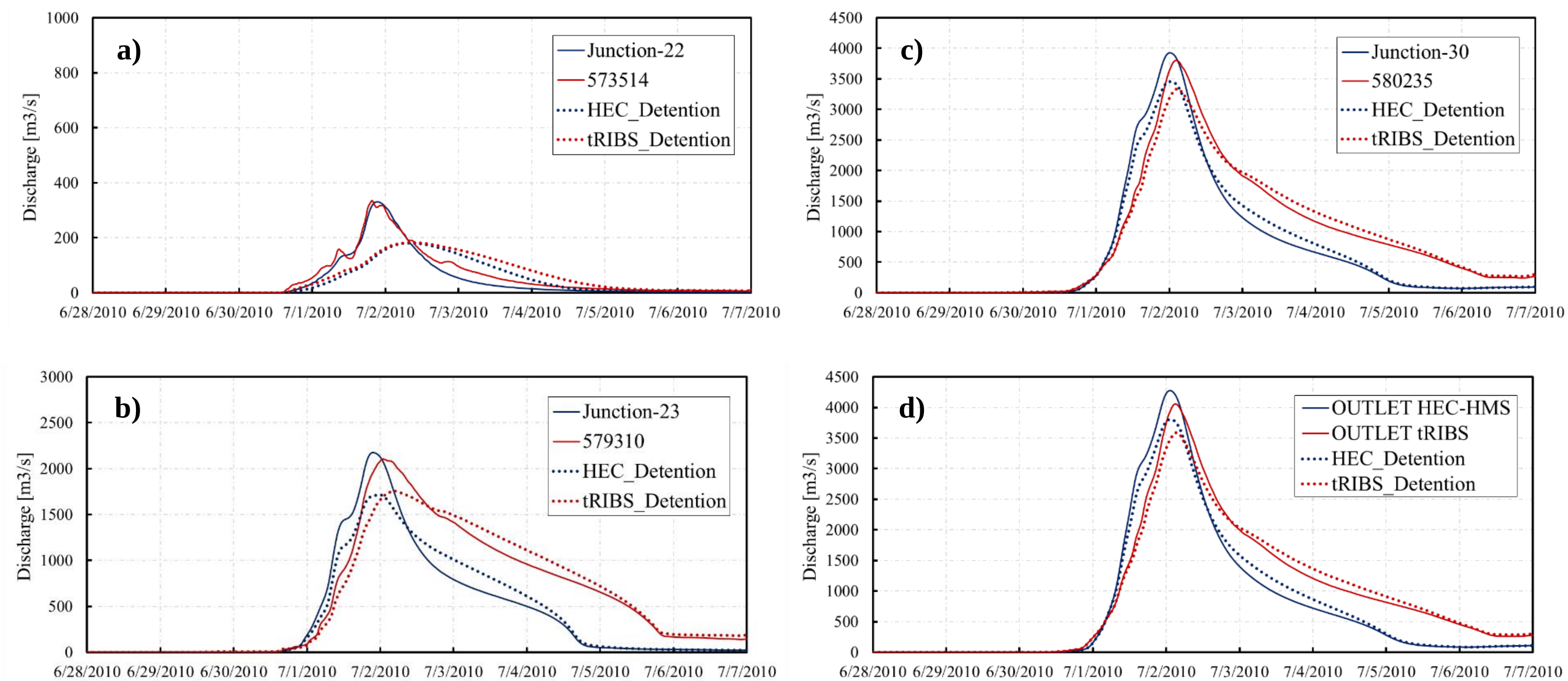

Figure 42. (a-d) Discharge hydrographs from HEC-HMS (blue) and tRIBS (red) for the third small dam at J-22 and discharges into subsequent locations downstream, including the outlet of the basin at Cadereyta.

A summary of the results for both models are shown in three main locations along the main channel that were studied in this analysis: the Entry to the City, receiving all discharges from the natural landscape (Figure 43 a, b). Site C, a confluence upstream of the main urban areas (Figure 43 c, d) and finally the outlet of the basin at Cadereyta (Figure 43 e, f).

The inclusion of a large dam at the Entry to the City showed favorable decreases in the peak flow at the outlet with a reduction of 16.5% in tRIBS and 23% in HEC-HMS. It was also found that an event of this magnitude would cause the water surface elevation at the new structure to go above the main spillway. The new artificial structure is able contain the pulse to some extent, although it would appear to be insufficient to larger, more intense storm events. The design of the structure at this location, mirroring the conditions at Rompepicos, can be indicated as a limitation given that an actual design of what could be constructed at this site is not available and outside the scope of this study. However, the response of this synthetic flood control structure can provide insights into the response of the Rompepicos dam if subjected to larger flood events. Higher intense storms could cause the water elevation to go over the main spillway and create considerable peak discharges as shown in Figures 43 a, b. Considering the fast response the watershed exhibited to this extreme event, with lag times as low as 10.92 hrs. (17.42 hrs. in tRIBS) in Site I and 11.92 hrs. (17.3 hrs. in tRIBS) in Site II (two locations in the upper basin), it highlights the risk of potential discharges going over the main spillway and how fast these can travel into the populated areas.

Additional scenarios presented at this location included the impact caused by the current hydraulic structure Rompepicos and inclusion of two small dams upstream from E-C. The current structure provided approximately 39% peak reduction at this site, stressing the crucial role this dam had in containing runoff from higher upstream areas. The two small detention dams located upstream from the Entry to the City also revealed promising results by reducing peaks incoming at this site by 13% (tRIBS) and 17% (HEC-HMS).

Site C, a key location just upstream of the main urbanized areas and a confluence of incoming runoff from the upper basin and the north-western regions, further displays the impact from the flood control scenarios analyzed in this study (Figure 43 c, d). At this location the full effect of the combination of small dams reveals the favorable delay in the flood wave and mitigation in the peak discharge by 17% in tRIBS and 20% in HEC-HMS.

Finally, the results at the basin outlet are presented in Figure 43 e, f. The current structure had significant value in containing runoff from the upper basin and potentially prevented greater damages to the city. The inclusion of the large artificial dam at E-C had a favorable mitigation impact, mainly by delaying the large flood wave incoming from the upper basin and preventing them from merging with incoming runoff from the north-western areas. The alternative to a large flood control structure scenario, in the form of three small dams, showed promising initial results by collectively delaying small flood pulses in upper regions before they grow in magnitude.

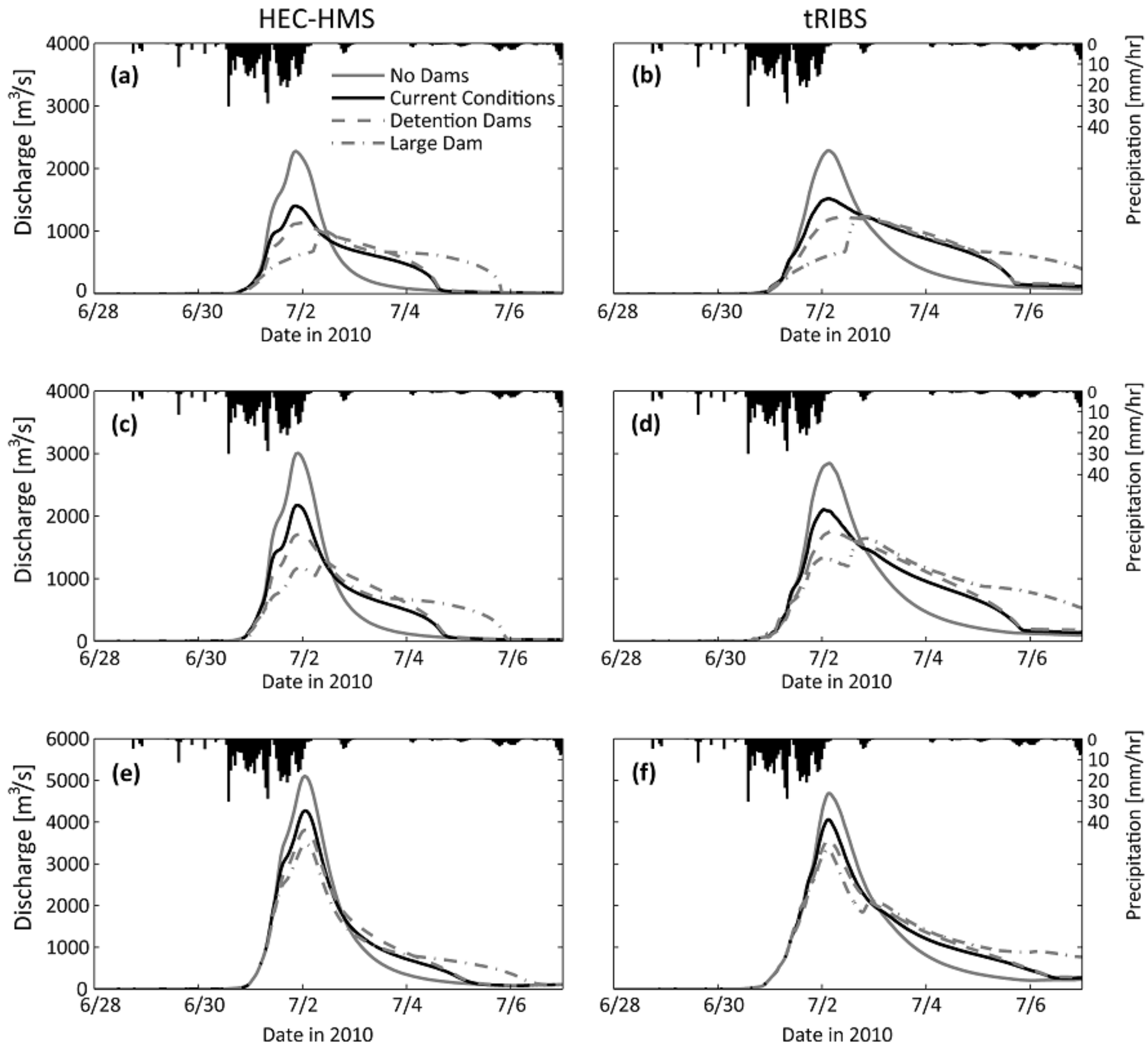

Figure 43. Comparison of the hydrologic responses from HEC-HMS (left) and tRIBS (right) for different hydraulic infrastructure scenarios at Entry to City (a, b), Site C, a confluence upstream of the urban area (c, d), and Basin Outlet at Cadereyta (e, f). The scenarios are labeled 'No Dam' (removal of Rompepicos Dam), 'Current Conditions' (with Rompepicos Dam), and 'Detention Dams' and 'Large Dam', both in addition to Rompepicos Dam. The hourly basin-averaged precipitation from the bias-corrected NLDAS product is shown in all cases.

CHAPTER 4

CONCLUSIONS AND FUTURE WORK

4.1 CONCLUSIONS

Three main goals can be highlighted in this study that were addressed through the use of two hydrological models:

1. Evaluate the proposed flood controls through a multi-model approach (semi and fully-distributed hydrological modeling) to provide stakeholder confidence for future decision making strategies.
2. Understand the hydrological response of the Santa Catarina watershed to high intensity events and identify the hydrological controls leading to flood hazards.
3. Evaluate the mitigation impact generated from current and additional hydraulic infrastructure in extreme rainfall events such as Hurricane Alex.

This study incorporated the strengths from two different hydrological models to generate data to best inform decision making processes in the Santa Catarina River Basin. The model calibration provided insights into the limitations found from the sparse availability and uneven temporal resolution in the streamflow gauges. The methods applied in the study yielded satisfactory results in establishing the best physical description of the basin with the limited-available data as a relatively low error in the peak discharge at the outlet could be achieved (251 m^3/s in tRIBS and 35.94 m^3/s in

HEC-HMS). The general good agreement between the two models added a level of confidence to the basins response to the storm event, particularly in the comparable total runoff generation over the entire simulation where a bias (B) of 0.99 and 0.8 for tRIBS and HEC-HMS respectively was obtained. A strong relation was found between the models' simulated hydrographs considering the different methods each model applies in their routing scheme.

The flood event diagnosis sub-divided the basin into three distinct units based on their intrinsic characteristics. This method served well to reveal the advantages and limitations of the semi-distributed model as physical parameters lumped into sub-basins can be at times non-representative of the actual conditions of the basin. Unit 1, characterized by having a mountainous and steeply sloped area revealed how spatial variations in the terrain, mainly slope variations, can have a significant role in complex terrains such as the Santa Catarina basin. HEC-HMS was susceptible to high discharges and quick peaks in the runoff with fast recessions due to its aggregated representation of the topographic conditions in the site. A key location was identified within Unit 2, the Entry to the City. The application of the two models to carry-out a flood event diagnosis allowed to identify in this ungauged location that a peak discharge of approximately 1500 m^3/s was generated and continued uncontrolled into the urban areas. This peak amount was comparable to the discharge going into the Rompepicos Dam, and finally mitigated by this structure. Unit 3 exposed the contribution of the urban areas to the growth of the flood wave. The larger coverage of impervious surfaces in this area added to a 60% increase in the runoff while only having a 22% increase of the contributing area.

The fully-distributed model (tRIBS) presented a set of spatially explicit distributed output at high resolutions reliant on the TIN generation. These spatially distributed results are of great significance when attempting to evaluate the basins response to the storm event. It was found that topographic attributes have strong a role in this basin's runoff mechanisms. Infiltration-excess runoff occurrence in the upper basin was dominant due to the highly efficient moisture redistribution provided by the high slopes while flatter terrains, or areas with topographic junctions promoted saturation of the soil profile.

The assessment of the hydrological impact from current and potential hydraulic infrastructures within the basin was done featuring three different scenarios using a newly developed reservoir routing tool for tRIBS based on the level pool routing method already available in HEC-HMS. The three scenarios considered were (1) evaluation of the current structure by removing the Rompepicos dam; (2) Implementation of an additional large structure at the Entry to the City and (3) the placement of three small detention basins.

The simulations showed that the current structure contributed to a mitigation of the flood peak of approximately 13.7% for tRIBS and 15% for HEC-HMS at the outlet of the basin. However, the impact from the current structure is more evident upstream of the urban areas with a reduction close to 39%, further displaying the large contribution to the growth of the flood wave from the populated areas.

The implementation of an additional large dam at the Entry to the City revealed favorable results in delaying the flood peak and presented reductions of 16.5% from tRIBS and 23% from HEC-HMS. The key information obtained from this scenario was that structure sharing similar characteristics as Rompepicos might not be sufficient to contain similar or larger extreme events. The results showed the water surface elevation surpassed the main spillway and while it was able to contain and delay the flood wave, considerable discharges still flowed downstream.

Alternative flood control structures were explored through three small detention dams placed in strategic locations with the main purpose of creating a collective delay of the flood peaks at upstream points. The initial results of this scenario exhibited promising results in their mitigation impact with 11.6% and 10.9% reductions in the peak discharge at the outlet for tRIBS and HEC-HMS respectively. This strategy yielded a lower impact than having a large flood control structure, however the implementation and maintenance costs of a large structure versus those of small localized detention dams are to be considered and represent an opportunity for further studies. The potential lower costs of setting a series of small dams has also the downside of generally having a greater impact on the environment than a large dam (Ohsugi et al. 2004).

A costly investment in a large structure that functions solely for extreme events can be justified by the downstream setting, the Monterrey Metropolitan Area, which represents one of the most important cities in the country and significant part of its economic development. This can be viewed as an investment on not only the security of the population, but on the infrastructure of city as well. Construction of a control structure could return the investment in the next extreme event. Dams like Rompepicos require approximately 46 million USD but far larger amounts have been invested in damages and repairs for the MMA in the past (Ferriño-Fierro et al. 2010).

4.2 FUTURE WORK

This work presents potential opportunities to further develop the study of the Santa Catarina River basin. In this study, the extreme storm event Hurricane Alex was examined and used to force the different simulations. To further understand the response of the basin and assess the value of additional hydraulic infrastructure, the examination of the Probable Maximum Precipitation or largest possible flood in this basin can be studied in the context of the different scenarios presented here. Simulating a larger Hurricane-induced flood event can reveal how the catchment is affected when water elevations at the Rompepicos dam surpass the spillway of the structure.

Simulating larger induced flood events also present the opportunity to consider hydraulic modeling in the main reach of the Santa Catarina River. Hydraulic models like HEC-RAS provide steady/unsteady flow simulations to calculate water surface profiles and see how these could affect urbanized settings. Different scenarios could be implemented with tools like the Dam break analysis and levee breaching and overtopping that could provide further insights for stakeholders and decision makers in the MMA.

The increasingly recurrent flood events in the region create a pressing need to further explore the set of solutions available and take actions in the best interest of the population. The refinement in the design of the different structures considered here utilizing the bathymetric data of the site would be of interest for the decision making process in establishing the required strategy for the catchment.

REFERENCES

Amador, J. A., Alfaro, E. J., Lizano, O. G., & Magaña, V. O. (2006). Atmospheric forcing of the eastern tropical Pacific: A review. *Progress in Oceanography*, *69*(2), 101-142.

Ashley, S. T., & Ashley, W. S. (2008). Flood fatalities in the United States. *J. Appl. Meteor. Climatol.*, *47*(3), 805-818. doi: http://dx.doi.org/10.1175/2007JAMC1611.1

Bashar, K. E., & Zaki, A. F. (2005). SMA Based Continuous Hydrologic Simulation of the Blue Nile. In *A paper published in the International Conference of UNESCO Flanders FUST FRIEND/NILE Project" Towards a Better Cooperation". Sharm El-Sheikh, Egypt*.

Bennett, T. H. (1998). *Development and application of a continuous soil moisture accounting algorithm for the Hydrologic Engineering Center Hydrologic Modeling System (HEC-HMS).* MS thesis, Dept. of Civil and Environmental Engineering, Univ. of California, Davis, Calif.

Bennett, T. H., & Peters, J. C. (2000). Continuous Soil Moisture Accounting in the Hydrologic Engineering Center Hydrologic Modeling System (HEC-HMS). *ASCE Technical Publication*. *Building Partnerships*: pp. 1-10. doi: 10.1061/40517(2000)149

Berga, L. (2006). El papel de las presas en la mitigación de las inundaciones. *Ingeniería Civil*, (Greso Internacional De Grandes Presas), 7-13.

Carlson, T. N., & Ripley, D. A. (1997). On the Relation Between NDVI, Fractional Vegetation Cover, and Leaf Area Index. *Remote Sensing of Environment*, *62*(3), 241- 252.

Carlyle-Moses, D., & Price, A. (2007). Modelling Canopy Interception Loss from a Madrean Pine-Oak Stand, Northeastern Mexico. *Hydrological Processes*, *21*(19), 2572-2580.

Cavazos, T. (1999). Large-scale circulation anomalies conducive to extreme precipitation events and derivation of daily rainfall in northeastern Mexico and southeastern Texas. *Journal of Climate*, *12*(5), 1506-1523.

Chaudhry, M. H. (1993). Open-channel flow. *Englewood Cliffs, NJ: Prentice-Hall*.

Chow, V. T. (1959). Open channel flow. *McGraw-Hill Book Co. Inc.: New York*.

Chu, X., & Steinman, A. (2009). Event and continuous hydrologic modeling with HEC-HMS. *Journal of Irrigation and Drainage Engineering*, *135*(1), 119-124.

Consejo Estatal para la Reconstrucción de Nuevo León (2010). *Plan Maestro: Corredor Integral de Movilidad Sustentable (Constitución-Morones Prieto) + Uso Recreativo y Deportivo público en el Lecho del Río Santa Catarina*. Nuevo Leon, Mexico.

Corbosiero, K. L., Dickinson, M. J., & Bosart, L. F. (2009). The contribution of eastern North Pacific tropical cyclones to the rainfall climatology of the southwest United States. *Monthly Weather Review*, *137*(8), 2415-2435.

Drainage, U. (2008). Flood Control District. *Urban Storm Drainage Criteria Manual*, *Vol. 1*, 6-14.

Emerson, C. H., Welty, C., & Traver, R. G. (2003). Application of HEC-HMS to model the additive effects of multiple detention basins over a range of measured storm volumes. In *World Water & Environmental Resources Congress* (Vol. 2003, pp. 1-8). doi: 10.1061/40685(2003)319

Farfán, L. M., Prieto, R., Martínez-Sánchez, J. & Padilla, R. (2015). *Ciclones Tropicales y su Influencia en México*. Conviviendo con la Naturaleza: El Problema de los Desastres Asociados a Fenómenos Hidrometeorológicos y Climáticos en México. Teresa Cavazos. 1st Edition. ILCSA S.A. de C.V.C. Tijuana, B.C., México.

Faurès, J. M., Goodrich, D. C., Woolhiser, D. A., & Sorooshian, S. (1995). Impact of Small-Scale Spatial Rainfall Variability on Runoff Modeling. *Journal of Hydrology*, *173*(1), 309-326.

Ferriño-Fierro, A., Guerra-Cobián, V., Bruster-Flores, J., De Lira-Reyes, G. & Cavazos-Gonzalez, R. (2010). *Control de Inundaciones en Zonas Urbanas, Caso de Estudio: Presa Rompe Picos Corral de Palmas Ubicada en Santa Catarina, Nuevo Leon, México,* Ciencia – FIC, no. 1, pp. 5-9.

Fleming, M., & Neary, V. (2004). Continuous hydrologic modeling study with the hydrologic modeling system. *Journal of hydrologic engineering*, *9*(3), 175-183. doi: http://dx.doi.org/10.1061/(ASCE)1084-0699(2004)9:3(175)

Funk, T. (2006). Heavy convective rainfall forecasting: A look at elevated convection, propagation, and precipitation efficiency. In *Proc. 10th Severe Storm and Doppler Radar Conf.* Des Moines, IA. National Weather Association.

Ganoulis, J., Skoulikaris, H., & Monget, J. M. (2008). Involving Stakeholders in Transboundary Water Resources Management: The Mesta/Nestos “Help Basin”. *Water SA*, *34*(4), 461-467.

Garen, D. C., & Moore, D. S. (2005). Curve Number Hydrology In Water Quality Modeling: Uses, Abuses, And Future Directions. Journal of the American Water Resources Association, vol. 41, issue 2, pp. 377-388. doi: 10.1111/j.1752-1688.2005.tb03742.x

González, G. R. (1973). *La lluvia en Monterrey, Nuevo León. Estudio Cronológico y Probabilístico*. Boletín Bimestral de la División de Ciencias Agropecuarias y Marítimas del ITESM. 147:1-7 pp.

Gropp, W., Lusk, E., Doss, N., & Skjellum, A. (1996). A high-performance, portable implementation of the MPI message passing interface standard. *Parallel computing*, *22*(6), 789-828.

Hawkins, G. A., Vivoni, E. R., Robles-Morua, A., Mascaro, G., Rivera, E., & Dominguez, F. (2015). A climate change projection for summer hydrologic conditions in a semiarid watershed of central Arizona. *Journal of Arid Environments*, *118*, 9-20. doi:10.1016/j.jaridenv.2015.02.022

Hawkins, R. H. (1984). A comparison of predicted and observed runoff curve numbers. Proceedings Specialty Conference, "*Water Today and Tomorrow*", Flagstaff AZ, *Amer Soc Civ Eng*, New York, 67-76.

Hawkins, R. H. (1993). Asymptotic determination of runoff curve numbers from data. *Journal of Irrigation and Drainage Engineering*, *119*(2), 334-345. doi: http://dx.doi.org/10.1061/(ASCE)0733-9437(1993)119:2(334)

Hengl, T., de Jesus, J. M., MacMillan, R. A., Batjes, N. H., Heuvelink, G. B., Ribeiro, E., Walsh, M. G. & Gonzalez, M. R. (2014). SoilGrids1km—Global Soil Information Based on Automated Mapping *PLoS One*, *9*(8), e105992

Hernandez, M., Miller, S. N., Goodrich, D. C., Goff, B. F., Kepner, W. G., Edmonds, C. M., & Jones, K. B. (2000). Modeling runoff response to land cover and rainfall spatial variability in semi-arid watersheds. In *Monitoring Ecological Condition in the Western United States* (pp. 285-298). Springer Netherlands.

Hernández U. A. & Bravo L.C. (2010). *Reseña del huracán “Alex” del Océano Atlántico*. Secretaría de Medio Ambiente y Recursos Naturales (SEMARNAT) Retrieved from http://smn.cna.gob.mx/ciclones/tempo2010/atlantico/Alex2010a.pdf

Hornberger, G. M., & Boyer, E. W. (1995). Recent Advances in Watershed Modelling. *Reviews of Geophysics*, *33*(S2), 949-957. doi: 10.1029/95RG00288

Hydrologic Engineering Center (2000). *Hydrologic Modeling System HEC-HMS Technical Reference Manual*, U. S. Army Corps of Engineers

Hydrologic Engineering Center (2010). *Hydrologic Modeling System HEC-HMS User's Manual, Version 3.5.0*, U. S. Army Corps of Engineers

Hydrologic Engineering Center (2015). *Hydrologic Modeling System HEC-HMS Applications Guide*, U. S. Army Corps of Engineers

ICOLD. (2006). Role of dams in flood mitigation. A review. Bulletin 131. ICOLD, Paris.

INEGI, Instituto Nacional de Estadistica y Geografia (1990). *Guia para la Interpretacion cartografica, climatología*. Aguascalientes, Ags.

INEGI, Instituto Nacional de Estadística y Geografía (2009). *SCNM: Sistema de Cuentas Nacionales de Mexico: Producto Interno Bruto por entidad federativa 2005-2009*. Segunda Versión. Aguascalientes, Ags.

INEGI, Instituto Nacional de Estadistica y Geografia. (2011). *Population by County in Nuevo Leon State*. Aguascalientes, Ags.

INEGI, Instituto Nacional de Estadística y Geografía (2014). *Banco de Información Económica (BIE)*. Retrieved from www.inegi.org.mx/sistemas/bie/default.aspx.

Innovation Consortium Project, (2013). *An Integrated Approach for Sustainable Water Resources Management in Latin America and the Caribbean: The San Juan River Basin Pilot Project*. Washington, D.C.

Iskenderian, H., 1995: Tropical cloud plumes and the interannual variability of precipitation over the southeastern United States and Mexico. Ph.D. dissertation, State University of New York at Albany, 147 pp. Available from University at Albany, State University of New York, 1400 Washington Ave., Albany, NY 12222.

ISRIC – World Soil Information, (2013). SoilGrids: An Automated System for Global Soil Mapping. Available for Download at http://soilgrids1km.isric.org

Ivanov, V. Y., Vivoni, E. R., Bras, R. L., & Entekhabi, D. (2004a). Catchment Hydrologic response with a fully distributed triangulated irregular network model. *Water Resources Research, 40*(11) doi: 10.1029/2004WR003218

Ivanov, V. Y., Vivoni, E. R., Bras, R. L., & Entekhabi, D. (2004b). Preserving High Resolution Surface and Rainfall Data in Operational-Scale Basin Hydrology: A Fully-Distributed Physically-Based Approach. *Journal of Hydrology, 298*(1), 80-111. doi:10.1016/j.jhydrol.2004.03.041

Kidd, C. H. R. (1978). A Calibrated Model for the Simulation of the Inlet Hydrograph for Fully Sewered Catchments. *Urban Storm Drainage*, 172-186.

Kosugi, K. (1999). General model for unsaturated hydraulic conductivity for soils with lognormal pore-size distribution. *Soil Sci. Soc. Am. J.* 63:270-277.

Land Processes Distributed Active Archive Center (LP DAAC), (2012), Leaf Area Index – Fraction of Photosynthetically Active Radiation 8-Day L4 Global 1km. NASA EOSDIS Land Processes DAAC, USGS Earth Resources Observation and Science (EROS) Center, Sioux Falls, South Dakota (https://lpdaac.usgs.gov), accessed at https://lpdaac.usgs.gov/dataset_discovery/modis/modis_products_table/mcd15a2

Maqueda, A. (2007). Assessment of Impacts of Land cover change on the San Juan River watershed. Retrieved from Laboratorio de Sistemas de Información Georreferenciada (LabSIG ITESM, 2011). http://albers.mty.itesm.mx/TesisAxa1.html

Mays, L. W. (2010). *Water resources engineering*. John Wiley & Sons.

McEnroe, B. M. (2010). Guidelines for continuous simulation of streamflow in Johnson County, Kansas, with HEC-HMS. *Department of Civil, Environmental and Architectural Engineering, Univ. of Kansas*.

Méndez-Barroso, L. A., Vivoni, E. R., Robles-Morua, A., Mascaro, G., Yépez, E. A., Rodríguez, J. C., Watts, C. J., Garatuza-Payan, J. & Saíz-Hernández, J. A. (2014). A Modeling Approach Reveals Differences in Evapotranspiration and its Partitioning in Two Semiarid Ecosystems in Northwest Mexico. *Water Resources Research, 50*(4), 3229-3252. doi:10.1002/2013WR014838

Milly, P. C. D., & Eagleson, P. S. (1988). Effect of storm scale on surface runoff volume. *Water Resources Research, 24*(4), 620-624. doi: 10.1029/WR024i004p00620

Mitchell, K. E., Lohmann, D., Houser, P. R., Wood, E. F., Schaake, J. C., Robock, A., Luo, L. (2004). The Multi-Institution North American Land Data Assimilation System (NLDAS): Utilizing Multiple GCIP products and partners in a continental Distributed Hydrological Modeling System. *Journal of Geophysical Research: Atmospheres (1984–2012), 109*(D7)

Morel-Seytoux, H. J. (1988). Recipe for simple but physically based modeling of the infiltration and local runoff processes. *Proc. 8th Annual Hydrology Days, Colorado State University*, 226-247.

Moreno, H. A., Vivoni, E. R., & Gochis, D. J. (2013). Limits to flood forecasting in the Colorado Front Range for two summer convection periods using radar nowcasting and a distributed hydrologic model. *Journal of Hydrometeorology*, *14*(4), 1075-1097. doi: http://dx.doi.org/10.1175/JHM-D-12-0129.1

Mualem, Y. (1976). A New Model Predicting the Hydraulic Conductivity of Unsaturated Porous Media. *Water Resour. Res*. 12:513-522.

Murillo, M. E. (2002). Estudio del Efecto del Cambio de Uso de Suelo en el Escurrimiento en la Subcuenca 24Bf “Monterrey”, Aplicando un Sistema de Información Geográfica. Retrieved from Laboratorio de Sistemas de Información Georreferenciada (LabSIG ITESM, 2011). http://albers.mty.itesm.mx/tesis/erendira.pdf

Myneni, R., Knyazikhin, Y., Glassy, J., Votava, P., & Shabanov, N. (2003). User’s guide: FPAR, LAI (ESDT: MOD15A2) 8-day composite NASA MODIS land algorithm. *Terra*.

Návar, J., & Synnott, T. J. (2000). Soil infiltration and land use in Linares, N.L., México. *Terra Latinoamericana*, *18*(3), 255-262.

Návar, J. (2012). Modeling annual discharge of six Mexico’s northern rivers. *Revista Ambiente & agua, 7(1),* 36-50. http://dx.doi.org/10.4136/ambi-agua.705

Nikolopoulos, E. I., Anagnostou, E. N., Borga, M., Vivoni, E. R., & Papadopoulos, A. (2011). Sensitivity of a mountain basin flash flood to initial wetness condition and rainfall variability. *Journal of Hydrology, 402*(3), 165-178. doi:10.1016/j.jhydrol.2010.12.020

Oak Ridge National Laboratory Distributed Active Archive Center (ORNL DAAC). (2014). MODIS subsetted land products, Collection 5. Available on-line [http://daac.ornl.gov/MODIS/modis.html] from ORNL DAAC, Oak Ridge, Tennessee, U.S.A. Accessed May 22, 2015. Subset obtained for MOD13Q1 product at 25.6374N,100.2299W, time period: 2000-02-18 to 2015-04-23, and subset size: 6.25 x 6.25 km

Ohsugi, M., Yasuda, N. and Okano, M. (2004). Dams and the environment, ICOLD symposium.

Pitman, J. I. (1989). Rainfall interception by bracken in open habitats—relations between leaf area, canopy storage and drainage rate. *Journal of Hydrology*, *105*(3), 317-334.

Ponce, V. M., & Hawkins, R. H. (1996). Runoff curve number: Has it reached maturity? *J. Hydrol. Eng.*, 10.1061/(ASCE)1084-0699(1996)1:1(11), 11-19

Ramirez, A. (2010). *Estudio hidrológico de la cuenca del rio Santa Catarina, N.L*. Technical Report Comissioned to Integrate Reconstrucción del río Santa Catarina después del Huracán Alex, CONAGUA, Monterrey.

Ramirez, A. (2011). *Evaluacion del funcionamiento de la Presa Rompepicos*, technical Report Comissioned to Integrate Reconstrucción del río Santa Catarina después del huracán Alex, CONAGUA, Monterrey.

Re, M. (2004). Annual Review: Natural Catastrophes 2004. *Knowledge series*. Munich.

Robles-Morua, A., Vivoni, E. R., & Mayer, A. S. (2012). Distributed Hydrologic Modeling in Northwest Mexico Reveals the Links Between Runoff Mechanisms and Evapotranspiration. *Journal of Hydrometeorology, 13*(3), 785-807. doi: http://dx.doi.org/10.1175/JHM-D-11-0112.1

Robles-Morua, A., Che, D., Mayer, A. S., & Vivoni, E. R. (2015). Hydrological Assessment Of Proposed Reservoirs In The Sonora River Basin, Mexico, Under Historical And Future Climate Scenarios. *Hydrological Sciences Journal, 60*(1), 50 66. doi:10.1080/02626667.2013.878462

Sakamoto, T., & Yasuda, N (2009). *Monitoring and Evaluating Dams and Reservoirs*. Water, Storage, Transport and Distribution. Encyclopedia of Life Supports Systems (EOLSS).

Saxton, K., Rawls, W., Romberger, J., & Papendick, R. (1986). Estimating Generalized Soil-Water Characteristics from Texture. *Soil Science Society of America Journal, 50*(4), 1031-1036

Schaap, M.G., Leij F.J. & van Genuchten, M. Th. (1999). A Bootstrap-Neural Network Approach to Predict Soil Hydraulic Parameters. *In*: van Genuchten, M.Th., F.J. Leij, and L. Wu (eds), Proc. Int. Workshop, *Characterization and Measurements of the Hydraulic Properties of Unsaturated Porous Media*, pp 1237-1250, University of California, Riverside, CA.

Seyfried, M. S., & Wilcox, B. P. (1995). Scale and the nature of spatial variability: Field examples having implications for hydrologic modeling. *Water Resources Research*, *31*(1), 173-184. doi: 10.1029/94WR02025

Singh S. R. & Jain M. K. (2015). Continuous Hydrological Modeling using Soil Moisture Accounting Algorithm in Vamsadhara River Basin, India. *Journal of Water Resource and Hydraulic Engineering 10/2015; 4*(4):398-408. doi: 10.5963/JWRHE0404011

Singh, V. P., & Woolhiser, D. A. (2002). Mathematical Modeling of Watershed Hydrology. *Journal of Hydrologic Engineering*, *7*(4), 270-292. doi: 10.1061/(ASCE)1084-0699(2002)7:4(270)

Sisto, N. P., & Ramírez, A. (2015). Flash Flood in the Monterrey metropolitan area, Mexico: Lessons from Hurricane Alex. Aguilar-Barajas, I., Mahlknecht, J., Kaledin, J., Kjellén, M., & Mejía-Betancourt, A. (Eds.). *Water and Cities in Latin America: Challenges for Sustainable Development*. Routledge.

Sivapalan, M., & Wood, E. F. (1986). Spatial heterogeneity and scale in the infiltration response of catchments. In *Scale problems in hydrology* (pp. 81-106). Springer Netherlands.

Smith, R. E., & Hebbert, R. H. B. (1979). A Monte Carlo analysis of the hydrologic effects of spatial variability of infiltration. *Water Resources Research*, *15*(2), 419-429. doi: 10.1029/WR015i002p00419

SMN, Servicio Meteorologico Nacional (2010). Normales Climatologicas por Estado. *Secretaría de Medio Ambiente y Recursos Naturales (SEMARNAT)* Mexico, D.F. Retrieved from http://smn.cna.gob.mx/index.php?option=com_content&view=article&id=184&tmpl=component

Solano, R., Didan, K., Jacobson, A., & Huete, A. (2010). MODIS Vegetation Index User's Guide (MOD13 series). *Vegetation index and phenology lab*.

Steiner, M., Smith, J. A., Burges, S. J., Alonso, C. V., & Darden, R. W. (1999). Effect of bias adjustment and rain gauge data quality control on radar rainfall estimation. *Water Resources Research*, *35*(8), 2487-2503.

Stone, J. J., Lane, L. J., & Shirley, E. D. (1992). Infiltration and runoff simulation on a plane. *Transactions of the ASAE*, *35*(1), 161-170.

Tingsanchali, T., & Tanmanee, S. (2012). Assessment of hydrological safety of Mae Sruai Dam, Thailand. *Procedia Engineering*, *32*, 1198-1204.

Tucker, G. E., Lancaster, S. T., Gasparini, N. M., & Bras, R. L. (2001). The Channel-Hillslope Integrated Landscape Development (CHILD) model. In R. S. Harmon, & W. W. Doe (Eds.), *Landscape Erosion and Sedimentation Modeling* (pp. 349-388). Norwell, Mass: Kluwer Academy.

United States Department of Agriculture (USDA): US Salinity Laboratory, (1999), ROSETTA Model: Year 1999, Version: 1.0. Retrieved from http://www.ars.usda.gov/News/docs.htm?docid=8953#top

Van Genuchten, M. T. (1980). A closed-form equation for predicting the hydraulic conductivity of unsaturated soils. *Soil Science Society of America Journal, 44*(5), 892-898.

Vazquez, R. F., Feyen, L., & Refsgaard, J. C. (2002). Effect of grid size on effective parameters and model performance. *Hydrological Processes*, VOL. 16, 355-372.

Vivoni, E. R., Ivanov, V. Y., Bras, R. L., & Entekhabi, D. (2004). Generation of triangulated irregular networks based on hydrological similarity. *Journal of Hydrologic Engineering, 9*(4), 288-302.

Vivoni, E. R., Ivanov, V. Y., Bras, R. L., & Entekhabi, D. (2005a). On the Effects of Triangulated Terrain Resolution on Distributed Hydrologic Model Response. *Hydrological Processes, 19*(11), 2101-2122.

Vivoni, E. R., Teles, V., Ivanov, V. Y., Bras, R. L., & Entekhabi, D. (2005b). Embedding Landscape Processes into Triangulated Terrain Models. *International Journal of Geographical Information Science, 19*(4), 429-457.

Vivoni, E. R., Entekhabi, D., Bras, R. L., Ivanov, V. Y., Van Horne, M. P., Grassotti, C., & Hoffman, R. N. (2006). Extending the predictability of hydrometeorological flood events using radar rainfall nowcasting. *Journal of Hydrometeorology, 7*(4), 660-677. doi: http://dx.doi.org/10.1175/JHM514.1

Vivoni, E., Entekhabi, D., Bras, R., & Ivanov, V. (2007). Controls on Runoff Generation and Scale-Dependence in a Distributed Hydrologic Model. *Hydrology and Earth System Sciences*, 11(5), 1683-1701

Vivoni, E. R., Mascaro, G., Mniszewski, S., Fasel, P., Springer, E. P., Ivanov, V. Y., & Bras, R. L. (2011). Real-world Hydrologic Assessment of a Fully-Distributed Hydrological Model in a Parallel Computing Environment. *Journal of Hydrology, 409*(1), 483-496. doi:10.1016/j.jhydrol.2011.08.053

Woolhiser, D. A., & Goodrich, D. C. (1988). Effect of storm rainfall intensity patterns on surface runoff. *Journal of Hydrology*, *102*(1), 335-354. doi:10.1016/0022-1694(88)90106-0

Xiang, T., Vivoni, E. R., & Gochis, D. J. (2014). Seasonal evolution of ecohydrological controls on land surface temperature over complex terrain. *Water Resources Research, 50*(5), 3852-3874. doi:10.1002/2013WR014787

Zupka, D. (1998). Economic impact of disasters. *UNDRO News*. Jan-Feb.

APPENDIX A

LEVEL POOL ROUTING CODE IN TRIBS

Header file “tReservoir.h” begins:

```
/***************************************************************************
**
**                    tRIBS Distributed Hydrologic Model
**
**          TIN-based Real-time Integrated Basin Simulator
**                    Ralph M. Parsons Laboratory
**                 Massachusetts Institute of Technology
**
**
**  tReservoir.h: Header for class tReservoir (see tReservoir.cpp) which inherets
**          tFlowNet, tKinemat and implements Level Pool Routing.
**
***************************************************************************/

#ifndef TRESERVOIR_H
#define TRESERVOIR_H

//=========================================================================
=====
//
//
//              Section 1: tReservoir Include Statements
//
//
//=========================================================================
=====


#include "tFlowNet/tResData.h"
#include "Headers/Inclusions.h"

using namespace std;

//=========================================================================
=====
//
//
//              Section 3: tReservoir Class Definitions
//
//
//=========================================================================
=====

class tReservoir
{
```

```
public:
 tReservoir();
 tReservoir(tInputFile &);
 ~tReservoir();
// void SendCout();
 void RunLevelPoolRouting(double);
 void ComputeInflow(double);
 void ComputeInitialSTQ();
 void ComputeSTQnext();
 void ComputeSTQ();
 void ComputeResQ();

 void SetResVariables(tInputFile &);
 void SetResNodes(tInputFile &);
 void readResNodeFile(char *);
 void readReservoirFile(char *);

 void setCurrResNode(int);
 int  getCurrResNode();

 void setCurrResType(int);
 int  getCurrResType();

 void setNReservoirs(int);
 int  getNReservoirs();

 void setResDischargeOut(double);
 double getResDischargeOut();

 void setResElevOut(double);
 double getResElevOut();

 void setModelTimeStep(double);
 double getModelTimeStep();

 int getNodetKinemat(int);
 int getTypetKinemat(int);

 void setResArraySize(int);
 int  getResArraySize();

protected:

 char resfile[kName];
 char resNodeFile[kName];

 tResData * reservoirNodes;
 tResData * reservoirTypes;
 int rType;
```

```
  int rNode;

  double resInflow; // Inflow = Ij + Ij+1
  double ResQinflow, ResQinflow2;

  // Values obtained through linear interpolation from data files:
  double STQ_0, initialH, initialS, initialQ;

  // Values with a "2" indicate they are from current time step
  // Values without a "2" are from previous time step:
  double resQ, resQ2, resH, resH2, resS, resS2, EDSdata, EDSdata2;

  double elevData;
  int interNum, interNum2;
  int lengthH; //Length of the data table provided for the reservoir
  double STQnext; // Storage-discharge function for the next time step
  double STQ, STQprev;
  double Q_0, H_0; // Outflow and elev from the Reservoir
  int RStep;
  int NumRes;
  double ResTimeDt, ;
  int ResTyp, ResNID, ArraySize;
  double ResOutflow, ResOutElev;

  int nReservoirs;

};

#endif // TRESERVOIR_H

//=====================================================================
//
//
//                    End tReservoir.h
//
//
//=====================================================================/
```

Main code for Reservoir module “tReservoir.cpp” begins:

```
/***************************************************************************
**
**                    tRIBS Distributed Hydrologic Model
**
**          TIN-based Real-time Integrated Basin Simulator
**                      Ralph M. Parsons Laboratory
**                  Massachusetts Institute of Technology
**
**
**  tReservoir.cpp: Functions for class tReservoir (see tReservoir.h)
**        A Finite-Element Kinematic Wave Routing Algorithm
**
***************************************************************************/

#include "tFlowNet/tReservoir.h"
#include "Headers/globalIO.h"

//=========================================================================
//
//
//              Section 1: tReservoir Constructors/Destructors
//
//
//=========================================================================

/***************************************************************************
**
**  tReservoir::tReservoir()
**
**  Constructor for tRIBS model use
**
***************************************************************************/
tReservoir::tReservoir()
{

}

tReservoir::tReservoir(tInputFile &inFile)
{
	nReservoirs = 0;
	SetResVariables(inFile);
	SetResNodes(inFile);
```

```
}



/***************************************************************************
**
**  tReservoir::~tReservoir()
**
**  Destructor
**
***************************************************************************/
tReservoir::~tReservoir()
{
	delete [] reservoirNodes;
	delete [] reservoirTypes;
}

//=========================================================================
//
//
//		Section 2: tReservoir Functions
//
//
//=========================================================================

/***************************************************************************\
**
**  tReservoir::RunLevelPoolRouting()
**
**  Runs the Reservoir component using the Level Pool Routing method.
**
\***************************************************************************/
void tReservoir::RunLevelPoolRouting(double Qin)
{
	/* Defines from which tResData class Type will the code read from */
	rType = getCurrResType();

	/* Defines from which tResData class Node will the code read from */
	rNode = getCurrResNode();

	ComputeInflow(Qin);
	ComputeSTQnext();

	return;
}

/***************************************************************************\
```

```
**
**  tReservoir::ComputeInflow()
**
**  Computes the Inflow into the reservoir from the upstream boundary node
**  in the current time step and the previous one.
**
\***************************************************************************/
void tReservoir::ComputeInflow(double Qinflow)
{
	// Call a function to Get current time step
	RStep = reservoirNodes[rNode].getRoutingStep();
	reservoirNodes[rNode].setInflow(Qinflow);

	if (RStep == 1) {
		ResQinflow2 = Qinflow;
		resInflow = 0 + ResQinflow2; // At initial time step inflow = 0
	}

	else {
		ResQinflow2 = Qinflow; // Get inflow at the upper BND node
		ResQinflow = reservoirNodes[rNode].getInflow(RStep-1);
		resInflow = ResQinflow + ResQinflow2; // = Ij + Ij+1
	}

	return;
}

/***************************************************************************
**
** tReservoir::ComputeInitialSTQ()
**
** Function to compute the inital [2Sj/dt - Qj] based on the inital level
** of the Reservoir
**
***************************************************************************/
void tReservoir::ComputeInitialSTQ() //Will need to read initial H.
{
	lengthH = reservoirTypes[rType].getResLines();

	//Read provided table for Elevation-Storage-Discharge data
	initialH = reservoirNodes[rNode].getInitial_H();

	for (int h=0; h!=lengthH; h++) {
		elevData = reservoirTypes[rType].getResElev(h);
		if (initialH > elevData)
			continue;
		else
			interNum = h;
			break;
```

```
	}

	//Get Discharge Q and Storage S at elevation H by linear interpolation.
	resQ = reservoirTypes[rType].getResDischarge(interNum-1);
	resH = reservoirTypes[rType].getResElev(interNum-1);
	resS = reservoirTypes[rType].getResStorage(interNum-1);
	resQ2 = reservoirTypes[rType].getResDischarge(interNum);
	resH2 = reservoirTypes[rType].getResElev(interNum);
	resS2 = reservoirTypes[rType].getResStorage(interNum);

	initialS = resS + (resS2-resS)*((initialH-resH)/(resH2-resH));
	initialQ = resQ + (resQ2-resQ)*((initialH-resH)/(resH2-resH));

	double timestepUsed = getModelTimeStep();

	//Obtain the Storage-Discharge function (2S/dt + Q) for the first time step.
	STQ_0 = resInflow + ((2.0*initialS/timestepUsed)-initialQ); //Read timestep used in the
model

	return;
}

/***************************************************************************
**
** tReservoir::ComputeSTQnext()
**
** Function to compute the [2Sj+1/dt - Qj+1] based on the Outflow.
**
***************************************************************************/
void tReservoir::ComputeSTQnext()
{
	if (RStep == 1){
		ComputeInitialSTQ();
		ComputeResQ();

		STQnext = STQ_0 - 2.0*Q_0;
		reservoirNodes[rNode].setSTQnext(STQnext, RStep);
	}

	else {
		ComputeSTQ();
		ComputeResQ();

		STQnext = STQ - 2.0*Q_0;
		reservoirNodes[rNode].setSTQnext(STQnext, RStep);
	}

	return;
}
```

```
/*************************************************************************
**
** tReservoir::ComputeSTQ()
**
** Function to compute the Storage-Discharge relation [2Sj+1/dt + Qj+1]
** of the Reservoir at the next time step.
**
*************************************************************************/
void tReservoir::ComputeSTQ()
{
	STQprev = reservoirNodes[rNode].getSTQnext(RStep-1); //Read STQ from previous
time step
	STQ = resInflow + STQprev;

	return;
}

/*************************************************************************
**
** tReservoir::ComputeResQ()
**
** Function to compute the Outflow [Qj+1] from the Reservoir using linear
** interpolation from the provided data table.
**
*************************************************************************/
void tReservoir::ComputeResQ()
{
	if (RStep == 1){
		Q_0 = initialQ;
		setResDischargeOut(Q_0);
		setResElevOut(initialH);
	}

	else {
		for (int x=0; x!=lengthH; x++) {
			EDSdata = reservoirTypes[rType].getResEDS(x);
			if (STQ > EDSdata)
				continue;
			else
				interNum2 = x;
				break;
		}

	resQ = reservoirTypes[rType].getResDischarge(interNum2-1);
	resQ2 = reservoirTypes[rType].getResDischarge(interNum2);
	EDSdata = reservoirTypes[rType].getResEDS(interNum2-1);
	EDSdata2 = reservoirTypes[rType].getResEDS(interNum2);
	resH = reservoirTypes[rType].getResElev(interNum2-1);
```

```
        resH2 = reservoirTypes[rType].getResElev(interNum2);

        Q_0 = resQ + (resQ2 - resQ)*((STQ-EDSdata)/(EDSdata2-EDSdata));
        H_0 = resH + (resH2 - resH)*((STQ-EDSdata)/(EDSdata2-EDSdata));

        setResDischargeOut(Q_0);
        setResElevOut(H_0);
        }
        return;
}
//=========================================================================
//
//
//              Section 3: tReservoir Read File Functions
//
//
//=========================================================================

/*************************************************************************
**
**  tReservoir::SetResVariables(tInputFile &inFile)
**
**  Initializes tResData object
**
*************************************************************************/
void tReservoir::SetResVariables(tInputFile &inFile)
{
        inFile.ReadItem(resfile, "RESDATA");
        readReservoirFile(resfile);

        return;
}

/*************************************************************************
**
**  tReservoir::SetResNodes(tInputFile &inFile)
**
**  Initializes tResData object
**
*************************************************************************/
void tReservoir::SetResNodes(tInputFile &inFile)
{
        inFile.ReadItem(resNodeFile, "RESPOLYGONID");
        readResNodeFile(resNodeFile);

        return;
}

/*************************************************************************
```

```
**
** tReservoir::readResNodeFile() Function
**
**
** Reads the Reservoir Polygon ID File which provides information concerning
** the selected nodes to be represented as Reservoirs.
**
** Format for the Reservoir Polygon ID File:
**
** Header:
** nReservoirs nNodeParams (3)
**
** Body:
** NodeID       ResNodeType             Initial_H
**
** NodeID          (int)             Node selected by the user to be a Reservoir
** ResNodeType  (int)             Type of Reservoir associated to the Node
** Initial_H        (double)       Initial Water Surface Elevation at the Reservoir [m]
**
*************************************************************************/
void tReservoir::readResNodeFile(char *resNodeFile)
{
	int nNodeParams;
	int NodeID, ResNodeType;
	double Initial_H;

	Cout<<"\nReading Reservoir Polygon ID File '";
	Cout<< resNodeFile<<"'..."<<endl<<flush;

	ifstream readFile(resNodeFile);
	if (!readFile) {
		cout << "File "<<resNodeFile<<" not found." << endl;
		cout<<"Exiting Program...\n\n"<<endl;
		exit(1);
	}

	readFile >> nReservoirs;
	setNReservoirs(nReservoirs);
	readFile >> nNodeParams;
	reservoirNodes = new tResData[nReservoirs];
	assert(reservoirNodes != 0);

	for (int count=0;count<nReservoirs;count++) {
		reservoirNodes[count].setResArraySize(getResArraySize());
		reservoirNodes[count].setRNum(0);
		for (int ct=0;ct<nNodeParams;ct++) {
			if (ct==0) {
				readFile >> NodeID;
				reservoirNodes[count].setResNodeID(NodeID);
```

```
                    }
                    if (ct==1) {
                              readFile >> ResNodeType;
                              reservoirNodes[count].setResNodeType(ResNodeType);
                    }
                    if (ct==2) {
                              readFile >> Initial_H;
                              reservoirNodes[count].setInitial_H(Initial_H);
                    }
          }
     }
     readFile.close();
}

/****************************************************************************
**
** tReservoir::readReservoirFile() Function
**
**
** Reads the Reservoir File which provides information concerning
** the different types of Reservoir specified by the user. Creates an
** array of tResData objects for storing data. (see tResData.h)
**
** Format for the Reservoir Data File:
**
** Header:
** nTypes        nResParams (4)
**
** Body:
** Type#         Elevation         Discharge         Storage
**
** Type#              (int)             1->N
** Elevation          (double)          Stage or water elevation at the Reservoir [m]
** Discharge          (double)          Discharge for each elevation  [m^3/s]
** Storage            (double)          Storage for each elevation  [1000 m^3]
**
****************************************************************************/
void tReservoir::readReservoirFile(char *resfile)
{
     int nTypes, nResParams, nLines;
     int ResType;
     double rElev, rDischarge, rStorage;
     double EDSdt, EDSstorage, EDSdischarge, EDSvalue;

     Cout<<"\nReading Reservoir Data File '";
     Cout<< resfile<<"'..."<<endl<<flush;

     ifstream readFile(resfile);
     if (!readFile) {
```

```
		cout << "File "<<resfile<<" not found." << endl;
		cout<<"Exiting Program...\n\n"<<endl;
		exit(1);
	}

	readFile >> nTypes;
	readFile >> nResParams;

	reservoirTypes = new tResData[nTypes];
	nLines = reservoirTypes[0].getnumLines(resfile);
	assert(reservoirTypes != 0);

	int currType = 0; //Initializes Reservoir Type
	reservoirTypes[currType].setRNum(0);

	for (int countLine=0;countLine < (nLines-1);countLine++) { //Reads all lines from the
file (excludes header)
		for (int ct=0;ct < nResParams;ct++) { // Reads parameters from each line (4)
			if (ct==0) {
				readFile >> ResType;
				if (ResType != currType) {
					currType++;
					reservoirTypes[currType].setResType(ResType);
				}
				else {
					reservoirTypes[currType].setResType(ResType);
					int NumType = reservoirTypes[currType].getRNum();
				}
			}
			if (ct==1) {
				readFile >> rElev;
				reservoirTypes[currType].setResElev(rElev);
			}
			if (ct==2) {
				readFile >> rDischarge;
				reservoirTypes[currType].setResDischarge(rDischarge);
				int NumDis = reservoirTypes[currType].getRNum();
			}
			if (ct==3) {
				readFile >> rStorage;

	reservoirTypes[currType].setResLines(reservoirTypes[currType].getRNum());
				reservoirTypes[currType].setResStorage(rStorage);
			}
		}
	}
	readFile.close();

	EDSdt = getModelTimeStep(); // Units in seconds
```

```
	for (int iter=0;iter < nTypes;iter++) {
		for (int param=0;param < reservoirTypes[iter].getResLines();param++) {
			EDSstorage = reservoirTypes[iter].getResStorage(param);
			EDSdischarge = reservoirTypes[iter].getResDischarge(param);
			EDSvalue = ((2*EDSstorage)/EDSdt) + EDSdischarge; // 2S/dt + Q
			reservoirTypes[iter].setResEDS(EDSvalue, param);
		}
	}
}




//=====================================================================
//
//
//		Section 4: tReservoir Set/Get Functions
//
//
//=====================================================================

void tReservoir::setNReservoirs(int resNum){NumRes = resNum;}
int  tReservoir::getNReservoirs(){return NumRes;}

void tReservoir::setCurrResNode(int resN){ResNID = resN;}
int  tReservoir::getCurrResNode(){return ResNID;}

void tReservoir::setCurrResType(int resT){ResTyp = resT;}
int  tReservoir::getCurrResType(){return ResTyp;}

void tReservoir::setResDischargeOut(double resQout){ResOutflow = resQout;}
double  tReservoir::getResDischargeOut(){return ResOutflow;}

void tReservoir::setResElevOut(double resHout){ResOutElev = resHout;}
double  tReservoir::getResElevOut(){return ResOutElev;}

void tReservoir::setModelTimeStep(double resTimeStep){ResTimeDt = resTimeStep;}
double  tReservoir::getModelTimeStep(){return ResTimeDt;}

void tReservoir::setResArraySize(int resArray){ArraySize = resArray;}
int  tReservoir::getResArraySize(){return ArraySize;}

// Get function for NODE ID and Type access from tKinemat
int tReservoir::getNodetKinemat(int tKNode)
{
	return reservoirNodes[tKNode].getResNodeID();
}
```

```
int tReservoir::getTypetKinemat(int tKType)
{
	return reservoirNodes[tKType].getResNodeType();
}

//======================================================================
//
//
//			End tReservoir.cpp
//
//
//======================================================================
```

APPENDIX B

HEC-GEOHMS MODEL SETUP

Overview of the ArcGIS Setup Steps using GeoHMS Tool

1. Obtain ASTER gDEM from NASA/METI (Ministry of Economy, Trade and Industry of Japan) at a resolution of 30 m (geoTIFF format)

2. Use the tool Mosaic to raster to merge the DEM tiles where the study site is located to have the final product for the Digital elevation map as shown in Figure B1.

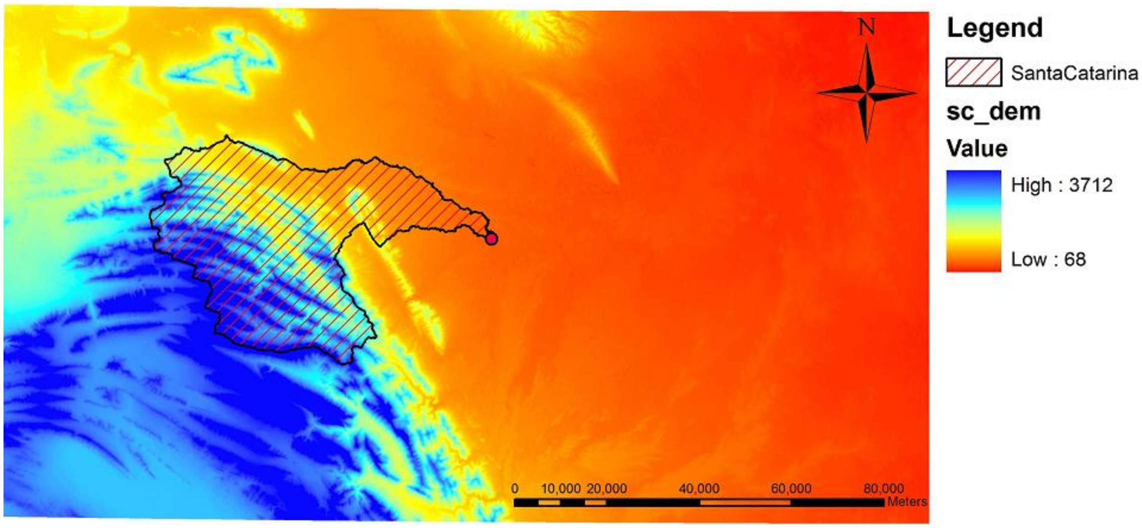

Figure B1. ASTER gDEM from NASA with a 30m resolution

3. Install HEC-geoHMS extension to preprocess the terrain and delineate the boundaries and river network. The following steps were done as described in detail in the User's Manual (2010).
    a. Fill Sinks
    b. Flow Direction
    c. Flow Accumulation
    d. Stream Definition (10 km^2) – condition specified by the user. In this model a condition of 10 km^2 was used since it was a good fit for the purposes of the study to capture spatial variability of the catchment without creating an un-manageable amount of sub-basins. 61 sub-basins resulted from this definition.
    e. Stream Segmentation
    f. Catchment Grid Delineation
    g. Catchment Polygon Processing
    h. Drainage Line Processing
    i. Adjoint Catchment Processing

4. HMS Project Setup

   The basin is defined here from out of the whole DEM by specifying the outlet of the basin.

   a. Start New project
   b. Add project Point (Cadereyta)
   c. Generate Project

5. Basin Processing
   a. Merge Subbasins (if necessary)
   b. Subdivide basin (this was done to capture areas of importance such as Rompepicos). This tool was used since initial divisions of the sub-basins did not capture the location of the Rompepicos Dam.
   c. River Length
   d. River Slope
   e. Basin Slope
   f. Longest Flowpath
   g. Basin Centroid
   h. Centroid Elevation
   i. Centroidal Longest Flowpath

6. Hydrologic Parameters
   a. Select HMS Processes
      i. Loss Method – Soil Moisture Accounting scheme
      ii. Transform Method – Kinematic Wave
      iii. Routing Method – Kinematic Wave
   b. Sub-basin Parameters from Raster
      i. Canopy Storage
         1. Derived from MODIS product MOD 15 – Leaf Area Index (LAI)
         2. Offset adjustment for LAI = 0.1*LAI
         3. S = 0.5*LAI (Canopy maximum storage)
         4. Raster calculator was used to transform any "Fill" values in the raster for urban and barren areas into an LAI value of zero and import it into the ArcMap project.
      ii. Surface Storage (see the methods section for the equations used)
      iii. Loss parameters obtained from the soil maps presented in the methods section.
      iv. Channel and overland planes roughness parameters from tabular values.

c. Kinematic Wave Parameters
   i. From Basin characteristics generated through HEC-geoHMS (slope, river network)

7. Transform NLDAS grid cells into precipitation gauges. Both hydrological models were forced using the same meteorological data from NLDAS. In HEC-HMS each pixel from the rainfall fields in NLDAS was converted to a rain gauge within the model and assigned a Thiessen weight using ArcGIS following Robles-Morua et al. (2015). The steps converting the pixels into points are:
   a. Raster to Point file tool in ArcGIS
   b. Assign gauge weight to the basin layer created through HEC-geoHMS using the Thiessen polygons tool
   c. Obtain individual time series for each "gauge" or pixel to be used in the meteorological model in HEC-HMS with the matlab code generated named *Read_NLDAS_ind_pixel_HMS.m* found in the matlab codes folder.

8. Prepare project for export into HEC-HMS to generate a basin model as seen in Figure B2.

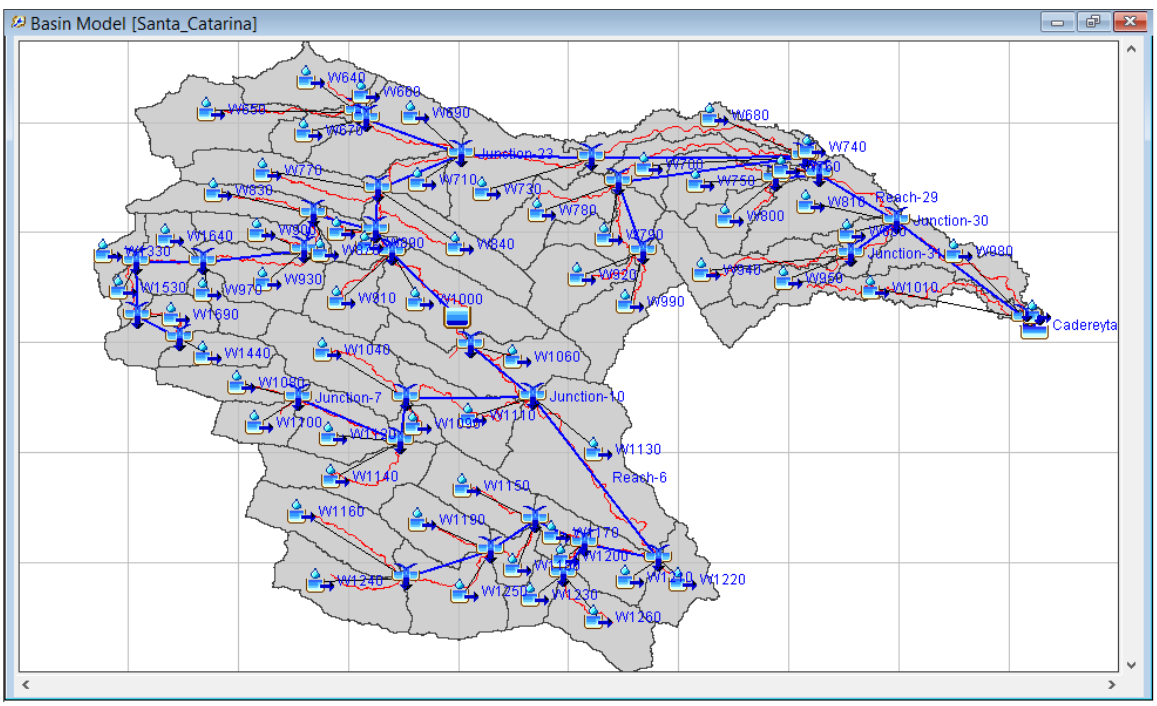

Figure B2. Basin Model generated in HEC-HMS

APPENDIX C

RESEARCH MATERIAL DATASETS

This appendix contains the description of the data used to complete this study. The datasets included are the following:

- Weather and precipitation forcing for both models
- GIS data repository on the Santa Catarina basin including spatial maps and relevant shapefiles and ASCII grids
- HEC-HMS and tRIBS model setup

Table C1 presented below describes the organization of the data as found in the delivered hard drive and a description of the contents.

Table C1

Hard drive folder organization.

Content	Path
Meteorological data	X:\Appendix_C\Met
GIS repository	X:\Appendix_C\GIS
HEC-HMS model	X:\Appendix_C\HEC
tRIBS model	X:\Appendix_C\tribs
tRIBS Reservoir code	X:\Appendix_C\tribs_reservoir
TIFF files	X:\Appendix_C\tiff

Meteorological data: This folder will contain the original NLDAS meteorological data in GRIB format (*.grb) that includes precipitation, solar radiation, and wind speed among others for the months of June and July 2010. The Matlab code used to extract the data is included in the script folder. Precipitation files, rainfall from gauges, observed streamflow from the gauge Cadereyta II and cumulative precipitation maps are included.

GIS repository: This contains all spatial maps used in the project such as the 30 m DEM, 1 km soil grids, land cover maps, MODIS datasets, reservoir points and corresponding contributing area delineation and rain gauges. The data is in the

WGS_1984_UTM_Zone14N projected coordinate system and a Geographic Coordinate System: GCS_WGS_1984 and Datum: D_WGS_1984. The “Basin” folder contains all the spatial maps: DEM, hillshade, MODIS, slope, soils, land cover, stream networks, contributing areas, etc. The “Location_points” folder includes all point files from GIS such as the rain gauges, outlet, dam locations, points of interest highlighted in the thesis, etc.

HEC-HMS model: This contains the HEC-HMS model setup as used for the simulations in this study. The “GISmodel” folder contains the river network and sub-basin model with an attached geodatabase file (*.gdb) with information on sub-basin parameters. It contains 4 basin models and the required paired data for the Storage-Discharge and Elevation-Storage functions.

<u>Basin Models</u>:

1) “Impervious_pervious”: the base case simulation
2) “NO_DAMS”: The Rompepicos dam is removed from the simulation
3) “FINAL_2dams”: Inclusion of a second large dam at the Entry to the City
4) “Detention_Basins”: Inclusion of three small detention dams

tRIBS model: Contains the tRIBS model setup in the format and organization required by the model. Included are the “*.in” files used for each simulation in the main folder which contain all associated datasets for each run. Included are the “Input”, “Output”, “Rain” and “Weather” folders containing the model forcings, soil/land cover parameters, reservoir nodes and elevation-discharge-storage information. Included are also the “*.sh” files required to run the model in the ASU Advance Computing Center cluster “OCOTILLO”.

<u>tRIBS runs:</u>

1) FINAL_Base.in : Base case simulation to recreate current conditions. Output file extension for hydrographs and tMesh output: “FINAL_base”.

2) FINAL_NO_Dam.in : Simulation to recreate conditions without any hydraulic structure in the site. The option to activate the reservoir routing is off. Output file extension for hydrographs and tMesh output: “FINAL_NO_Dam”.
3) FINAL_2dam.in : Simulation to include a second large dam at the Entry to the City. Output file extension for hydrographs and tMesh output: “FINAL_2dam”.
4) FINAL_detention_dam.in : Inclusion of three small detention dams. Output file extension for hydrographs and tMesh output: “FINAL_detention_dam”.

tRIBS Reservoir Code: Contains the tRIBS code presented in Appendix A that enables the use of assigned nodes to route as reservoirs given the necessary information by the user. For more information on compilation and setup, visit the tRIBS model site at: http://vivoni.asu.edu/tribs.html

TIFF Files: This folder contains 600-dpi compressed Tagged Image File Format (*.tiff) and Illustrator Encapsulated PostScript (*.eps) versions of the figures used for the thesis and additional figures created for the development of a manuscript. In addition to the figures, the file used to generate tables is included as well.